京都大学学術情報リポジトリ
KURENAI 紅
Kyoto University Research Information Repository

京都大学
KYOTO UNIVERSITY

Title	DUCTILITY AND ENERGY DISSIPATION OF CONCRETE BEAM MEMBERS AND THEIR DAMAGE EVALUATION BASED ON HYSTERETIC DISSIPATED ENERGY(Dissertation_全文)
Author(s)	Inoue, Susumu
Citation	Kyoto University (京都大学)
Issue Date	1994-01-24
URL	http://dx.doi.org/10.11501/3074844
Right	
Type	Thesis or Dissertation
Textversion	author

Kyoto University

(2)

DUCTILITY AND ENERGY DISSIPATION OF CONCRETE BEAM MEMBERS AND THEIR DAMAGE EVALUATION BASED ON HYSTERETIC DISSIPATED ENERGY

September 1993

Susumu INOUE

ACKNOWLEDGEMENTS

I am deeply grateful to Dr. Manabu Fujii, Professor of Department of Civil Engineering at Kyoto University, for his supervision of my research, scholarly guidance and invaluable advice. I also wish to express my sincere gratitude to Dr. Toyoaki Miyagawa, Associate Professor of Department of Civil Engineering at Kyoto University, for his helpful guidance and heartfelt encouragement.

I am also deeply indebted to Professor Shiro Morita and Professor Kenzo Toki of Kyoto University for their critical review of the manuscript.

I am deeply indebted to Dr. Kiyoshi Okada, Professor Emeritus of Kyoto University, who guided me as a researcher in concrete engineering field and supervised my research for the first two years until his retirement. I also feel earnestly grateful to Dr. Kazuo Kobayashi, Professor of Department of Civil Engineering at Osaka Institute of Technology, for his helpful advice, valuable suggestions and continuous encouragement.

I wish to express my gratitude to Dr. Hirokazu Iemura, Associate Professor of Kyoto University and Dr. William Tanzo of Saitama University for their kind review and revise of the manuscript. I also thank Dr. Kazuyuki Izuno of Ritsumeikan University, Mr. Makoto Kimura of Kyoto University, Mr. Tatsuo Kawahigashi of Kinki University and Mr. Shinichi Igarashi of Kanazawa University for their continuous encouragement.

I also would like to express my appreciation to Mr. Atsushi Hattori for his kind help in experimental and analytical works. Thanks are also due to Mr. Takahiro Fujita, Mr. Yoshihiro Katsuno, Mr. Toshihiko Matsumoto, Mr. Keiji Ikushima, Mr. Yukio Igo, Mr. Ken Takahashi, Mr. Kunihisa Isono, Mr. Seiji Nakata, Mr. Koji Tsukada, Mr. Kenichi Takao, Mr. Yuji Fukushima, Mr. Shiro Fujii and all the other students who studied together in Construction Materials Laboratory for their kind help in experimental works. Appreciation should be also expressed to Mrs. Eri Okamoto for her help in typing this manuscripts.

I also would like to thank my parents for their encouragement.

Lastly, I wish to thank my wife Atsuko and our daughter Saki for their understanding and encouragement.

TABLE OF CONTENTS

LIST OF ABBREVIATIONS

ACI: American Concrete Institute.
AIJ: Architectural Institute of Japan.
ASCE: American Society of Civil Engineers.
CAJ: Cement Association of Japan.
FIP: Fédération Internationale de la Précontrainte.
GBRC: General Building Research Corporation.
JCI: Japan Concrete Institute.
JSCE: Japan Society of Civil Engineers.
PCI: Precast/Prestressed Concrete Institute.

LIST OF SYMBOLS

a: shear span length.
A_p: area of prestressing steel.
A_s: area of reinforcing steel.
b: width of section.
c: cover thickness for hoops.
C_{cf}: confining coefficient for maximum stress.
$C_{c\varepsilon m}$: confining coefficient for strain at maximum stress.
C_{f0}: confining coefficient for stress degradation gradient.
d: effective depth of section or
diameter of longitudinal bar [in Chapter 2].
d_p: depth of prestressing steel.
d_s: depth of reinforcing steel.
D: minimum length or diameter of cross section.
D': minimum leg of a hoop.
DI: damage index.
E_c: elastic modulus of concrete.
E_d: dissipated energy at each deflection amplitude.
E_d': non-dimensional dissipated energy at each deflection amplitude.
E_i: tangent modulus of stress – strain curve of plain concrete.
f_c: maximum stress of confined concrete.
f'_c: compressive strength of concrete or
maximum stress of plain concrete [in Chapter 2].
f'_{ck}: design compressive strength of concrete.
f_{ps}: stress in prestressing steel at ultimate state.
f_{pu}: tensile strength of prestressing steel.
f_{py}: yield strength of prestressing steel.
f_{sy}: yield strength of reinforcing steel.
f_{syh}: yield strength of transverse steel or hoop.
f_{su}: tensile strength of reinforcing steel.
f(n): damage reducing factor.
h_{eq}: equivalent coefficient of damping.
l: span length or buckling length [in Chapter 3].

M: flexural moment.
n: number of loading cycle or
number of intervals having specified length of s [in Chapter 3].
p: longitudinal reinforcement ratio.
p_w: shear reinforcement ratio.
P: applied load.
P_{cr}: flexural cracking load.
P_{max}: maximum load at each deflection amplitude.
P_u: maximum ultimate load.
P_u': calculated maximum ultimate load.
P_y: yield load.
P_{ycal}: calculated yield load.
q: longitudinal steel index.
q_p: prestressing steel index.
q_s: reinforcing steel index.
s: spacing of transverse steel or hoop.
V_c: shear resistance of concrete.
α: restoring index.
δ: deflection.
δ_{max}: deflection amplitude applied at the first cycle of Series-B beam [in Chapter 5].
δ_u: deflection at ultimate state.
δ_y: yield deflection.
δ_{ycal}: calculated yield deflection.
$\Delta\varepsilon$: increment in longitudinal strain.
$\Delta\varepsilon_{coc}$: $\varepsilon_{coc}-\varepsilon_{co}$ or $\varepsilon_{coc}'-\varepsilon_{co}'$.
ΔP: increment in applied load.
ε: longitudinal strain.
ε_b: strain at buckling initiation of longitudinal bar.
ε_c: strain in concrete.
ε_{co}: strain at the maximum stress of confined concrete.
ε_{co}': strain at the maximum stress of plain concrete.
ε_{coc}: strain at onset of stress degradation of confined concrete.
ε_{coc}': strain at onset of stress degradation of plain concrete.
ε_{c20}: strain at $\sigma=0.2f_c$.
ε_{sh}: strain at onset of strain hardening of reinforcing bar.
ε_{su}: strain at tensile strength of reinforcing bar.

ε_{sy}: strain at yielding of reinforcing bar.
ϕ: diameter of bar or curvature of section.
λ: mechanical degree of prestress.
μ: ductility factor.
θ: stress degradation gradient [Chapter 2] or rotation angle [Chapter 4].
ρ_s: volumetric ratio of transverse steel or hoop.
σ: longitudinal stress.
σ_p: introduced prestress.
$\Sigma E_d'$: accumulated non-dimensional energy dissipated actually during loading.
$\Sigma E_{d\,ult}'$: non-dimensional total dissipated energy until ultimate state.

CHAPTER 1

INTRODUCTION

1.1 GENERAL REMARKS

Most of the present seismic design codes for concrete structures, including the JSCE Standard Specification for Design and Construction of Concrete Structures [1], allow plastic deformation depending on the degree of expected earthquake damages based on Newmark's constant energy law [2]. This concept of seismic design makes concrete structures safe and economical by assuming the required serviceability after earthquakes and allowing some degree of damages according to their serviceability. On the other hand, this means that concrete structures should maintain the strength above the yield strength up to at least the allowable plastic deformation adopted in the design that allows certain degree of damage during earthquakes. Therefore, it becomes necessary to provide a sufficient amount of ductility to concrete structures so that they should not collapse during the expected earthquakes.

As one of the methods for improving the ductility of concrete structures and members, lateral confinement of concrete in compression zone of section is very effective. In recent years, many research works had been done on the ductility improvement of reinforced concrete members by lateral confinement, and these results had been reflected on the provisions for structural details in various seismic codes. Concerning the laterally confined concrete itself, Kent et al. [3] proposed the stress – strain model for confined concrete, which had been modified by Park et al. [4] into the well-known modified Kent and Park model.

Although the effects of various factors on the fundamental properties of confined concrete has been discussed [5], compressive ductility of confined concrete is largely dependent upon the size and shape of specimen and strength of materials used. Therefore, still many stress – strain models for confined concrete have been proposed in recent years [6–8]. While all of these proposed models claim to represent general properties of confined concrete, some problems still remain about their applicability to general types of specimen with various sizes and shapes and strength of materials. From this view point, it is necessary to develop a suitable stress – strain model for confined concrete to be used in estimating the ductility

improvement of flexural members due to confined concrete, especially in the prediction of ultimate deformability during earthquakes.

In evaluating the ductility of concrete structures and members, there are often discussions on how the ultimate state of a member should be defined. Ductility of a member is largely dependent on the definition of the ultimate state since ductility is usually expressed in terms of the ratio of the deformation at the ultimate state to that at the first yielding of the member, that is, ductility factor. Therefore, a rational and reasonable definition of the ultimate state of a member is necessary for ductility evaluation. Park [9] summarized alternative definitions for maximum ultimate displacement, which correspond to 1) limit strain of concrete under compression, 2) peak load, 3) some small reduction in load carrying capacity after peak load and 4) fracture or buckling of reinforcement. Among these definitions, 3) and 4) seem to be reasonable because most structures have some capacity for deformation after the peak load without significant reduction in load carrying capacity. In general cases, however, definition corresponding to small reduction in load carrying capacity, for example 20% of peak load, is used. This is mainly because that buckling of longitudinal compression reinforcement and fracture of transverse reinforcement cannot be easily predicted, especially under reversed cyclic loading as experienced during earthquakes.

As for the buckling of longitudinal bars in reinforced concrete members, Suzuki et al.[10] and Papia et al. [11] proposed equations for predicting the strain at buckling initiation. However, each method for determining buckling initiation point was different, resulting in different strains at buckling initiation. In addition, the effects of influencing factors on the buckling of longitudinal bars in confined concrete have not been made clear. Since the researches dealing with this field are very few, further investigations are necessary in order to establish a rational method for determining buckling initiation and to evaluate the ductility of a member in which ultimate state is determined by buckling of compression reinforcement.

As mentioned previously, ductility of reinforced concrete members could be improved largely by lateral confinement. However, a reinforced concrete member with under-reinforced section has an adequate amount of ductility under pure bending even if it is not provided with lateral confinement. In case of flexural members, therefore, ductility improvement due to lateral confinement is more effective in prestressed concrete than in reinforced concrete because higher compressive ductility is required in prestressed concrete section due to the existence of axial force. Researches on ductility improvement of prestressed

concrete beams by lateral confinement had been done by Park et al. [12], Muguruma et al. [13] Suzuki et al. [14] and so on. Nevertheless, further investigations on the effectiveness of lateral confinement under different conditions are still necessary, especially for cases of unbonded prestressed concrete and partially prestressed concrete subjected to reversed cyclic loads.

At the present state, safety of concrete structures under earthquake loads is usually examined by means of deformation ductility under unidirectional monotonous loads. During large earthquakes, however, ductility of concrete members is significantly reduced due to load repetitions at large deformations compared with the predicted ductility under monotonous loads. In such cases, it had been often pointed out that reinforced concrete members which were designed to fail in flexure with sufficient shear capacity tended to show brittle shear failure. Therefore, it leaves much to be investigated on the ductility of a member under reversed cyclic loading.

The evaluation of seismic damages of concrete structures is very important in order to repair or strengthen the deteriorated structures as soon as possible after severe earthquakes. Up to now, the evaluation of damages after earthquakes has been done usually based on the investigation of the appearance of deteriorated structures [15] or the maximum response deformation experienced during earthquakes. However, damages of concrete structures are caused not only by excessive deformation but also load reversals and repetitions as mentioned previously. Therefore, evaluation of seismic damage should be done considering the effects of both of excessive deformation and load repetitions. In this case, maximum response deformation would be an indicator for the former, while dissipated or absorbed energy during earthquakes would be for the latter.

From these view points, some damage indicators have been proposed in recent years. Park et al. [16] proposed "Damage Index", which is expressed by a linear function of maximum deformation and hysteretic dissipated energy. Stephens et al. [17] also proposed "Damage Function" based on the low cycle fatigue theory. These indicators are supposed to be reasonable and to have potential effectiveness for the evaluation of seismic damage of reinforced concrete structures. However, considerable degree of uncertainty is still remained as for the effects of various factors on the energy dissipation properties of reinforced and prestressed concrete members and the difference in final failure mode as seen between reinforced concrete and prestressed concrete under reversed cyclic loading.

1.2 ORGANIZATION OF THIS THESIS

This research is done in order to clarify the effects of various factors on the ductility and energy dissipation properties of reinforced, partially prestressed and prestressed concrete beam members in a quantitative sense. Fundamental investigations are also done for the establishment of seismic damage evaluation based on hysteretic dissipated energy of these members.

In Chapter 2, effects of various factors on the fundamental properties of laterally confined concrete are investigated. From the test results, a new stress – strain model for confined concrete is proposed and its applicability to theoretical moment – curvature analysis is discussed.

In Chapter 3, applicability of various methods for determining the buckling initiation point of longitudinal bars in confined concrete is examined. In addition, effects of various factors on the strain at buckling initiation of longitudinal bars are investigated.

In Chapter 4, improvement of flexural inelastic deformation properties under reversed cyclic loading due to confined concrete is examined mainly about partially prestressed concrete and unbonded prestressed concrete.

In Chapter 5, energy dissipation properties of partially prestressed concrete beams under reversed cyclic loading are discussed and the effects of various factors on the accumulation process of dissipated energy are investigated. An example of damage index based on hysteretic dissipated energy is also proposed.

In Chapter 6, energy dissipation properties of reinforced concrete beams are discussed by focussing mainly on the effects of longitudinal reinforcement ratio and shear reinforcement ratio. An example of damage index is also proposed and its applicability is examined by using 1/3 scale bridge pier model specimens.

Finally in Chapter 7, concluding remarks of the whole chapters of this thesis are summarized in addition to some comments for future investigations.

REFERENCES OF CHAPTER 1

1) Japan Society of Civil Engineers, "Standard Specification for Design and Construction of Concrete Structures," Part 1 [Design], 1991. [in Japanese]
2) Veletsos, A. S. and Newmark, N. M., "Effect of Inelastic Behavior on the Response of Simple Systems to Earthquake Motions," Proc. of Second World Conference on Earthquake Engineering, Vol.2, pp.895–912, 1960.
3) Kent, D. C. and Park, R., "Flexural Members with Confined Concrete," Journal of the Structural Division, ASCE, Vol.97, No.ST7, pp.1969–1990, 1971.
4) Park, R., Priestley, M. J. N. and Gill, W. D., "Ductility of Square-Confined Concrete Columns," Journal of the Structural Division, ASCE, Vol.108, No.ST-4, pp.929–950, 1982.
5) Park, R. and Paulay, T., "Reinforced Concrete Structures," John Wiley & Sons, 1975.
6) Muguruma, H., Watanabe, F., Katsuta, S. and Tanaka, H., "Modeling of Stress – Strain Curve for Confined Concrete," Proc. of CAJ, No.34, pp.429–432, 1980. [in Japanese]
7) Sheikh, S. A., "Confined Concrete Subjected to Axial and Bending Loads," Proc. of the 8th World Conference on Earthquake Engineering, Vol.V, pp.869–876, 1984.
8) Mander, J. B., Priestley, M. J. N. and Park, R. "Theoretical Stress – Strain Model for Confined Concrete," Journal of Structural Engineering, ASCE, Vol.114, No.8, pp.1804–1823, 1988.
9) Park, R., "Ductility Evaluation from Laboratory and Analytical Testing," Proc. of Ninth World Conference on Earthquake Engineering, Vol.VIII, pp.605–616, 1988.
10) Suzuki, K., Nakatsuka T., Nagata, N. and Inoue, K., "Buckling Behavior of Longitudinal Compressive Reinforcement in Confined Concrete with Circular Spiral Reinforcement," Proc. of the JCI, Vol.9, No.2, pp.151–156, 1987. [in Japanese]
11) Papia, M. and Russo, G., "Compressive Concrete Strain at Buckling of Longitudinal Reinforcement," Journal of Structural Engineering, ASCE, Vol.115, No.2, pp.382–397, 1989.
12) Thompson, K. J. and Park, R., "Ductility of Prestressed and Partially Prestressed Concrete Beam Sections", PCI Journal, Vol.25, No.2, pp.46–70, 1980.

13) Muguruma, H., Watanabe, F., Tanaka, H. and Katsuda, S., "Improving the Ductility of Prestressed Concrete Beam by Using the High Yield Strength Hoop Reinforcement," Proc. of JCI 2nd Conference, pp.377–380, 1980. [in Japanese]
14) Suzuki, K., Nakatsuka, T., Hiramatsu, K. and Nagata, S., "High Ductile Behavior of Partially Prestressed Concrete Beams with Confined Concrete in the Compression Zone," Proc. of JCI 7th Conference, pp.485–488, 1985. [in Japanese]
15) Public Works Research Center, "Manual for Restoration Methods for Civil Engineering Structures Damaged during Earthquakes," Ministry of Construction, 1987. [in Japanese]
16) Park, Y. J. and Ang, A. H–S., "Mechanistic Seismic Damage Model for Reinforced Concrete," Journal of Structural Engineering, ASCE, Vol.111, No.4, pp.722–739, 1985.
17) Stephens, J. E. and Yao, J. T. P., "Damage Assessment Using Response Measurements," Journal of Structural Engineering, ASCE, Vol.113, No.4, pp.787–801, 1987.

CHAPTER 2

FUNDAMENTAL PROPERTIES OF LATERALLY CONFINED CONCRETE

2.1 GENERAL REMARKS

Concrete itself is a brittle material with an ultimate compressive strain of at most 0.3%. However, it is well known that the compressive ductility of concrete can be improved significantly by confining laterally with spirals or hoops. By confining concrete laterally, triaxial compressive stress condition is formed under applied longitudinal stress, resulting in enhancement in compressive deformability and strength. In addition, these transverse reinforcements prevent premature buckling of longitudinal reinforcement and also play a role as web reinforcements. Furthermore, high–strength hoops or spirals with yield strength of more than 80kgf/mm^2 have been used as lateral confinement for high–strength concrete for the development of high–rise and high–ductility buildings.

As for laterally confined concrete, many research works have been done in recent years, and the fundamental properties of that have been made clear to some extent. It has been also indicated, however, that there are many factors having influences on the properties of confined concrete. The appropriate amount of lateral confinement which will give sufficient safety to concrete structures under earthquake load has not been unified yet as can be seen in the different recommended values of lateral confinement among several code provisions. In addition, it has became necessary to evaluate the deformability of concrete members well into the post–elastic range in case of examining the ultimate limit state under earthquake loads as the limit state design has been introduced in the design of concrete structures. In such cases, stress – strain models of concrete considering confining effects should be necessary.

From a view point of assessing the ductility of concrete members under flexure and/or compression, it is desirable to establish a rational stress – strain model of confined concrete.

In this chapter, a new stress – strain model of laterally confined concrete is proposed based on the results of uniaxial compression tests on the column specimens having a circular or square section. And then, its applicability to

theoretical moment – curvature analysis of flexural members is discussed.

2.2 REVIEW OF PREVIOUS RESEARCH WORKS

2.2.1 General Properties of Confined Concrete

As main factors having influences on the compressive properties of confined concrete, the following variables can be listed generally [1].

1. ratio of transverse steel for lateral confinement.
2. yield strength of transverse steel.
3. spacing of transverse steel.
4. diameter of transverse steel.
5. shape of transverse steel (spiral or hoop, circular or square).
6. strength of concrete.
7. existence of strain gradient in cross section.
8. loading rate.

Other factors other than the above mentioned ones may have some influences on the physical properties of confined concrete.

It is reported that the enhancement in strength and ductility of confined concrete becomes larger by using circular spirals than by square hoops, and also that the effectiveness of lateral confinement can be achieved more easily in lower strength concrete than higher strength one [1].

As an example of indices representing the degree of confinement, the average confining stress (σ_r) were proposed as follows [2].

$$\sigma_r = \frac{2A_s\sigma_s}{sD} = p_s\sigma_s$$
$$= p_s f_{syh} \text{ (at the yielding of transverse steel)} \qquad (2\text{–}1)$$

Where, A_s: area of transverse steel, σ_s: stress in transverse steel, s: spacing of transverse steel, D: minimum length of cross section, p_s: ratio of transverse steel ($=2A_s/sD$) and f_{syh}: yield strength of transverse steel.

From the uniaxial compressive loading tests conducted on circular column

specimens with circular spirals and hoops, it was reported that the stress in transverse steel reaches its yield strength at $s/D \leq 0.7$ if the yield strength is approximately 3000kgf/cm^2. Considering this result, the index, $p_s f_{syh}$ should be available. On the other hand, in case of high–strength transverse steel with yield strength of more than 10000kgf/cm^2, transverse steel dose not yield even at the ultimate state of the specimen under some arranging conditions [3, 4 and 5]. Therefore, the stress in transverse steel (σ_s) cannot always be replaced by its yield strength (f_{syh}).

As for the use of high–strength steels as transverse reinforcement, some disadvantages had been indicated previously. For instance, 1) utility of their strength is not as good as ordinary–strength ones, 2) failure mode of concrete at a large deformation becomes more brittle due to their elastic confinement and 3) spalling of core concrete, which is already in the plastic deformation range, is accelerated at unloading by elastic confinement [2]. In recent years, however, the use of high–strength steel as transverse reinforcement has become under consideration due to the spread of high–strength concrete.

Tests results on confined concrete with high–strength transverse steel (f_{syh}=14000kgf/cm^2) [3 and 5] showed that the improvement in compressive ductility of concrete could be more effectively achieved by using high–strength transverse steel than by ordinary–strength one and that the use of high–strength transverse steel was desirable in case of high–strength concrete because a larger confining force became necessary in order to restrain the transverse deformation compared with ordinary–strength concrete. Other advantages of high–strength transverse steels were also reported, for examples, the prevention of buckling of longitudinal reinforcement and fatigue rupture of transverse steel [6 and 7].

However, compressive failure mode of high–strength concrete is more brittle than ordinary–strength one. Therefore, a more detailing arrangement of transverse steels is necessary in case of high–strength concrete even when confined by high–strength transverse steels.

2.2.2 Stress – Strain Models for Confined Concrete

Various stress – strain model for laterally confined concrete have been proposed [8–14].

Fujii et al. [8] proposed the stress – strain model for confined concrete as

shown in Fig.2-1, which was derived from the experimental data together with the previous ones by other researchers and by modifying the confining coefficients proposed by Iyengar [9] and Muguruma et al. [10]. Each confining coefficient was given by Eq.(2-2).

$$C_{cf},\ C_{c\varepsilon m},\ C_{c\varepsilon u}=\rho_s{}^a[1-s/(kD)](f_{syh})^b(f'_c)^c \qquad (2\text{-}2)$$

Where, C_{cf}, $C_{c\varepsilon m}$ and $C_{c\varepsilon u}$: confining coefficients for the maximum stress, strain at the maximum stress and strain at the ultimate state, respectively, ρ_s: volumetric ratio of transverse hoop, s: spacing of hoops, D: minimum length of cross section, f_{syh}: yield strength of hoop, f'_c: compressive strength of plain concrete, a, b, c and k: experimental coefficients.

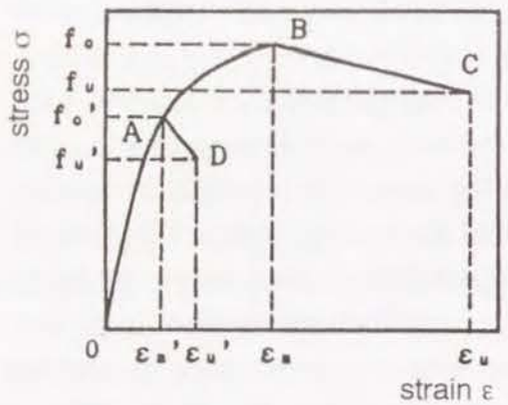

O – A $\quad \sigma = E_i\varepsilon + \dfrac{f_c' - E_i\varepsilon_m'}{(\varepsilon_m')^2}\varepsilon^2, \quad 0 \leqq \varepsilon \leqq \varepsilon_m'$

A – B $\quad \sigma = \dfrac{f_c' - f_c}{(\varepsilon_m' - \varepsilon_m)^3}(\varepsilon - \varepsilon_m)^3 + f_c,$

$\varepsilon_m' \leqq \varepsilon \leqq \varepsilon_m$

B – C $\quad \sigma = \dfrac{f_u - f_c}{\varepsilon_u - \varepsilon_m}(\varepsilon - \varepsilon_m) + f_c, \quad \varepsilon_m < \varepsilon < \varepsilon_u$

$\varepsilon_m' = 2.20 \times 10^{-3}, \quad \varepsilon_u' = 3.50 \times 10^{-3}$

$E_i = 189000 \times \sqrt{f_c'/200} \quad (\mathrm{kgf/cm^2})$

Fig.2-1 Stress – strain model proposed by Fujii et al. [8]

On the other hand, Park et al. [11] proposed the well-known modified Kent & Park model as shown in Fig.2-2. As for the modified Kent & Park model, however, it was reported that this model was not applicable to confined concrete with high-strength hoops because they might not yield even at the maximum stress [12].

Other models considering the strain gradient in cross section [13], cyclic load repetition and strain rate [14] were also proposed in recent years.

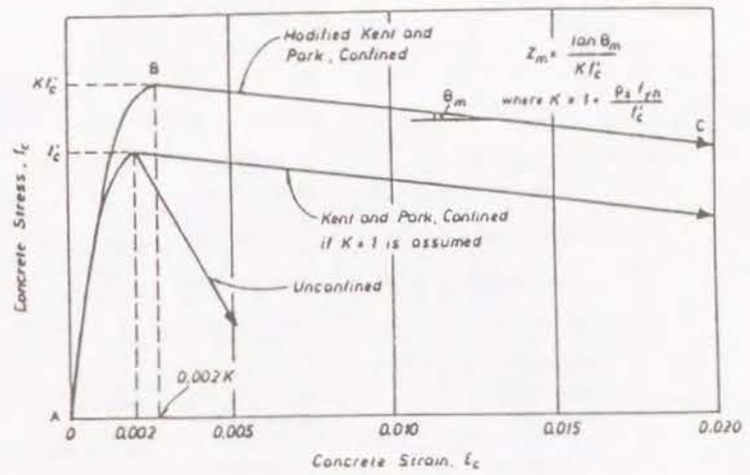

Region AB ($\varepsilon_c < 0.002K$)

$$f_c = Kf'_c\left[\frac{2\varepsilon_c}{0.002K} - \left(\frac{\varepsilon_c}{0.002K}\right)^2\right]$$

Region BC ($\varepsilon_c > 0.002K$)

$$f_c = Kf'_c[1 - Z_m(\varepsilon_c - 0.002K)]$$

$$Z_m = \frac{0.5}{\dfrac{3 + 0.29f'_c}{145f'_c - 1{,}000} + \dfrac{3}{4}\rho_s\sqrt{\dfrac{h''}{s_h}} - 0.002K}$$

$$K = 1 + \frac{\rho_s f_{yh}}{f'_c}$$

Fig.2-2 Modified Kent and Park model [11]

2.3 EXPERIMENTAL PROCEDURES [15]

2.3.1 Specimens

Column specimens having a circular (ϕ15cm) or square (15cm x 15cm) section and length of 30cm were used for uniaxial compressive loading tests. These specimens are shown schematically in Fig.2-3. All these specimens were not provided with axial reinforcement and cover concrete in order to eliminate their effects. Welded circular or square hoops with several kinds of yield strengths and diameters were used as transverse steel for lateral confinement.

2.3.2 Test Variables

The main test variables adopted were as follows.

(1) volumetric ratio of hoops (ρ_s): between 0.62%-4.02%.

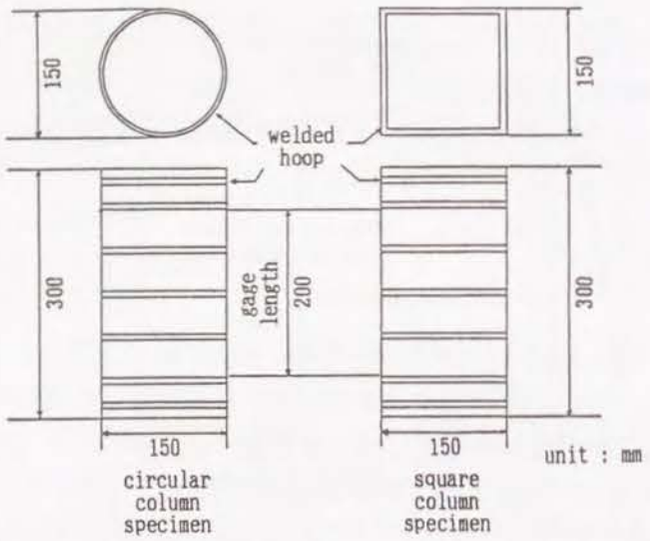

Fig.2-3 Dimensions of column specimens

Table 2-1 Details of test variables

	compressive strength of concrete f'_c (kgf/cm^2)	yield point of hoop f_{syh} (kgf/cm^2)	volmetric ratio of hoop ρ_s (%)	diameter of hoop (mm)	s/D ratio
circular column specimen	300, 500	3280~8630	0.62~4.02	3.5, 6.0	0.086~0.753
square column specimen	300, 500	3280~8630	0.62~2.50	3.5, 6.0	0.180~0.753

(2) yield strength of hoops (f_{syh}): between 3280kgf/cm^2~8630kgf/cm^2.
(3) design compressive strength of concrete (f'_{ck}): 300kgf/cm^2 and 500kgf/cm^2.
(4) spacing of hoops (s/D): between 0.086~0.753, where s: spacing of hoops and D: minimum length of cross section.
(5) shape of cross section: circular and square.

The details of these variables are indicated in Table 2-1.

2.3.3 Loading Method

All specimens were subjected to uniaxial compressive load up to failure.

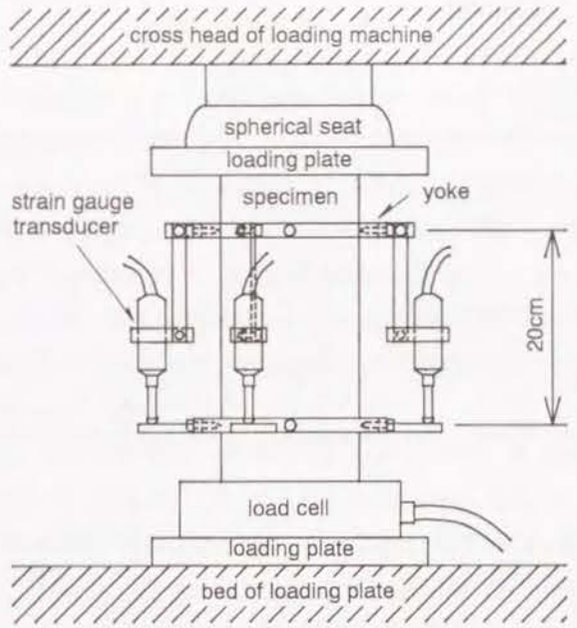

Fig.2-4 Loading and measuring apparatuses

During the loading tests, the longitudinal displacement of the specimen was measured by four displacement transducers arranged on four sides of the specimen together with the applied load. In addition, strains in transverse steels were measured by electric resistance strain gages. These details are shown in Fig.2-4.

2.4 RESULTS OF TESTS AND DISCUSSIONS [15]

As indexes which characterize the stress - strain relationship of confined concrete, f_c/f'_c and $\varepsilon_{co}/\varepsilon_{co}'$ were used in this study. The former shows the ratio of the maximum stress of confined concrete (f_c) to that (f'_c) of plain (unconfined) concrete, and the latter shows the ratio of strain at the maximum stress (ε_{co}) of confined concrete to that (ε_{co}') of plain concrete. The characteristics of stress - strain relationship in the falling branch region can be expressed by a limit strain, for example, the strain at which the stress reduces to 80% of the maximum stress [8 and 10]. However, the gradient of stress degradation in the falling branch region, θ, was used here because a more degraded stress - strain curve should be necessary for the moment - curvature analysis of concrete flexural members well into the inelastic range.

2.4.1 Effects of Test Variables

In Fig.2-5, Fig.2-6 and Fig2-7 are shown the effects of volumetric ratio of transverse hoops on the values of f_c/f'_c, $\varepsilon_{co}/\varepsilon_{co}'$ and θ, respectively. As shown in Fig.2-6 and Fig.2-7, the values of f_c/f'_c and $\varepsilon_{co}/\varepsilon_{co}'$ increase almost linearly with increasing value of ρ_s, although scattering of data is observed in some cases. On the other hand, the value of θ is almost in inverse proportion to ρ_s-value as seen in Fig.2-7. However, the effectiveness of transverse hoops for improving compressive ductility of concrete is more remarkable in circular column specimens than that in square ones.

Fig.2-8, Fig.2-9 and Fig.2-10 show the effects of yield strength of transverse hoops on the values of f_c/f'_c, $\varepsilon_{co}/\varepsilon_{co}'$ and θ, respectively. As seen in Fig.2-8-(a), the value of f_c/f'_c increases with increasing value of f_{syh} although its increasing ratio becomes smaller with increasing value of f_{syh} in case of circular column specimens. In case of square column specimens, the effect of f_{syh} on the value of f_c/f'_c is not remarkably observed as seen in Fig.2-8-(b). On the other hand, the value of $\varepsilon_{co}/\varepsilon_{co}'$ increases with increasing the value of f_{syh}. However, its increasing ratio is larger in circular column specimens than in square ones as seen in Fig.2-9. The value of θ decreases with increasing value of f_{syh} in both cases of circular and square column specimens.

Fig.2-11, Fig.2-12 and Fig.2-13 show the effects of compressive strength of concrete on the values of f_c/f'_c, $\varepsilon_{co}/\varepsilon_{co}'$ and θ, respectively. It can be observed from Fig.2-11 and Fig.2-12 that the values of f_c/f'_c and $\varepsilon_{co}/\varepsilon_{co}'$ tend to decrease with increasing value of f'_c although their decreasing ratio is smaller in case of square column specimens than those in circular ones. On the other hand, the value of θ increases with increase in f'_c.

In Fig.2-14 and Fig.2-15 are shown the effects of s/D ratio on the values of f_c/f'_c and $\varepsilon_{co}/\varepsilon_{co}'$, respectively. From these figures, it can be observed that the values of f_c/f'_c and $\varepsilon_{co}/\varepsilon_{co}'$ decrease with increasing value of s/d when compared at almost the same ρ_s-value.

Based on the above test results and the previous researches [5, 8], the relationships as summarized in Table 2 were obtained between these indexes and test variables.

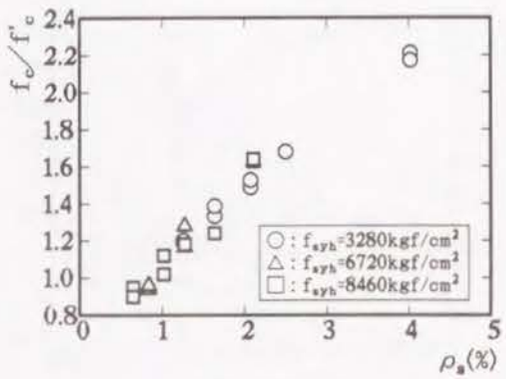

(a) circular column specimens (f'_{ck}=300kgf/cm²)

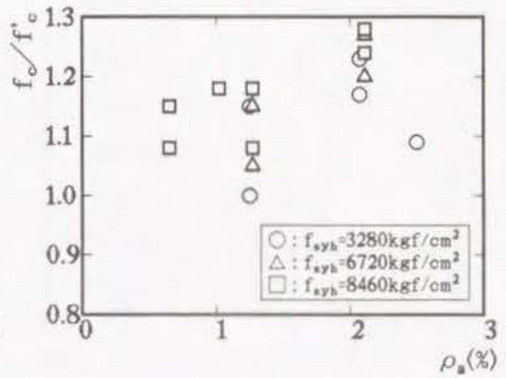

(b) square column specimens (f'_{ck}=300kgf/cm²)

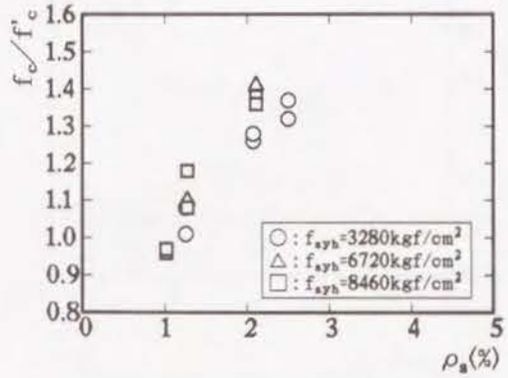

(c) circular column specimens (f'_{ck}=500kgf/cm²)

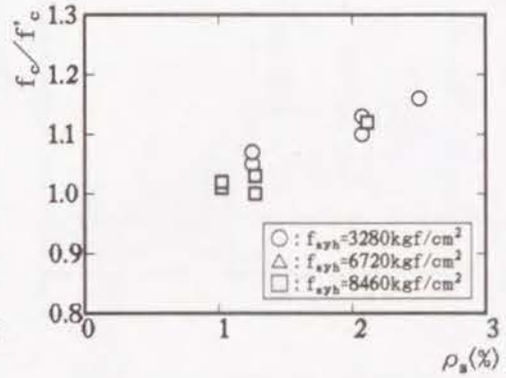

(d) square column specimens (f'_{ck}=500kgf/cm²)

Fig.2-5 Effects of volumetric ratio of hoops on f_c/f'_c-value

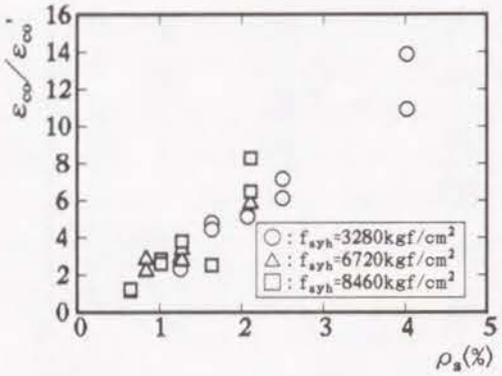

(a) circular column specimens
(f'_{ck}=300kgf/cm²)

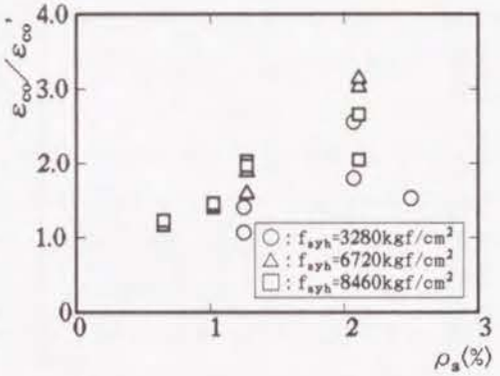

(b) square column specimens
(f'_{ck}=300kgf/cm²)

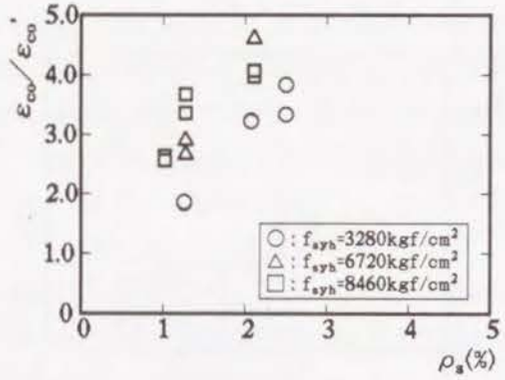

(c) circular column specimens
(f'_{ck}=500kgf/cm²)

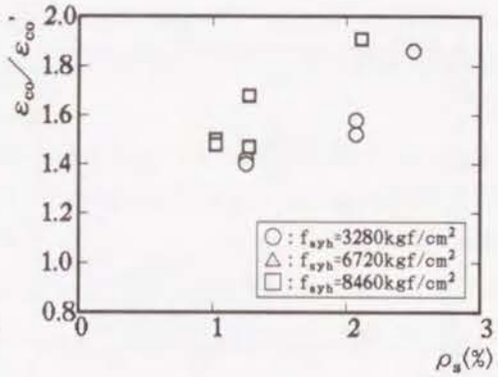

(d) square column specimens
(f'_{ck}=500kgf/cm²)

Fig.2-6 Effects of volumetric ratio of hoops on $\varepsilon_{co}/\varepsilon_{co}'$-value

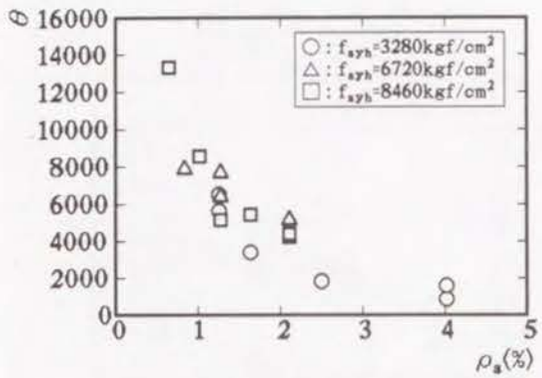

(a) circular column specimens
(f'_{ck}=300kgf/cm²)

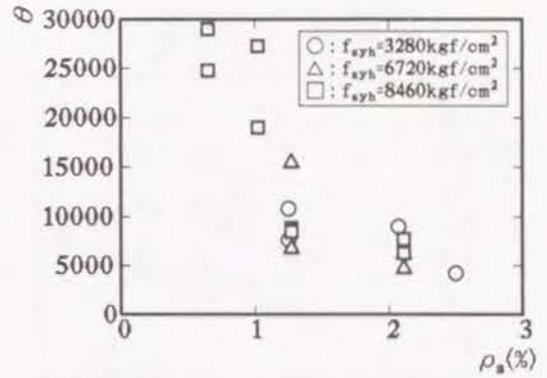

(b) square column specimens
(f'_{ck}=300kgf/cm²)

Fig.2-7 Effects of volumetric ratio of hoops on θ-value

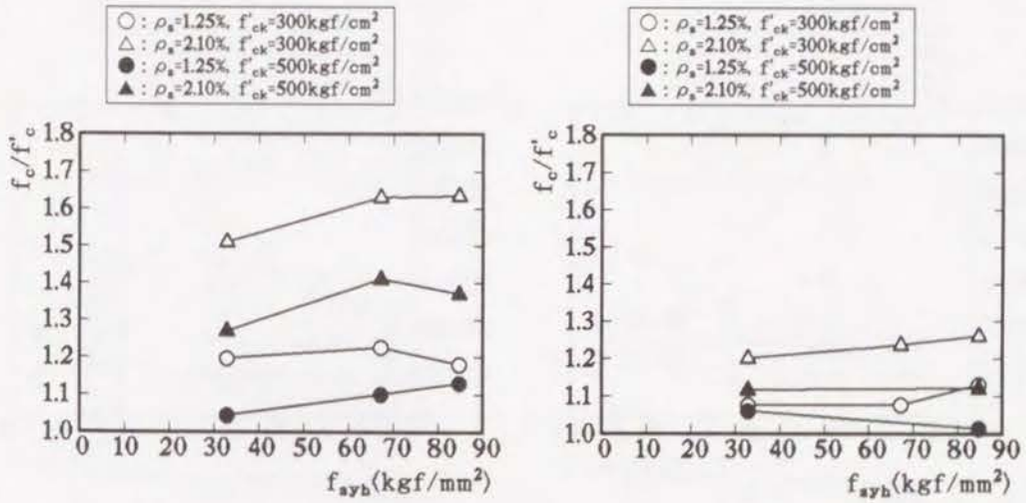

(a) circular column specimens (b) square column specimens

Fig.2-8 Effects of yield strength of hoops on f_c/f'_c-value

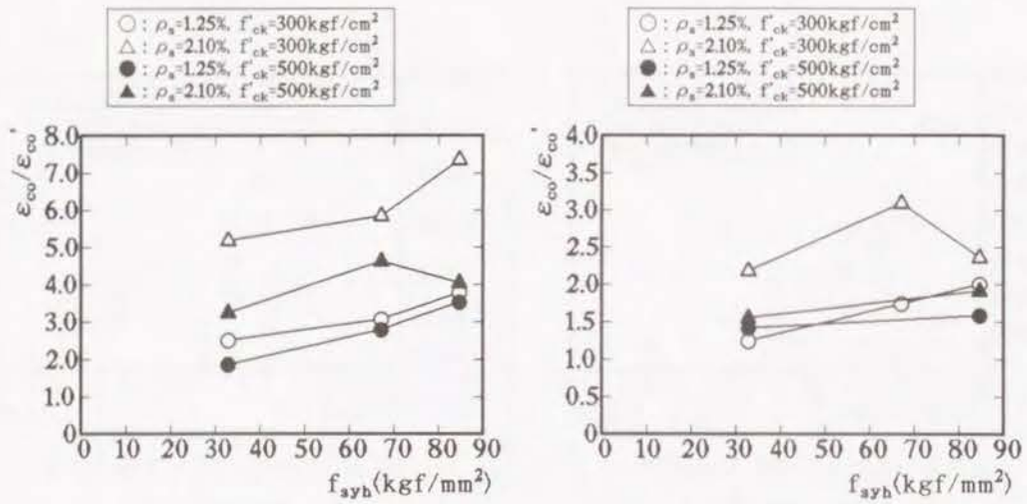

(a) circular column specimens (b) square column specimens

Fig.2-9 Effects of yield strength of hoops on $\varepsilon_{co}/\varepsilon_{co}'$-value

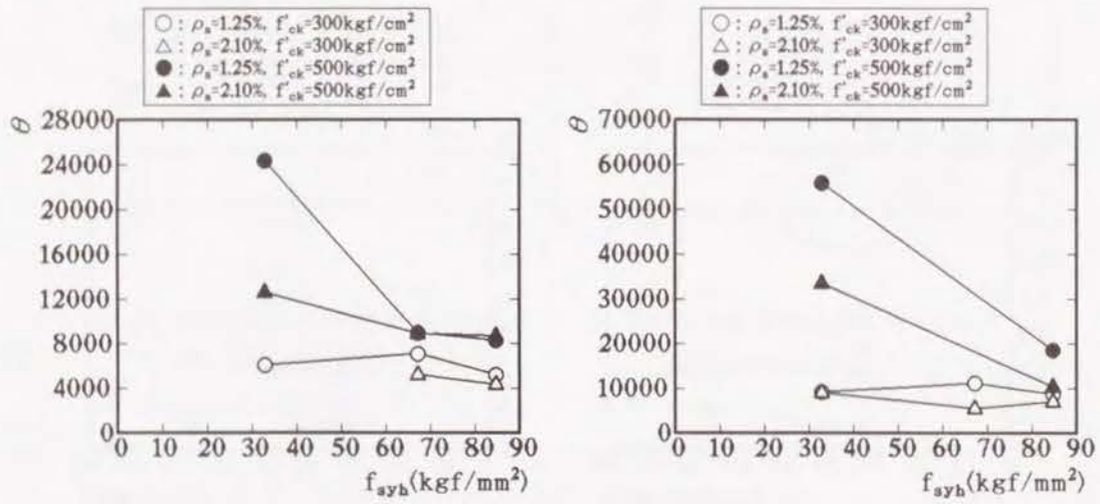

(a) circular column specimens (b) square column specimens

Fig.2-10 Effects of yield strength of hoops on θ-value

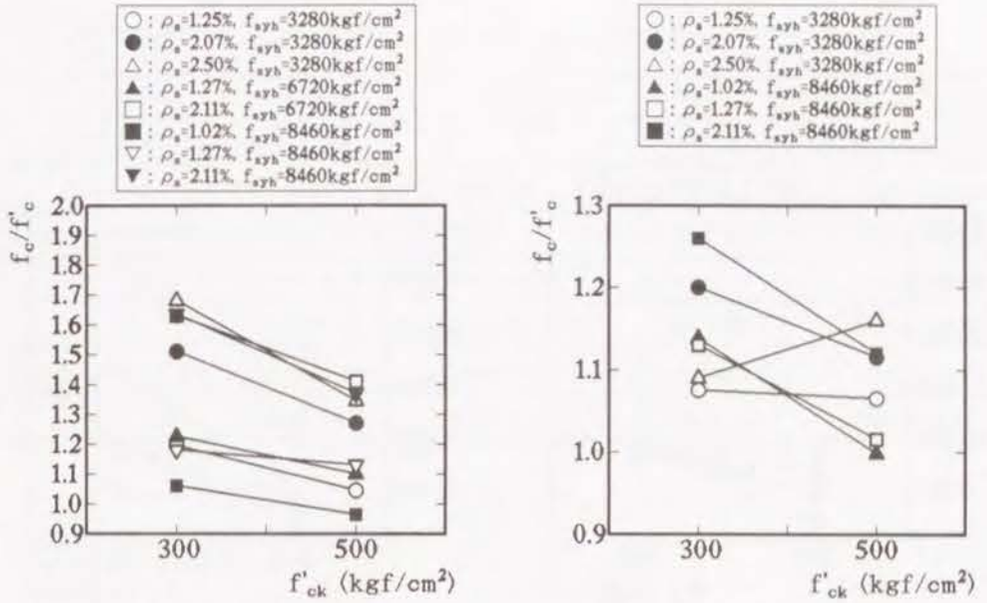

(a) circular column specimens (b) square column specimens

Fig.2-11 Effects of compressive strength of concrete on f_c/f'_c-value

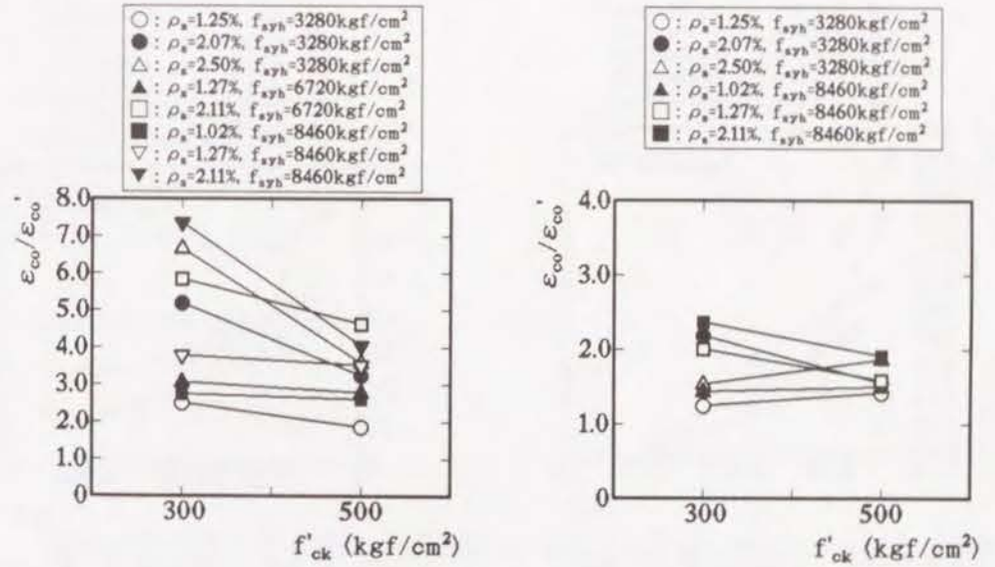

(a) circular column specimens (b) square column specimens

Fig.2-12 Effects of compressive strength of concrete on $\varepsilon_{co}/\varepsilon_{co}'$-value

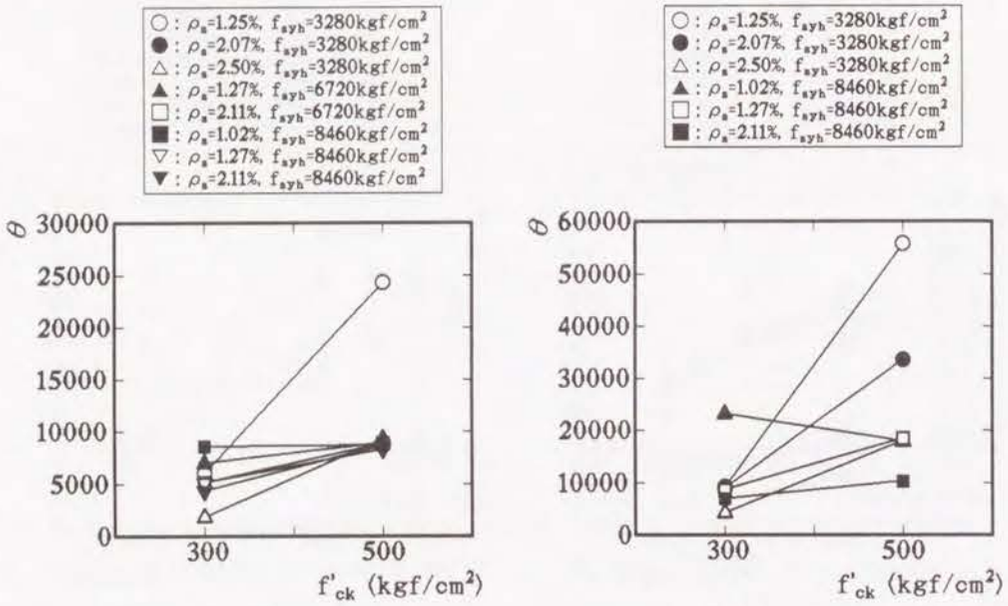

(a) circular column specimens　　(b) square column specimens

Fig.2–13　Effects of compressive strength of concrete on θ–value

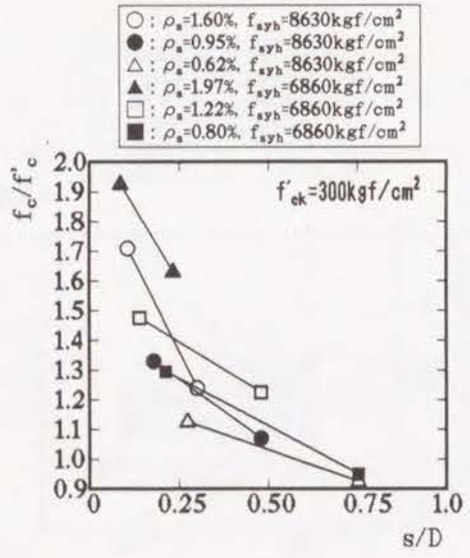

Fig.2–14　Effects of s/D ratio on f_c/f'_c–value (circular column specimens)

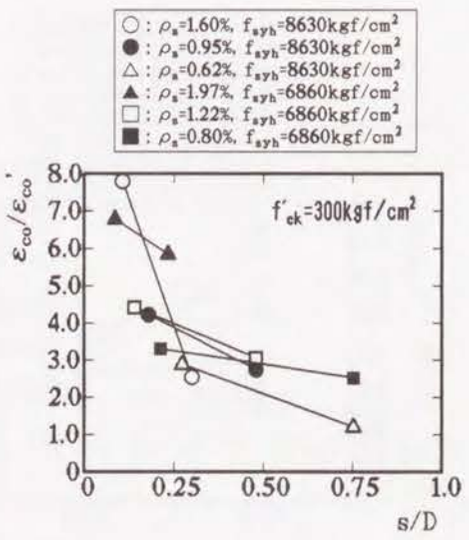

Fig.2–15　Effects of s/D ratio on $\varepsilon_{co}/\varepsilon_{co}'$–value (circular column specimens)

Table 2–2　Relationships between each index and test variable

		volumetric ratio of hoop ρ_s	yield point of hoop f_{syh}	comp. strength of concrete f'_c	s/D ratio
circular column specimen	f_c/f'_c	linear to ρ_s	linear to $\sqrt{f_{syh}}$	inverse to f'_c	linear to s/D
	$\varepsilon_{co}/\varepsilon_{co}'$	linear to ρ_s	linear to f_{syh}	inverse to f'^2_c	linear to s/D
	θ	inverse to ρ_s	inverse to f_{syh}	linear to f'^2_c	no relation
square column specimen	f_c/f'_c	linear to ρ_s	no relation	no relation	linear to s/D
	$\varepsilon_{co}/\varepsilon_{co}'$	linear to ρ_s	linear to $\sqrt{f_{syh}}$	inverse to f'^2_c	linear to s/D
	θ	inverse to ρ_s	inverse to f_{syh}	linear to f'^2_c	no relation

2.4.2 Confining Coefficients

As the indexes representing confining effects, the concept of "confining coefficients" [5, 8 and 10] were applied to the test results. That is, confining coefficients C_{cf}, $C_{c\varepsilon m}$ and C_{θ} for the maximum stress, the strain at the maximum stress and the stress degradation gradient, respectively, which indicate the effectiveness of confinement quantitatively, were determined as follows based on Table 2–2.

For circular column specimens,

$$C_{cf}=\rho_s[1-s/(k_1D)]\sqrt{f_{syh}}/f'_c \quad (2-3)$$

$$C_{c\varepsilon m}=\rho_s[1-s/(k_2D)]f_{syh}/(f'_c)^2 \quad (2-4)$$

$$C_{\theta}=(f'_c)^2/(\rho_s f_{syh}) \quad (2-5)$$

For square column specimens,

$$C_{cf}=\rho_s(1-s/D) \quad (2-6)$$

$$C_{c\varepsilon m}=\rho_s(1-s/D)\sqrt{f_{syh}}/(f'_c)^2 \quad (2-7)$$

$$C_{\theta}=(f'_c)^2/(\rho_s f_{syh}) \quad (2-8)$$

The parameters k_1 and k_2 in Eq.(2–3) and Eq.(2–4), respectively, indicate the maximum limit values of s/D ratio over which the effectiveness of confinement cannot be obtained. As far as these tests are concerned, k_1 and k_2 were found to be 0.51 and 0.95 respectively, although k_1=0.80 and k_2=1.70 in Ref. [8].

Fig.2–16 and Fig.2–17 show the relationships between f_c/f'_c, $\varepsilon_{co}/\varepsilon_{co}'$, θ and

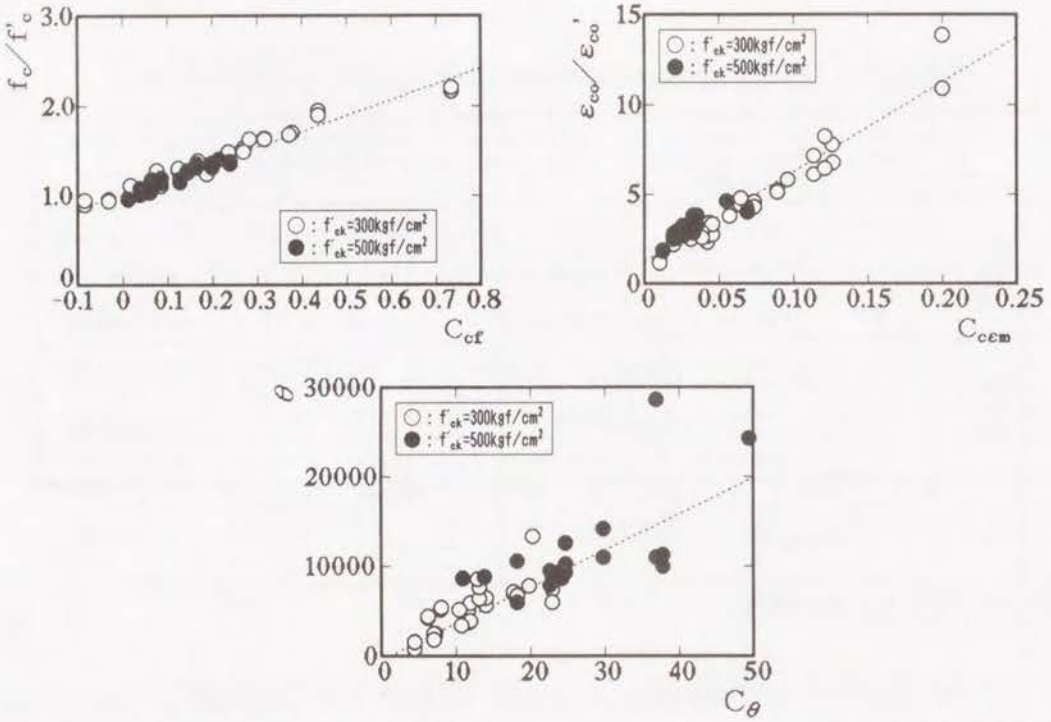

Fig.2–16 Relationship between f_c/f'_c, $\varepsilon_{co}/\varepsilon_{co}'$, θ and each confining coefficient (circular column specimens)

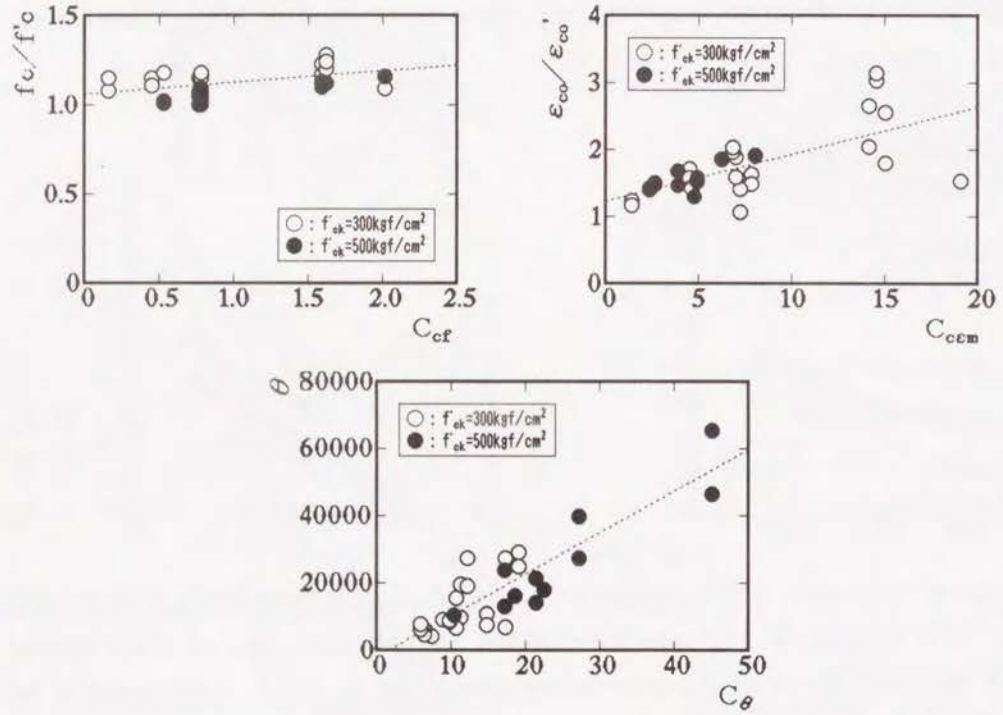

Fig.2–17 Relationship between f_c/f'_c, $\varepsilon_{co}/\varepsilon_{co}'$, θ and each confining coefficient (square column specimens)

each confining coefficient for circular and square column specimens, respectively. As indicated in these figures, each index can be expressed almost by a linear function of each confining coefficient. The details of these equations are as follows.

For circular column specimens,

$$f_c/f'_c=1.75C_{cf}+1.02 \quad (2\text{–}9)$$

$$\varepsilon_{co}/\varepsilon_{co}'=50.0C_{c\varepsilon m}+1.25 \quad (2\text{–}10)$$

$$\theta=406C_\theta-507 \quad (2\text{–}11)$$

For square column specimens,

$$f_c/f'_c=0.065C_{cf}+1.06 \quad (2\text{–}12)$$

$$\varepsilon_{co}/\varepsilon_{co}'=709C_{c\varepsilon m}+1.22 \quad (2\text{–}13)$$

$$\theta=1234C_\theta-2140 \quad (2\text{–}14)$$

2.4.3 A New Stress – Strain Model for Confined Concrete

From the previous mentioned results, a new stress – strain model for confined concrete as shown in Fig.2–18 is proposed.

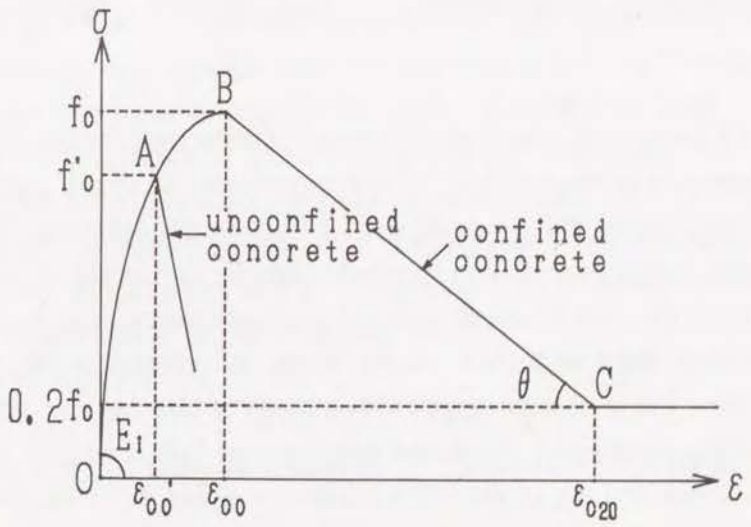

Fig.2–18 Proposed stress – strain model

The details are as follows.

(1) Region O–A ($0 \leq \varepsilon \leq \varepsilon_{co}'$):

$$\sigma = E_i \varepsilon + \frac{f_c' - E_i \varepsilon_{co}'}{(\varepsilon_{co}')^2} \varepsilon^2 \qquad (2\text{–}15)$$

(2) Region A–B ($\varepsilon_{co}' < \varepsilon \leq \varepsilon_{co}$):

$$\sigma = f_c + \frac{(\varepsilon - \varepsilon_{co})^3}{(\varepsilon_{co}' - \varepsilon_{co})^3} (f_c' - f_c) \qquad (2\text{–}16)$$

(3) Region B–C ($\varepsilon_{co} < \varepsilon \leq \varepsilon_{c20}$):

$$\sigma = f_c - \theta(\varepsilon - \varepsilon_{co}) \qquad (2\text{–}17)$$

(4) Region C– ($\varepsilon_{c20} < \varepsilon$):

$$\sigma = 0.2 f_c \qquad (2\text{–}18)$$

Where, $\varepsilon_{co}' = 2.20 \times 10^{-3}$ and $E_i = 189000 \times \sqrt{f_c'/200}$ (kgf/cm^2) in accordance with Ref. [8].

Fig.2–19 compares the proposed model, the model proposed by Fujii et al. [8] and modified Kent & Park model [11] with the measured stress – strain curves.

It is clearly shown that modified Kent & Park model estimates the maximum stress of square column specimens somewhat largely and tends to underestimate the strain at the maximum stress of both circular and square column specimens. In addition, modified Kent and Park model tends to underestimate the strength degradation after the maximum stress in both case of circular and square column specimen. On the other hand, the model proposed by Fujii et al. can estimate well the maximum stress and the strain at the maximum stress, but it cannot express the stress – strain relationship well into the falling branch region. Compared with these two models, the proposed model can express well the stress – strain relationship of confined concrete including the stress degradation branch.

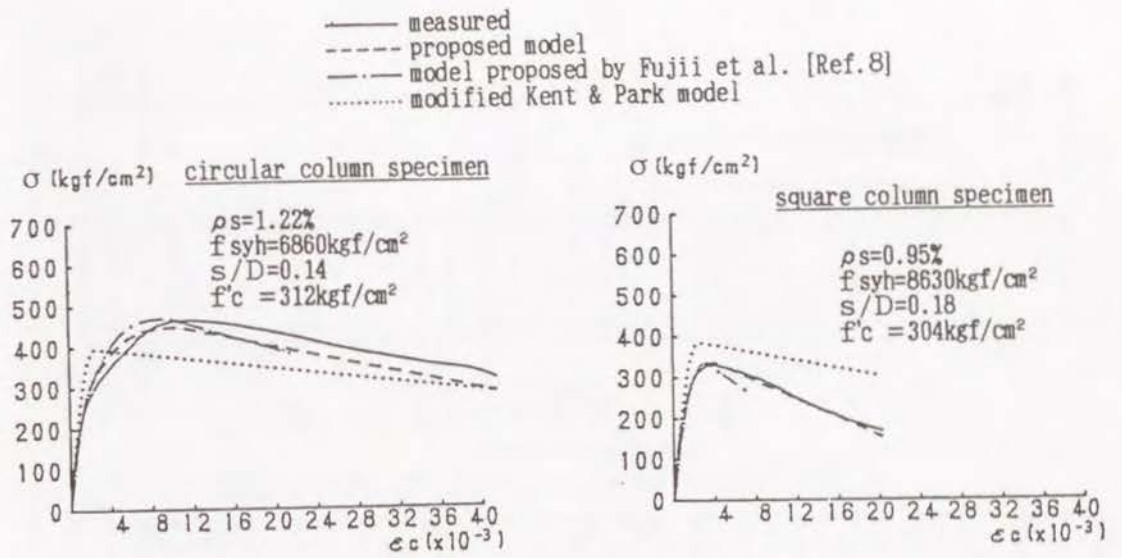

Fig.2–19 Measured and calculated stress – strain curves

2.5 VERIFICATION OF THE PROPOSED STRESS – STRAIN MODEL [15, 16]

2.5.1 Beam Specimens

Verification of the proposed stress – strain model for confined concrete was done by the analysis of moment – curvature (M – ϕ) relationship of reinforced, partially prestressed and prestressed concrete beams [12, 17]. The specimens used for the analysis had a rectangular cross section of width x full depth = 10 x 20 cm and total length of 160 cm as shown in Fig.2–20. These specimens had several volumetric ratios of transverse hoops and steel index, and were tested under symmetrical two–point loads (shear span length: 60cm, flexural span length: 20cm). ϕ6mm hoops with the same quality as used in the column specimens were used for lateral confinement (50cm region over mid–span).

2.5.2 Procedure of the Analysis of Moment – Curvature Relationship

Theoretical moment – curvature analysis on the above specimens was done by well–known iterative method based on compatibility of strains and equilibrium of forces. In the calculation of M–ϕ relationship, stress – strain models for reinforcing

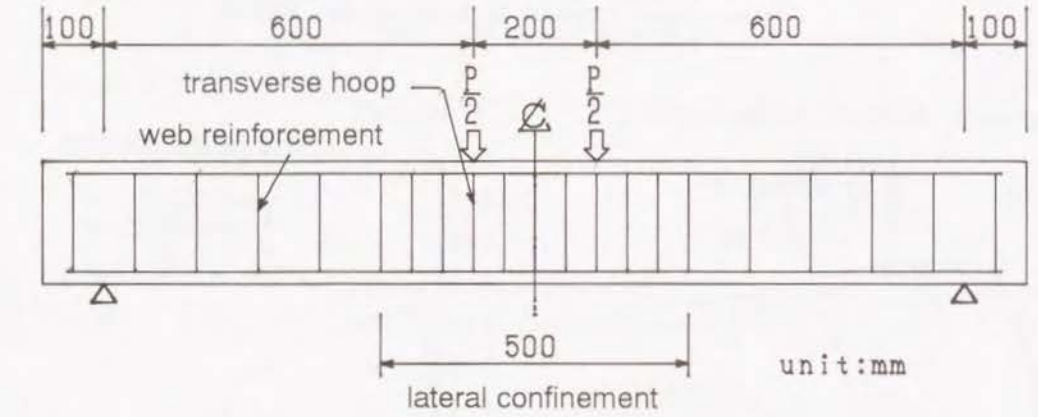

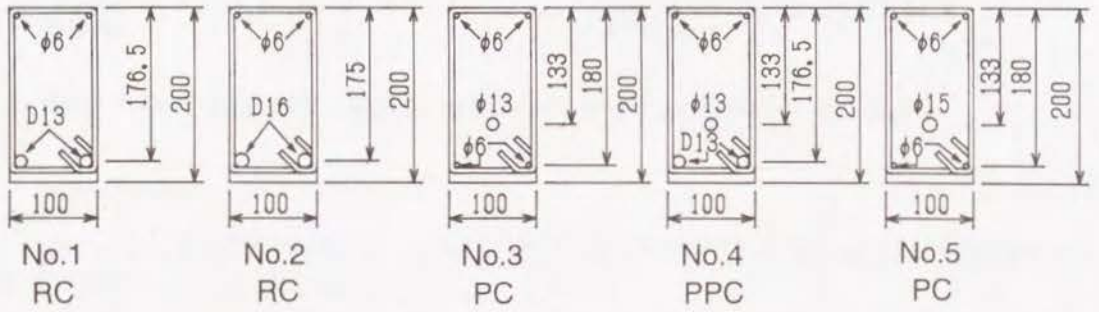

Fig.2-20 Dimensions of beam specimens

steel and prestressing steel are necessary in addition to the stress - strain model for confined concrete. As the stress - strain model for reinforcing steel, tri-linear type model as shown in Fig.2-21 were used, in which the strain at the onset of strain hardening (ε_{sh}) was determined as 5 times of that at the yielding (ε_{sy}) according to the results of tensile tests. As the model for prestressing steel, on the other hand, the model proposed by Blakeley et al. [18] as shown in Fig.2-22 was used.

When applying stress - strain model for confined concrete, which is obtained from uniaxial tests, to M - ϕ analysis of flexural members, the effect of strain gradient in section has been sometimes discussed [13]. The strain at the maximum stress of plain concrete under uniaxial compression is at most 0.002, while that under flexural compression becomes approximately 0.0035. JSCE also uses this value as the limit strain of concrete when examining ultimate limit state of sectional failure of members subjected to flexural moment or flexure and axial forces [19]. Considering these facts, the modified proposed model as shown in Fig.2-23, in

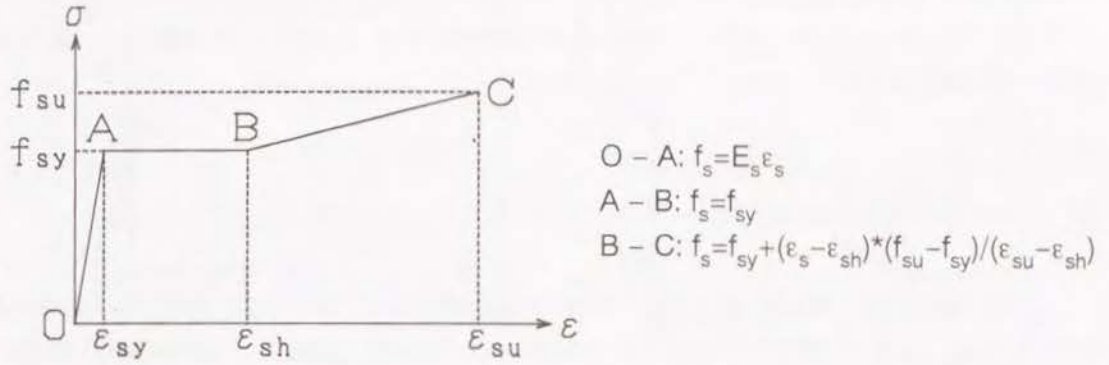

Fig.2-21 Stress - strain model for reinforcing steel

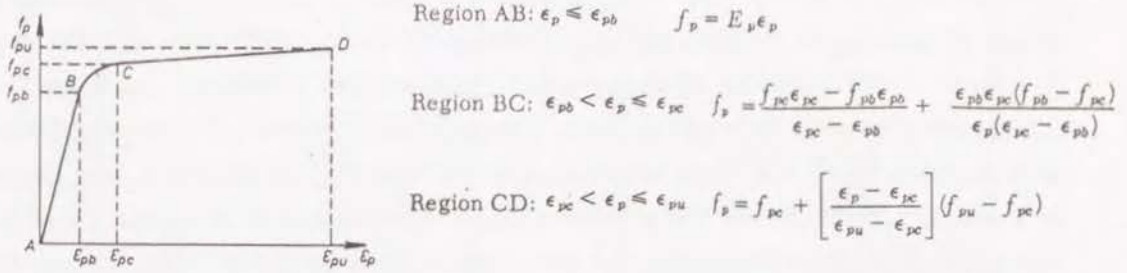

Fig.2-22 Stress - strain model for prestressing steel [18]

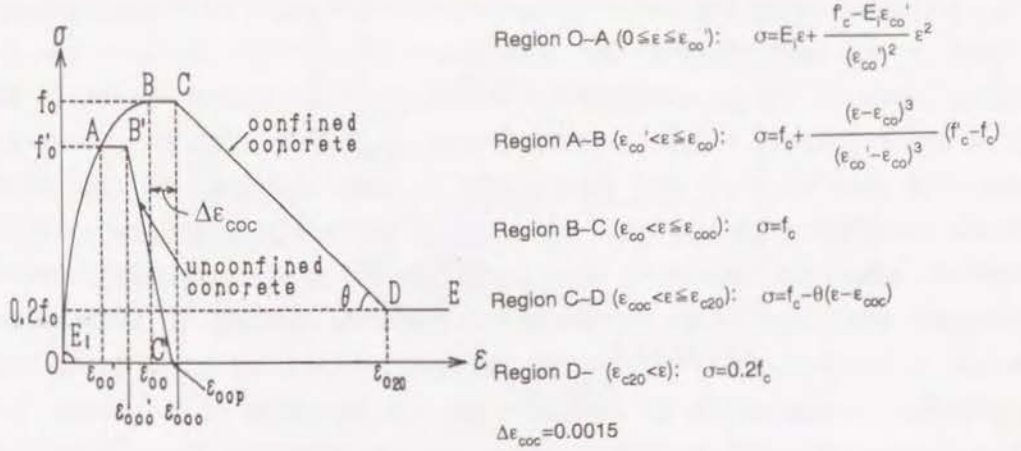

Fig.2-23 Modified proposed model considering strain gradient in section

which the length of strength holding region after reaching the maximum stress (B–C in Fig.2–23) is set as 0.0015, was also used in the analysis in addition to the modified Kent & Park model for comparison.

2.5.3 Results and Discussions

In Fig.2–24 are shown the measured moment – curvature curves together with the calculated ones using the proposed model, modified proposed model considering strain gradient and modified Kent & Park model.

In case of the beams with the value of longitudinal steel index (q) less than 0.218, the calculated curves by using each model are scarcely different from one another and coincided well with the measured one. This is mainly because the value of steel index is relatively small and therefore the contribution of concrete to the beam ductility may be relatively small. In case of the beam with the q–value of 0.288, the difference between the calculated curve obtained by the proposed model and those by using the other two models becomes larger. In this case, the moment in the calculated curve by the proposed model commences to decrease at smaller curvature compared with that in the calculated curves using the other two models, although the calculated curve by using the proposed model could represent best the measured one. In case of the beams with large steel indexes of q=0.380 and 0.388, on the other hand, the difference between the calculated curve by using the modified proposed model and that by using modified Kent and Park model becomes significant. In this case, modified Kent and Park model seems to estimate well the measured curve until larger curvature levels than the proposed model even if the effect of strain gradient was considered. These results, however, do not always indicate that modified Kent and Park model is most suitable. As mentioned previously, modified Kent and Park model tends to underestimate the strength degradation after the maximum stress of column specimen under uniaxial compression, and it can be supposed that this tendency resulted in rather better agreement in the analysis. In addition, the calculated curve even by using modified Kent and Park model tends to underestimate the curvature of the beam with q=0.380 at which the load carrying capacity begins to decrease. Considering that the measured curve is also dependent on the size of the specimen and some other restraining effects, for examples, restraining action of beam deformation at the supports and strain gradient in the longitudinal direction of the beam, it is impossible

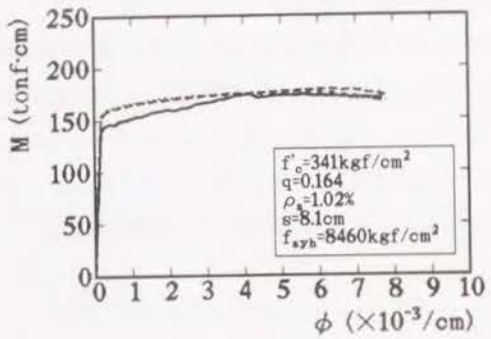

(a) No.1

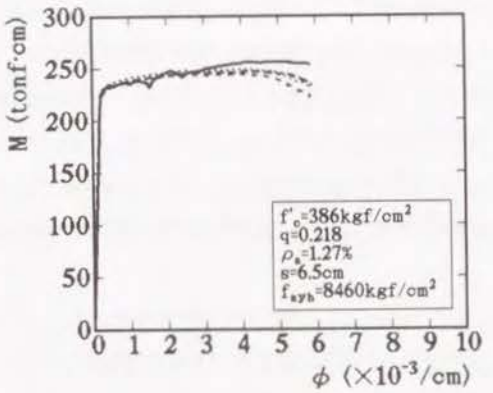

(b) No.2

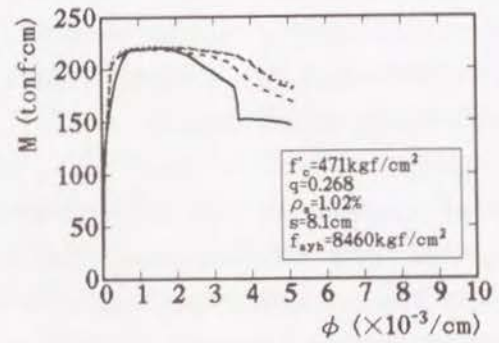

(c) No.3

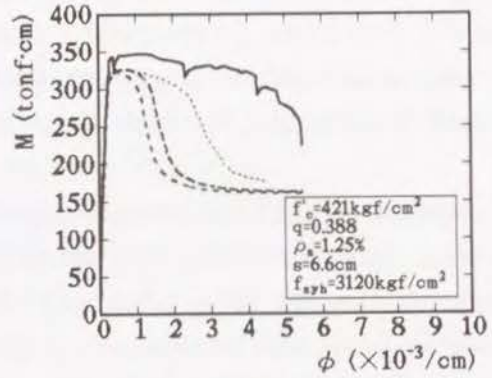

(d) No.4

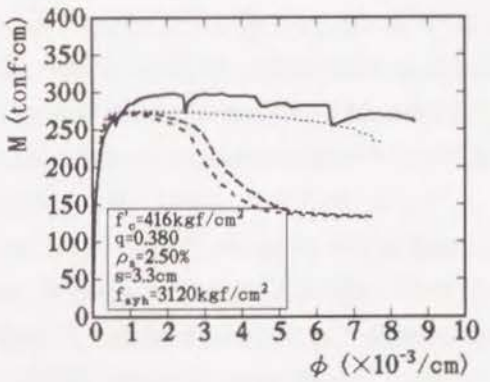

(e) No.5

——— : measured
····· : calculated by modified Kent & Park model
– – – – : calculated by proposed model
–·–·– : calculated by proposed model (considering strain gradient)

Fig.2–24 Comparison between the measured and calcurated M – φ curves

to determine the most suitable model only from these results.

Form the results of theoretical moment – curvature analysis of flexural members, the proposed stress – strain model for confined concrete is reasonable for the beams with q=0.168–0.268, which is within the range of the q–values of ordinary flexural members. However, further investigations into the effects of other factors, especially the effect of strain gradient in section, should be necessary.

2.6 CONCLUSIONS OF CHAPTER 2

In this chapter, fundamental properties of laterally confined concrete are investigated by uniaxial loading tests on circular and square column specimens. From the test results, a new stress – strain model for laterally confined concrete is proposed and its applicability to theoretical moment – curvature analysis of flexural members is discussed. The main conclusions obtained are as follows.

(1) Improvement of compression ductility of concrete by lateral confinement becomes more remarkable with increasing volumetric ratio of hoops, and with decreasing strength of concrete and s/D ratio. The increase in yield strength on transverse hoop also improves the compression ductility. However, its improving effect is relatively small compared with those of volumetric ratio of hoops, compressive strength of concrete and s/D ratio. These improving effects are more remarkably observed in circular column specimens than in square column ones.

(2) As the indexes which characterize the stress – strain relationship of concrete, the ratio of the maximum stress of confined concrete to that of unconfined concrete (f_c/f'_c), the ratio of the strain at the maximum stress of confined concrete to that of unconfined concrete ($\varepsilon_{co}/\varepsilon_{co}'$) and the stress degradation gradient after the maximum stress (θ) are used in this chapter. These indexes correlate well with each corresponding confining coefficient, which is defined considering the effects of test variables, and can be represented by a linear function of each confining coefficient.

(3) A new stress – strain model for laterally confined concrete, which considers the stress degradation after the maximum stress well into a large deformation, is proposed based on the above mentioned indexes and corresponding confining coefficients.

(4) Moment – curvature relationship of ordinary under–reinforced flexural members with steel index of less than 0.3 can be well estimated by using the proposed stress – strain model. As for the applicability to over–reinforced sections with steel index of more than 0.3, on the other hand, further investigations are necessary in addition to the effects of strain gradient in section.

REFERENCES OF CHAPTER 2

1) Park, R. and Paulay, T., "Reinforced Concrete Structures," John Wiley & Sons, 1975.
2) Suzuki, K., Nakatsuka, T. and Yoshida, H., "Strength and Deformation Characteristics of Confined Concrete with Circular Reinforcement," Journal of the Society of Materials Science, Japan, Vol.34, No.376, pp.33–39, 1985. [in Japanese]
3) Muguruma, H., Watanabe, F., Tanaka, H., Sakurai, K. and Nakamura, H., "Effect of Confinement by High Yield Strength Hoop Reinforcement," Proc. of CAJ, No.32, pp.444–448, 1978. [in Japanese]
4) Muguruma, H., Watanabe, F., Tanaka, H., Sakurai, K. and Nakamura, E., "Effect of Confinement by High Yield Strength Hoop Reinforcement upon the Compressive Ductility of Concrete," Proc. of the 22th Japan Congress on Materials Research, pp.377–382, 1979.
5) Muguruma, H., Watanabe, F., Iwashimizu, T. and Mitsueda, R., "Ductility Improvement of High Strength Concrete by Lateral Confinement," Transactions of the JCI, Vol.5, pp.403–410, 1983.
6) Hisatoku, T., Kato, Y., Segawa, T.,Ide, K., Sumi, A., Usui, S. and Yamada, M., "Experimental Studies on RC Columns Confined by High Strength Hoops and Case Study for the Design of High–Rise Building," GBRC, Vol.44, pp.6–18, 1986. [in Japanese]
7) Sugano, S., Nagashima, T., Kimura, H. and Tamura, A., "Experimental Studies on Seismic Behavior of High Strength Concrete Columns Laterally Reinforced with High Strength Steel Bars," Takenaka Technical Research Report, No.38, pp.35–53, 1987. [in Japanese]
8) Fujii, M., Miyamoto, A., Hiraoka, Y. and Ohyama, H., "Practical Formulation of Stress – Strain Curve of Confined Concrete," Review of the 40th General Meeting of CAJ, pp.226–229, 1986.
9) Iyengar, K. T. S., "Stress – Strain Characteristics of Concrete Confined in Steel Binders," Magazine of Concrete Research, Vol.22, No.72, pp.173–184,

1970.
10) Muguruma, H., Watanabe, F., Katsuta, S. and Tanaka, H., "Modeling of Stress – Strain Curve for Confined Concrete," Proc. of CAJ, No.34, pp.429–432, 1980. [in Japanese]
11) Park, R., Priestley, M. J. N. and Gill, W. D., "Ductility of Square–Confined Concrete Columns," Journal of the Structural Division, ASCE, Vol.108, No.ST–4, pp.929–950, 1982.
12) Matsumoto, T., "Stress – Strain Model for Confined Concrete and Its Application to Reinforced Concrete Beams," Master Thesis of Kyoto University, 1988. [in Japanese]
13) Sheikh, S. A., "Confined Concrete Subjected to Axial and Bending Loads," Proc. of the 8th World Conference on Earthquake Engineering, Vol.V, pp.869–876, 1984.
14) Mander, J. B., Priestley, M. J. N. and Park, R. "Theoretical Stress – Strain Model for Confined Concrete," Journal of Structural Engineering, ASCE, Vol.114, No.8, pp.1804–1823, 1988.
15) Fujii, M., Kobayashi, K., Miyagawa, T., Inoue, S. and Matsumoto, T., "Investigation on Application of Stress – Strain Relationship of Laterally Confined Concrete," Review of the 42nd General Meeting of CAJ, pp.246–249, 1988.
16) Inoue, S., Hattori, A., Miyagawa, T., Fujii, M. and Kobayashi, K., "Application of Rectangular Hoop as Lateral Confinement for Concrete Beam Members," CAJ Proceedings of Cement & Concrete, No.43, pp.340–340, 1989.
17) Hattori, A., "Fundamental Studies on the Application of Lateral Confinement to Concrete Beam Members," Graduation Thesis of Kyoto University, 1989. [in Japanese]
18) Blakeley, R. W. G. and Park, R., "Prestressed Concrete Sections with Cyclic Flexure," Journal of the Structural Division, ASCE, Vol.99, No.ST8, pp.1717–1742, 1973.
19) Japan Society of Civil Engineers, "Standard Specification for Design and Construction of Concrete Structures," Part 1 [Design], 1986.

CHAPTER 3

BUCKLING OF LONGITUDINAL BARS IN CONFINED CONCRETE

3.1 GENERAL REMARKS

As indicated in Chapter 2, compressive ductility of concrete can be improved significantly by lateral confinement using transverse steels such as hoops or spirals. Many research works have been done on the improvement of inelastic deformation properties of reinforced concrete (RC) members by using confined concrete. However, some of them indicated that buckling of longitudinal bars must occur in RC members at the ultimate state even if they are provided with an adequate amount of lateral confinement. Although buckling of longitudinal bars is supposed to be one of important factors which determine the ultimate state of RC members, only a few research works had dealt with buckling of longitudinal bars in confined concrete. This is mainly due to the fact that the criterion of the buckling initiation of longitudinal bars has not been strictly defined. Therefore, it is necessary to establish the effective method to determine the buckling initiation point of longitudinal bars in RC members in addition to investigating the influences of various factors on the strain of longitudinal bar at buckling.

In this chapter, investigation is done on the effective methods which determine the strain at buckling initiation of longitudinal bars in RC column specimens and their applicability is discussed. In addition, the influences of spacing of hoops, diameter of longitudinal bars, cover thickness for hoops and number of intervals having the specified length on the determined strain at buckling are also discussed.

3.2 REVIEW OF PREVIOUS RESEARCH WORKS

3.2.1 Judging Methods for Buckling Initiation

When discussing the buckling of longitudinal bars in RC members, the first important problem is how to determine the buckling initiation point. Up to now,

however, a unified method has not been established for determining the buckling initiation point and only a few research works [1–5] were reported.

Suzuki et al. [1] proposed a method for judging buckling initiation point based on the idea that the largest effect of the buckling of longitudinal bars on RC members was the reduction in load carrying capacity. In this method, the following characteristic points exhibited on the load – longitudinal strain curve of RC column specimens, confined concrete and longitudinal bar were used for judgment.

(1) Maximum load point in load – longitudinal strain curve of RC column specimens in case that the absolute value of strength reducing gradient in confined concrete is smaller than the strength increasing gradient of longitudinal bar in strain hardening region (point (i) in Fig.3–1).

(2) Point at which load carrying capacity commences to decrease remarkably in load – longitudinal strain curve of RC column specimens in case that the absolute value of strength reducing gradient in confined concrete is larger than the strength increasing gradient of longitudinal bar in strain hardening region (point (ii) in Fig.3–1).

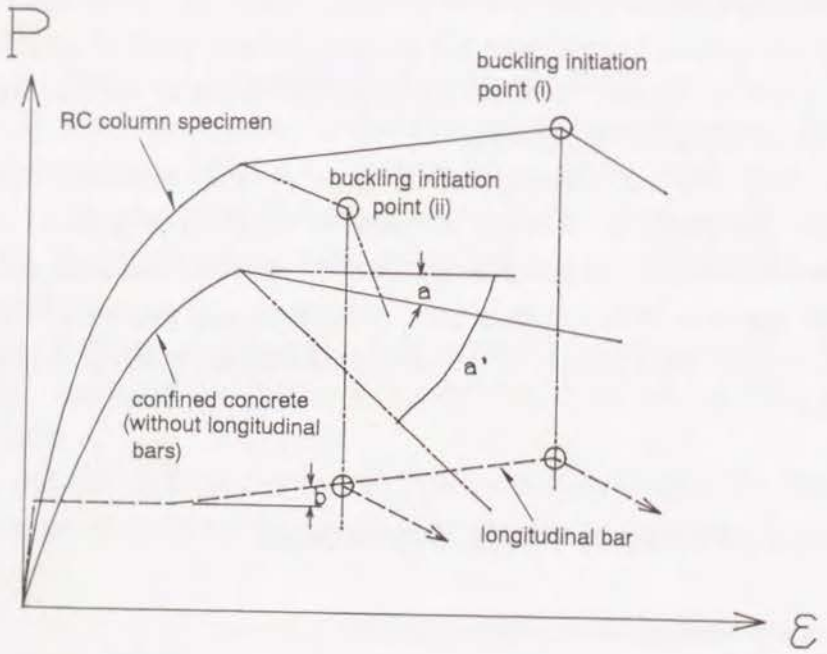

Fig.3–1 Definition of buckling initiation proposed by Suzuki et al. [1]

The point at which the ratio of increase in lateral displacement of longitudinal bar to increase in longitudinal strain ($\Delta\delta_H/\Delta\varepsilon$) turns to be positive in $\Delta\delta_H/\Delta\varepsilon$ – longitudinal strain curve was also added to the characteristic point for judging the buckling initiation [2].

Koyanagi et al. [3] also proposed a method based on transformation point appearing in the strength descending branch in load – displacement curves of RC column specimens.

Another method based on the sudden change in the readings of strain gauges attached so as to face each other on the surface of longitudinal bars was also proposed by Maruyama et al. [4].

The reviewing research of these proposed methods by Yoshida et al. [5] indicated that the strain at buckling initiation obtained by the method proposed by Suzuki et al. was approximately 40% of that by the method proposed by Koyanagi et al.

3.2.2 Buckling of Longitudinal Bar in RC Columns and Beams

Gosain et al. [6] indicated that two buckling mode shapes of longitudinal bar in RC flexural members as schematically shown in Fig.3–2 could be assumed if the slope was considered to be zero at both ends of each span between stirrups. The resulting effective buckling length, assuming no end translation was one–half the stirrup interval (Fig.3–2–(a)), while equal to one stirrup interval considering end translation (Fig.3–2–(b)). It was also indicated that the actual effective length factor ($k=l_k/s$, l_k: buckling length, s: interval of stirrups) fell somewhere between 0.5–1.0.

On the other hand, Scribner et al. [7] indicated that the buckling of longitudinal bar could occur not only within single stirrup interval (Fig.3–2) but also over a length greater than one stirrup interval as schematically shown in Fig.3–3. He also recommended that lateral ties with diameters at least half as large as the diameter of longitudinal bar should be used in RC members subjected to inelastic cyclic flexure. However, even very large ties could not guarantee that longitudinal bars would not buckle under inelastic cyclic flexure.

Suzuki et al. [1] reported the effects of spacing of transverse hoops in RC circular column specimens. They indicated that the limit value of the spacing of hoops, for which buckling occurs within single hoop interval, was approximately 0.7D (D: diameter of cross section of specimen) and that buckling could occur over

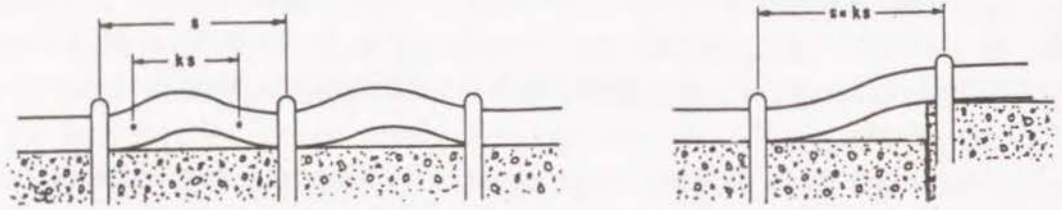

(a) no translation, k=1/2　　(b) with translation, k=1

Fig.3-2　Buckling mode shapes [6]

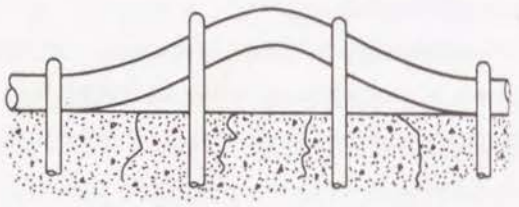

Fig.3-3　Buckling mode spanning three tie intervals [7]

a length greater than one hoop interval in case of s≤0.7D.

Maruyama et al. [4] investigated the effects of the arrangement details of longitudinal bars and transverse hoops on the buckling of longitudinal bars in RC members, and reported that the degree of influence on buckling of longitudinal bar became larger in the order of (spacing of hoops) ≧(diameter of longitudinal bar) ≧(diameter of hoop) ≧(mechanical properties of longitudinal bar) ≧(effective length of hoop) and also that a closer spacing of hoops was desirable for prevention of buckling of longitudinal bar under the same volumetric ratio of transverse hoops.

As for the compressive strain of concrete at buckling initiation of longitudinal bars (ε_{cr}), Papia et al. [8] proposed the following equations based on their analytical and experimental studies [9] for the case that buckling occurs within the strain hardening region of longitudinal bar.

$$\varepsilon_{cr}=\varepsilon_{ho}+[0.75(\mathrm{Log}\ k-2.5)(\lambda_{max}-\lambda)^{1.5\lambda-\zeta}+\eta(1-\xi 1.5^{(0.2\lambda-2)}(0.029\lambda^2-2.67\lambda+64)]10^{-} \quad (3-1)$$

Where,

$\zeta=0.17(\lambda_{max}/54)^{0.75}$: parameter for the maximum slenderness.

$\eta=(345/f_{sy})^{0.5}$: parameter for the yield strength of longitudinal bar.

$\xi=1-(f_{su}/1.5f_{sy})^{0.5}$: parameter for the hardening capacity of longitudinal bar.

ε_{ho}: strain at which the hardening of longitudinal bar begins.

$k=4q\omega_t E_{hot}/(hl)$: parameter for lateral stiffness.

ω_t: cross sectional area of transverse hoops.

E_{hot}: tangent modulus at onset of strain hardening in transverse steel.

h: length of the side of the perimeter hoop.

q: coefficient depending on the geometry of perimeter hoop. $q=\sqrt{2}$ for octagonal hoops, while in other cases q=2.

$\lambda=4l/d$: slenderness of longitudinal bar hinged between two consecutive supports.

d: diameter of longitudinal bar.

l: center to center spacing of hoops.

λ_{max}: limiting value of λ under which the strain hardening is achievable. $\lambda_{max}=54$ for $f_{su}/f_{sy}=1.5$, while $\lambda_{max}=62$ for $f_{su}/f_{sy}=1.7$.

f_{sy}: yield strength of longitudinal bar.

f_{su}: maximum strength of longitudinal bar.

Comparing the test results obtained by other researchers with the values calculated by Eq.(3-1), it was reported that the strain at buckling of longitudinal bars could be well estimated by Eq.(3-1).

On the other hand, Suzuki et al. [1] proposed the following equations for estimating the strain at buckling initiation of longitudinal bars in circular column specimens.

$$\varepsilon_{bu}=4.0\times10^{-4}\times[(D/s)-(1/0.7)]A_s f_{syh}+0.2 \quad (\%) \quad \text{for } 0<s/D<0.7 \quad (3-2a)$$

$$\varepsilon_{bu}=0.2 \quad (\%) \quad \text{for } 0.7\leq s/D \quad (3-2b)$$

Where,

ε_{bu}: strain at buckling initiation of longitudinal bar.

A_s: area of transverse hoop.

f_{syh}: yield strength of transverse hoop.

s: spacing of hoops.

D: diameter of cross section of specimen.

These equations were derived from the test results of circular column specimens and their applicability was limited. Therefore, they proposed a new equation applicable to both circular and square column specimens based on their

further investigation [2] as given below.

$$\varepsilon_{bu}=[(6-\phi)/90]\alpha\beta_2 p_s f_{syh}+1 \quad (\%) \qquad (3-3)$$

Where,

$\alpha=0.7+0.075n$

$\beta_2=1.0-1.0/(n+1.9)$

ϕ: diameter of longitudinal bar in cm.

n: number of sub ties.

p_s: ratio of transverse hoop area to area of core concrete.

Eq.(3-3) could estimate well the strain at buckling initiation of longitudinal bars. However, the applicability of Eq.(3-3) should be limited within the range of $\alpha\beta_2 p_s f_{syh}<7$, s/D<0.3 and f'c of approximately 300kgf/cm^2.

Some other researches [10~14] dealing with buckling of longitudinal bars in RC members were also reported in recent years.

3.3 EXPERIMENTAL PROCEDURES [15, 16]

3.3.1 Specimens

As shown in Fig.3-4, RC square column specimens (10cm x 10cm x 40cm) with four longitudinal bars at each corner were used in this study. Test variables were as follows.

(1) Spacing of hoops (s)

Suzuki et al. [1] reported that the effect of spacing of hoops on the buckling of longitudinal bar was influenced by the value of s/D (D: minimum length of cross section of specimen) and that the effect became large in the region of s/D<0.7. Maruyama et al. [4] also reported that the influence of spacing of hoops was most significant. Considering these results, three levels of spacing of hoops, that is, s=4cm, 6cm and 8cm were selected here. These values corresponded to the s/D values of 0.4, 0.6 and 0.8, respectively.

Welded square hoops made of ϕ6mm mild steel bars ($f_{syh}\cong$3100kgf/cm^2) were used for the lateral confinement.

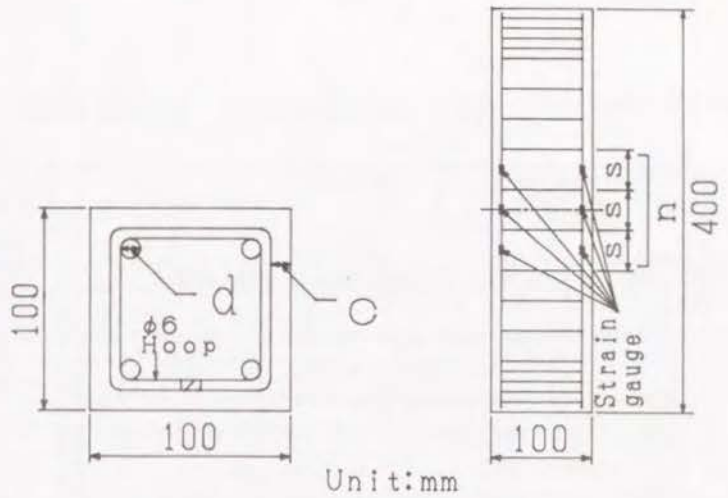

Fig.3-4 Dimensions of test specimen

(2) Diameter of longitudinal bars (d)

As the diameter of longitudinal bars, 10mm (D10 deformed bar) and 13mm (D13 deformed bar) were adopted. In addition to these specimens with longitudinal bars, some specimens without longitudinal reinforcement were prepared in order to investigate the load carrying capacity of longitudinal bars in confined concrete.

(3) Cover thickness for hoops (c)

In almost all specimens, the clear cover outside the transverse hoops was set to be zero. However, some specimens with cover thickness of 5 or 10mm were also prepared in order to investigate the effects of cover thickness on buckling of longitudinal bars.

(4) Number of intervals having the specified length of s (n)

In order to control the buckling initiation region of longitudinal bar, the specified spacing of hoops (s cm) was provided at the mid height of the column specimens with only one interval (n=1) or three intervals (n=3), considering that buckling could occur over the length greater than single hoop interval. Outside of this region, hoops were placed at 2.5cm interval to prevent premature deterioration.

Properties of the materials used are listed in Table 3-1. The details of the specimens are also listed in Table 3-2.

Table 3-1 Properties of materials

concrete		
compressive strength f'_c (kgf/cm²)		elastic modulus E_c (kgf/cm²)
cylinder	square column	cylinder
442	334～347	3.44×10^5
reinforcing bar		
kind	yield strength f_{sy} (kgf/cm²)	tensile strength f_{su} (kgf/cm²)
φ6	3060～3120	4040～4320
D10	3300～4000	4610～5750
D13	3550～3560	4910～5080

Table 3-2-(a) Details of specimens and results of tests

Specimen	s (cm)	d (mm)	c (mm)	n	s/D'	buckling mode	buckling length l (cm)	average strain in 25cm region at buckling initiation εb (×10⁻⁶) * Method I	Method II	Method III	Method IV
D10-No.1	4	10	0	1	0.400	②	4.0	7820 (7588)	26820 (5963)	24300 (8630)	15520 (23150)
D10-No.2	4	10	0	1	0.400	②	4.0	6880 (7275)	15880 (6075)	8629 (10400)	—
D10-No.3	4	10	0	1	0.400	④	4.5	—	11384	—	—
D10-No.4	4	10	0	3	0.400	③	8.0	8800	12440	10450	11240
D10-No.5	4	10	0	3	0.400	⑤	12.0	—	10121	—	—
D10-No.6	4	10	5	1	0.444	②	4.0	—	8695	—	—
D10-No.7	4	10	5	1	0.444	②	4.0	—	9370	—	—
D10-No.8	4	10	5	3	0.444	②	4.0	—	9702	—	—
D10-No.9	4	10	5	3	0.444	①	2.0	—	7818	—	—
D10-No.10	4	10	10	1	0.500	③	8.0	—	7475	—	—
D10-No.11	4	10	10	1	0.500	②	4.0	—	10493	—	—
D10-No.12	4	10	10	3	0.500	②	4.0	—	8463	—	—
D10-No.13	4	10	10	3	0.500	①	2.0	—	11668	—	—
D10-No.14	6	10	0	1	0.600	①	3.0	8710 (6233)	10730 (5042)	15540 (18800)	9180 (6233)
D10-No.15	6	10	0	1	0.600	①	3.0	9160 (8908)	9160 (11617)	9280 (9800)	—
D10-No.16	6	10	0	1	0.600	①	3.0	8280 (8033)	8280 (8033)	8820 (9590)	—
D10-No.17	6	10	0	3	0.600	⑤	18.0	9670	8160	8820	10540
D10-No.18	6	10	0	3	0.600	③	12.0	—	8130	8820	—
D10-No.19	6	10	0	3	0.600	①	3.0	8560	6980	—	—
D10-No.20	8	10	0	1	0.800	①	4.0	4020 (4525)	4020 (3238)	5420 (5770)	4020 (4038)
D10-No.21	8	10	0	1	0.800	①	4.0	3940 (4044)	3940 (4044)	7510 (12780)	—
D10-No.22	8	10	0	1	0.800	①	4.0	4140 (5044)	4140 (3094)	5420 (5180)	—
D10-No.23	8	10	0	1	0.800	①	4.0	—	4679	—	—
D10-No.24	8	10	0	1	0.800	①	4.0	—	5047	—	—
D10-No.25	8	10	0	3	0.800	①	4.0	4080	4080	—	5620
D10-No.26	8	10	0	3	0.800	①	4.0	3230	3120	7330	—
D10-No.27	8	10	0	3	0.800	①	4.0	3740	3060	5680	—
D10-No.28	8	10	0	3	0.800	①	4.0	—	5171	—	—
D10-No.29	8	10	0	3	0.800	①	4.0	—	4978	—	—
D10-No.30	8	10	5	1	0.889	①	4.0	—	4658	—	—
D10-No.31	8	10	5	1	0.889	①	4.0	—	6436	—	—
D10-No.32	8	10	5	3	0.889	①	4.0	—	3848	—	—
D10-No.33	8	10	5	3	0.889	①	4.0	—	3968	—	—
D10-No.34	8	10	10	1	1.000	①	4.0	—	4221	—	—
D10-No.35	8	10	10	1	1.000	①	4.0	—	4273	—	—
D10-No.36	8	10	10	3	1.000	①	4.0	—	3370	—	—
D10-No.37	8	10	10	3	1.000	①	4.0	—	4810	—	—

* the values within parenthese indicate the strains in the center s cm region at buckling initiation.

Table 3-2-(b) Details of specimens and results of tests

Specimen	s (cm)	d (mm)	c (mm)	n	s/D'	buckling mode	buckling length l (cm)	average strain in 25cm region at buckling initiation εb (×10⁻⁶) # Method I	Method II	Method III	Method IV
D13-No.1	4	13	0	1	0.400	①	2.0	7620 (9588)	11220 (14206)	11230 (15080)	—
D13-No.2	4	13	0	1	0.400	②	4.0	8250 (9150)	9240 (10950)	10560 (10940)	—
D13-No.3	4	13	0	3	0.400	⑤	12.0	8140	17460	6530	10250
D13-No.4	4	13	0	3	0.400	⑤	12.0	9020	12570	10450	—
D13-No.5	4	13	0	3	0.400	④	6.0	—	9173	—	—
D13-No.6	4	13	5	1	0.444	②	4.0	—	13354	—	—
D13-No.7	4	13	5	1	0.444	⑤	9.0	—	22021	—	—
D13-No.8	4	13	5	3	0.444	④	6.0	—	15230	—	—
D13-No.9	4	13	10	1	0.500	②	4.0	—	19235	—	—
D13-No.10	4	13	10	1	0.500	②	4.0	—	11949	—	—
D13-No.11	4	13	10	3	0.500	②	4.0	—	10836	—	—
D13-No.12	6	13	0	1	0.600	①	3.0	9420 (11096)	13360 (11096)	15540 (5230)	9420 (4575)
D13-No.13	6	13	0	3	0.600	⑤	18.0	8200	12640	12180	17040
D13-No.14	6	13	0	3	0.600	③	12.0	8090	12770	7120	—
D13-No.15	6	13	0	3	0.600	①	3.0	5820	9540	6260	—
D13-No.16	8	13	0	1	0.800	①	4.0	4080 (4244)	4080 (4244)	7700 (12760)	4080 (4244)
D13-No.17	8	13	0	1	0.800	①	4.0	3620 (3756)	3440 (2575)	5330 (10430)	—
D13-No.18	8	13	0	1	0.800	②	8.0	—	4337	—	—
D13-No.19	8	13	0	3	0.800	①	4.0	2430	4190	3750	3360
D13-No.20	8	13	0	3	0.800	①	4.0	4850	4050	3920	—
D13-No.21	8	13	0	3	0.800	①	4.0	4290	4560	4191	—
D13-No.22	8	13	5	1	0.889	①	4.0	—	4995	—	—
D13-No.23	8	13	5	1	0.889	①	4.0	—	5522	—	—
D13-No.24	8	13	5	3	0.889	①	4.0	—	3813	—	—
D13-No.25	8	13	10	1	1.000	②	8.0	—	5662	—	—
D13-No.26	8	13	10	1	1.000	②	8.0	—	3891	—	—
D13-No.27	8	13	10	3	1.000	①	4.0	—	5028	—	—
D13-No.28	8	13	10	3	1.000	②	8.0	—	4815	—	—

the values within parenthese indicate the strains in the center s cm region at buckling initiation.

3.3.2 Loading Setups

Specimens were loaded uniaxially up to failure with care so that the eccentricity of load should be minimized. During test, the applied load was measured by a load cell, and longitudinal deformations in 25cm region including s cm region were measured by electric strain gauge transducers (gauge length: 50mm) attached on the specimens through the yokes. In some specimens, longitudinal deformations in the center s cm region (center of three intervals having the length of s cm in case of the specimens with n=3) were also measured by displacement transducers (gauge length: 10mm). In addition, strains in each longitudinal bar within s cm region were measured in some specimens by two electric strain gauges (gauge length: 2mm), which were attached so as to face each other on the surface of bars. The measuring points of strain in longitudinal bars were shown in Fig.3-4 and the details of loading and measuring apparatuses are shown in Fig.3-5.

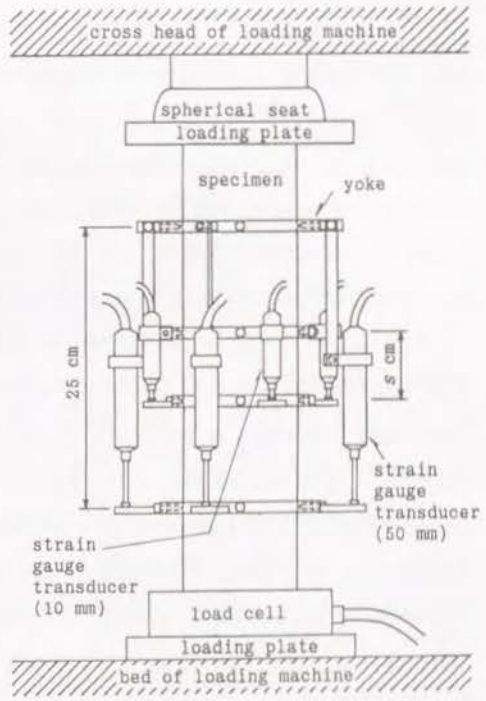

Fig.3-5 Loading and measuring apparatuses

3.4 RESULTS OF TESTS AND DISCUSSIONS [15, 16]

3.4.1 Methods for Determining the Buckling Initiation Point

Except for some specimens, in which the load carrying capacity reduced at an early stage due to the deterioration of confined concrete near both ends of the specimens before buckling initiation, the buckling of longitudinal bars occurred within the region where the transverse hoops was arranged at the spacing of s cm. In this study, the longitudinal strain in both the center s cm region and 25cm region at buckling initiation of longitudinal bar were estimated by the following four different methods.

(1) Method I

As shown in Fig.3-6-(a), the strain in the center s cm region (① in Fig.3-6-(a)) increases similarly to the strain in (25-s) cm region (③), which means the region where the center s cm region is subtracted from 25cm region, until the initiation of buckling. However, once the buckling of longitudinal bar occurs within the center s cm region, the strain in this region commences to increase abruptly while the strain in (25-s) cm region increases very little or none. In this method, the buckling initiation point is defined as the point where the strain increment in the center s cm region becomes to deviate from that in (25-s) cm region (■ mark in Fig.3-6-(a)). In case of the specimens with n=3, buckling can occur in another two intervals having the length of s cm outside the center s cm region. In such case, an opposite phenomenon can be observed, that is, the strain in (25-s) cm region begins to increase abruptly while the increase in the strain in the center s cm region becomes very little. Therefore, the point at which the strain in the center s cm region separates from that in (25-s) cm region can be regarded as buckling initiation point.

(2) Method II

This method is similar to that proposed by Suzuki et al. [1] and Koyanagi et al. [3], based on the idea that the largest effect of the buckling of longitudinal bars on RC members is reduction in load carrying capacity. In this method, the relationship between the gradient of load – longitudinal strain curve ($\Delta P/\Delta\varepsilon$) and longitudinal strain (ε) is firstly obtained as indicated in Fig.3-6-(b). As seen in the figure, the gradient of a load – longitudinal strain curve turns to be negative immediately after passing the maximum load and decreases to the minimum point due to the crushing and spalling of cover concrete. After that, the gradient begins to increase up to the maximum point (●mark in Fig.3-6-(b)) and then decreases again. In this method, this maximum point is defined as the buckling initiation point because this point is supposed to represent the abrupt reduction of the load carrying capacity due to the buckling of longitudinal bars if the decreasing ratio in load carrying capacity of confined concrete is assumed to be constant. When the spacing of hoops is relatively large, the buckling of longitudinal bars occurs immediately after passing the maximum load and the maximum point does not appear [1]. In such a case, the buckling initiation point is defined as the maximum load point. This method can be available to both of the strain in the center s cm region and the average strain in 25cm region at buckling of longitudinal bar.

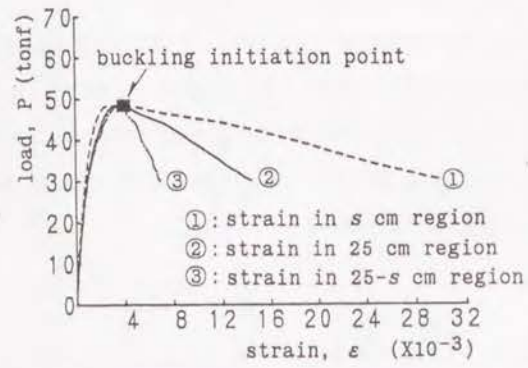

(a) METHOD I

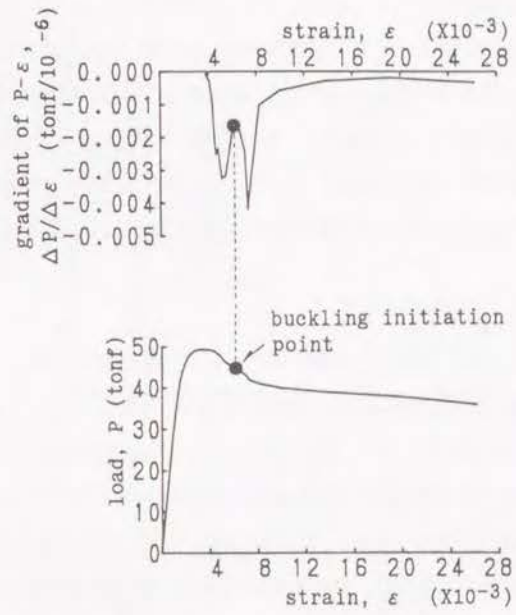

(b) METHOD II

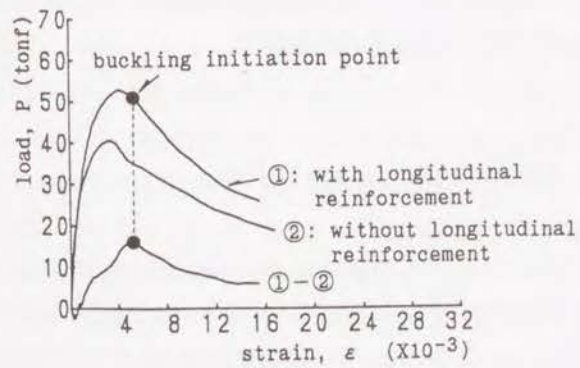

(c) METHOD III

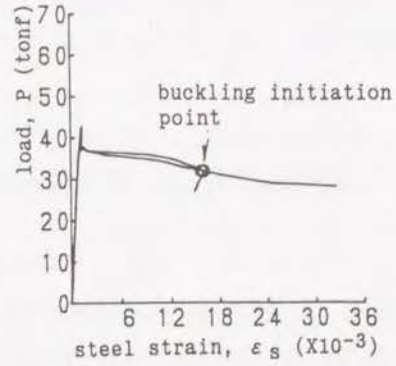

(d) METHOD IV

Fig.3-6 Methods for determining the buckling initiation of longitudinal bars

(3) Method III

By subtracting the load – longitudinal strain curve of the specimen without longitudinal bars from that of the specimen with longitudinal bars, the load – longitudinal strain curve of longitudinal bar can be obtained as shown in Fig.3-6-(c) if the stress – strain curve of confined concrete used in both specimens is assumed to be the same. In this method, the buckling initiation point is defined as the maximum load point of the curve (●mark in Fig.3-6-(c)) because this curve is supposed to represent the load carried by longitudinal bars.

(4) Method IV

Maruyama et al. [4] reported that the buckling initiation could be decided by the sudden change in the readings of strain gauges attached so as to face each other on the surface of longitudinal bars. Once the buckling of longitudinal bar commences, the compressive strain at the internal side of bar increases abruptly while the strain at the opposite side begins to decrease as shown in Fig.3-6-(d). In this method, the separating point is defined as the buckling initiation point (○mark in Fig.3-6-(d)).

In Table 3-2 are shown the average strains in 25cm region of each specimen at the buckling of longitudinal bars obtained from the above mentioned four methods. The strains in the center s cm region are also indicated as for the specimens in which the strains in the s cm region were measured.

3.4.2 Comparison of Strain at Buckling Obtained from Each Method

Fig.3-7-(a) and (b) show the strains in the center s cm region and 25cm region at buckling of longitudinal bars obtained from four different methods about the specimens with n=1 in which the buckling occurred within s cm region. In these figures, the horizontal axis shows the strains at buckling obtained from Method I (ε_b(I)), while the vertical axis shows the strains derived from Method II, III and IV (ε_b(II), ε_b(III) and ε_b(IV), respectively) for the corresponding specimens, which are plotted by different marks.

As for the strains in the center s cm region, the strains at buckling obtained from Method II tend to give a little smaller values within the region of ε_b<0.008 and a little larger values in the region of ε_b>0.008 compared with those obtained from

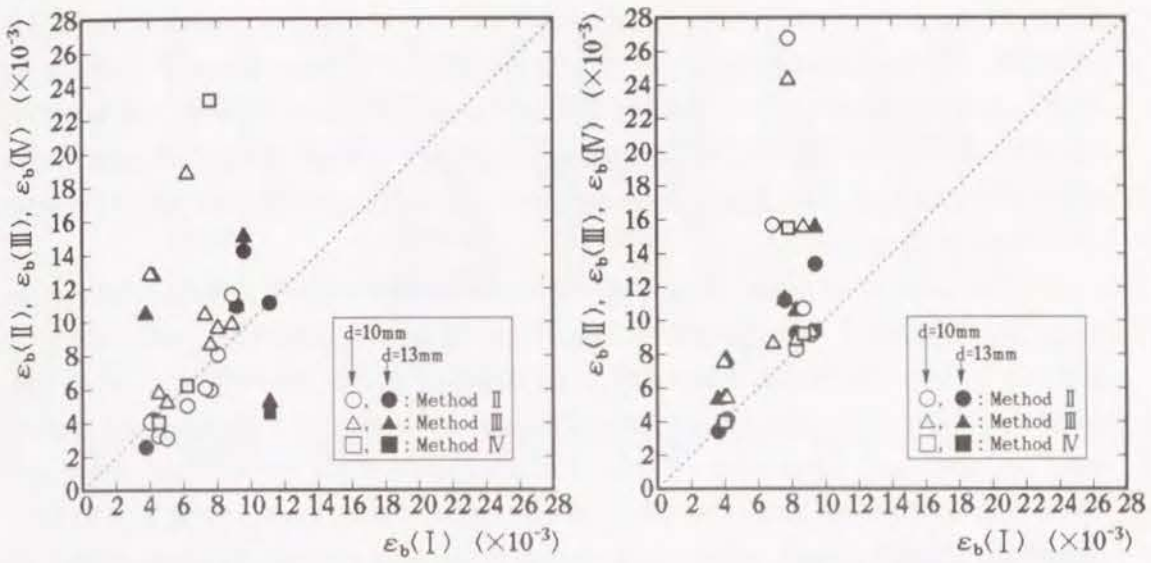

(a) s cm region (b) 25cm region

Fig.3-7 Comparison of strains at buckling initiation obtained from each method

Method I. In this case, however, the difference between these two methods is relatively small. This tendency is similar irrespective of diameter of bars. From these results, Method II is supposed to be one of the effective methods to determine the buckling initiation point of longitudinal bar in confined concrete. In the specimens which did not show the clear reduction in load carrying capacity in P – ε curve, however, the maximum point in $\Delta P/\Delta\varepsilon$ – ε curve does not clearly appeared. In such cases, the determined strains at buckling may be a little uncertain. This tendency is sometimes seen in the specimens with a smaller spacing of hoops and becomes more significant in case of the average strain in 25cm region, resulting in giving considerably larger values than those by Method I.

The strains at buckling obtained from Method III indicate larger values compared with those from Method I in case of d=10mm and the difference between Method III and Method I is larger than that between Method II and Method I. In case of d=13mm, this difference becomes considerably large. These tendencies are observed in both of the strains in the center s cm region and 25cm region. In the P – ε curves of the specimens without longitudinal bars, the increase in load carrying capacity caused by the confining effect due to the interaction of longitudinal bars and transverse hoops is not included. Therefore, in the P – ε curves obtained by subtracting the P – ε curves of the specimens without longitudinal bars from

those of the specimens having longitudinal bars, the above mentioned effects are included. If it is assumed that these effects are the same irrespective of spacing of hoops and diameter of bars, Method III may be used for determining the buckling initiation. However, the scattering also exists in the P – ε curves of the specimens without longitudinal bars. From these reasons, it is supposed that Method III should be in supplementary use.

The strains at buckling by Method IV sometimes show the same values as those by Method I, while some values are considerably different from those by Method I. This method is supposed to be effective if the buckling occurs at the position where the strain gauges are attached. However, the determined strains may be uncertain if the buckling occurs at another position. In addition, there are some possibilities that strain gauges may be broken before the buckling due to their sensitivity. From these reasons, it is desirable that Method IV should be in supplementary use with another methods.

As for the average strain in 25cm region at buckling of longitudinal bars, the value obtained from Method I is supposed to give a lower limit one (Fig.3-7-(b)).

It is supposed that Method I might be a very effective method when the buckling point or the failure zone could be predicted to a certain extent as seen in the case of the specimens with n=1 used in this study. In general cases, however, there exist some difficulties in selecting the specified length to measure the longitudinal deformations because the buckling zone of longitudinal bars cannot be easily predicted.

As mentioned above, it is difficult to choose the best method for determining the buckling initiation of longitudinal bars because each method has advantages and disadvantages simultaneously. Considering the scattering of test data, however, Method I or II should be used mainly for determining the strains at buckling, while Method III and IV should be in supplementary use.

3.4.3 Buckling Mode and Effective Buckling Length

In Fig.3-8 are shown schematically the buckling mode of longitudinal bars observed in the specimens. The buckling mode and effective buckling length of each specimen are also indicated in Table 3-2. The effective buckling length is considered to be one-half the hoop interval (s) in case of no end translation (Fig.3-2-(a)), while equal to one hoop interval in case of end translation (Fig.3-2-(b)).

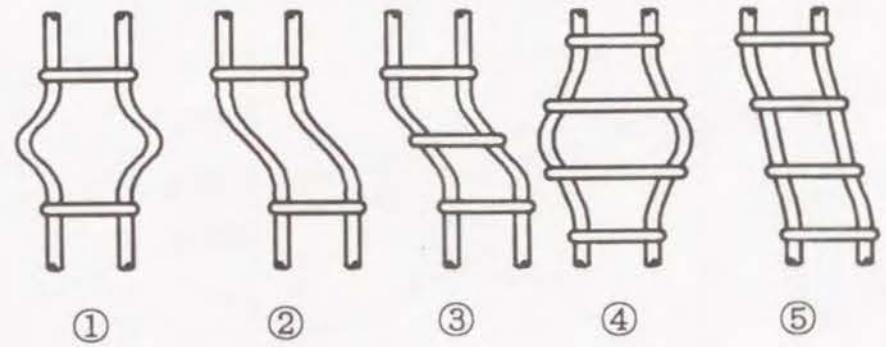

Fig.3-8 Schema of buckling mode observed in the specimens

The specimens with d=10mm and n=1 show the buckling mode ① without exception in case of s=6cm or 8cm, resulting in the calculated effective buckling length of 3cm for s=6cm and 4cm for s=8cm. In case of the specimens with s=4cm, on the other hand, the buckling mode ② is more frequently observed rather than the buckling mode ①, resulting in the effective buckling length close to 4cm.

As for the specimens with d=10mm and n=3, only the buckling mode ① is observed in the specimens with s=8cm, while the buckling mode spanning more than two hoop intervals, that is, the buckling mode ③, ④ and ⑤, become to be observed in the specimens with smaller s-values. These results implies that the possibility of the occurrence of buckling spanning over several hoop intervals increases with decreasing spacing of hoops in case of the specimens with n=3.

In the specimens with D13 deformed bars (d=13mm), similar tendency to the specimens with D10 deformed bars (d=10mm) is observed as for the influence of spacing of hoops (s) and number of intervals (n). However, the buckling modes accompanied by end translation (buckling mode ②, ③ and ⑤) are more frequently observed in the specimens with d=13mm. This suggests that the effective buckling length becomes a little larger with increasing diameter of longitudinal bars.

As far as the specimens used, the effect of cover thickness (c) on the buckling mode and effective buckling length is scarcely recognized.

3.4.4 Strain at Buckling Initiation

In Fig.3-9 are shown some examples of load – longitudinal strain curves

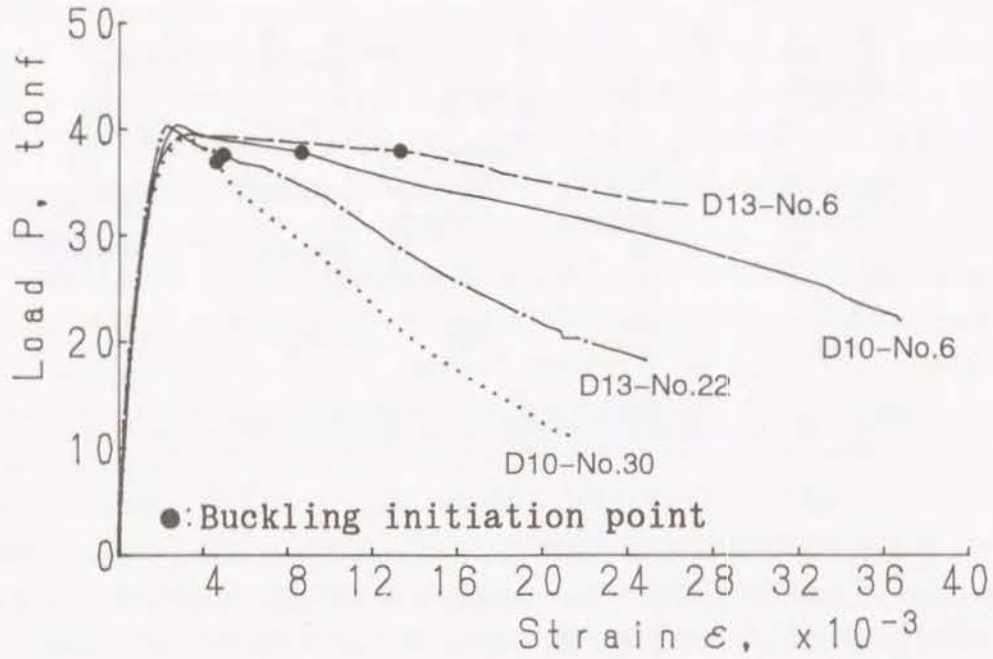

Fig.3–9 Examples of load – longitudinal strain relationship

obtained from the strains in 25cm region.

The strain at buckling initiation is inevitably different according to the length where the strain is measured. In some of the tested specimens, the strains in the center s cm region were measured together with the average strains in 25cm region. However, the length of s cm region is different due to the kinds of specimen and buckling of longitudinal bars did not always occur in the center s cm region in the specimens with n=3.

On the other hand, Method I and II are supposed to be one of good methods for determining the strain at buckling initiation. However, Method I can not be applied to all the specimens because the strains in the center s cm region was not always measured in all of them. Therefore, the average strains in 25cm region at buckling initiation obtained from Method II are used in the following discussions.

In Fig.3–10 are shown the effects of spacing of hoops (s) on the strain at buckling initiation (ε_b) for specimens without cover concrete (c=0). In this figure, the average value among the specimens with the same test variables is indicated. The strain at buckling initiation is remarkably affected by the spacing of hoops, that is, ε_b–value decreases with increasing s–value. This tendency can be observed irrespective of diameter of longitudinal bar (d) and number of intervals having the

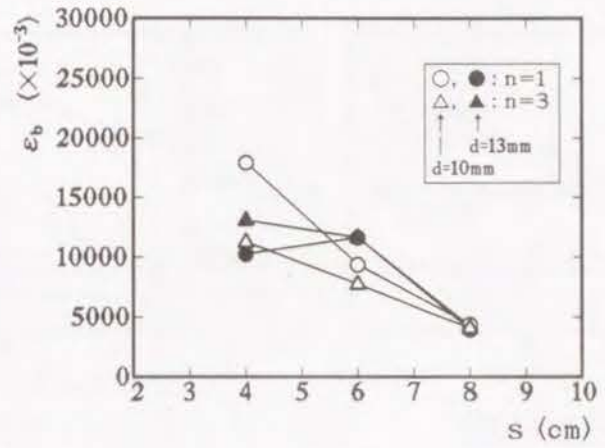

Fig.3–10 Effects of spacing of hoops on the strain at buckling initiation

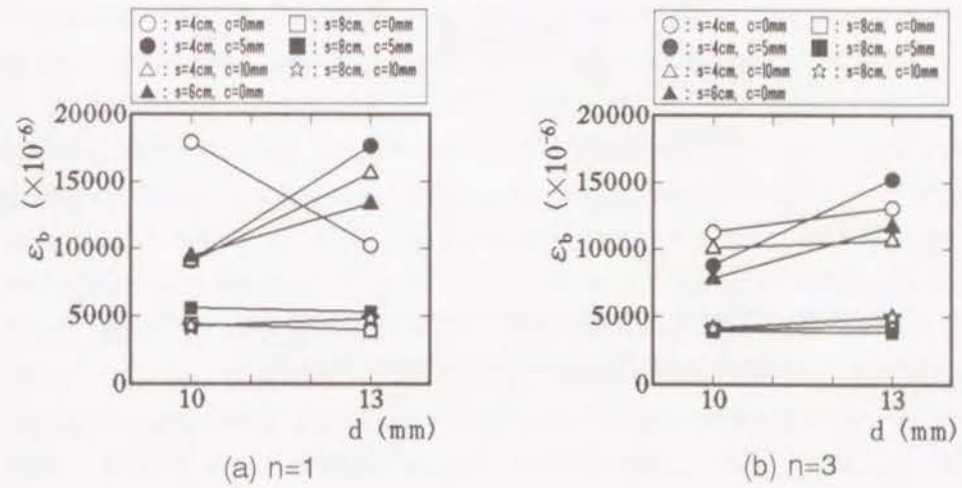

Fig.3–11 Effects of diameter of longitudinal bars on the strain at buckling initiation

length of s (n), although some scattering of data exists.

Fig.3–11 shows the effects of diameter of longitudinal bar (d). In case of s=4cm and 6cm, the strain at buckling becomes larger in the specimens with d=13mm than that in those with d=10mm except for only one case with s=4cm, c=0mm and n=1. In the specimens with s=8cm, on the other hand, ε_b–value is ranged between 4000–5000x10^{-6} irrespective of bar diameter. This is because the

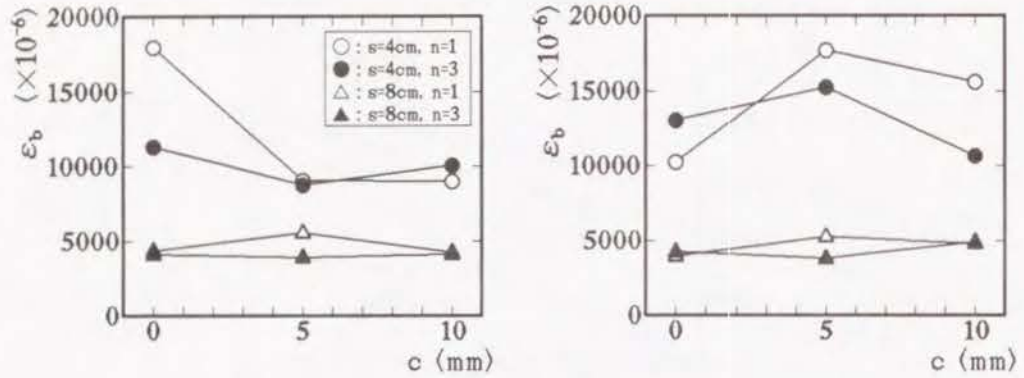

(a) d=10mm (b) d=13mm

Fig.3-12 Effects of cover thickness for hoops on the strain at buckling initiation

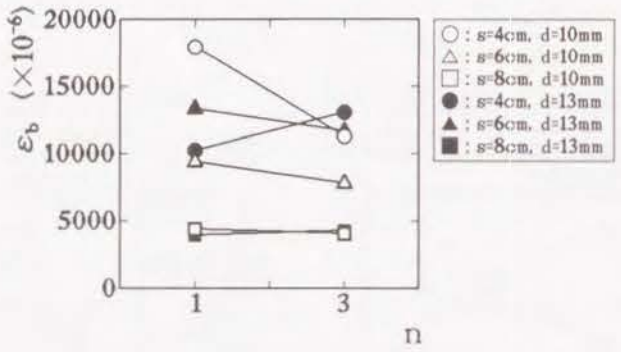

Fig.3-13 Effects of number of intervals having the specified length on the strain at buckling initiation

buckling of longitudinal bars occurs immediately after the maximum load point due to a relatively large spacing of hoops and consequently the influences of bar diameter dose not appear.

Fig.3-12 and Fig.3-13 show the effects of cover thickness for hoops (c) and number of intervals having the length of s (n), respectively. In case of s=4cm, ε_b-value becomes largest at c=5mm in the specimens with d=10mm while this becomes largest at c=0mm in the specimens with d=13mm. In case of s=8cm, on the other hand, the effects of cover thickness on ε_b-value are not obviously recognized. As for the effects of n, ε_b-value in the specimens with n=3 tend to become somewhat smaller than that in the specimens with n=1 except for the case of s=4cm and d=13mm. This is mainly due to that possibility of the buckling of

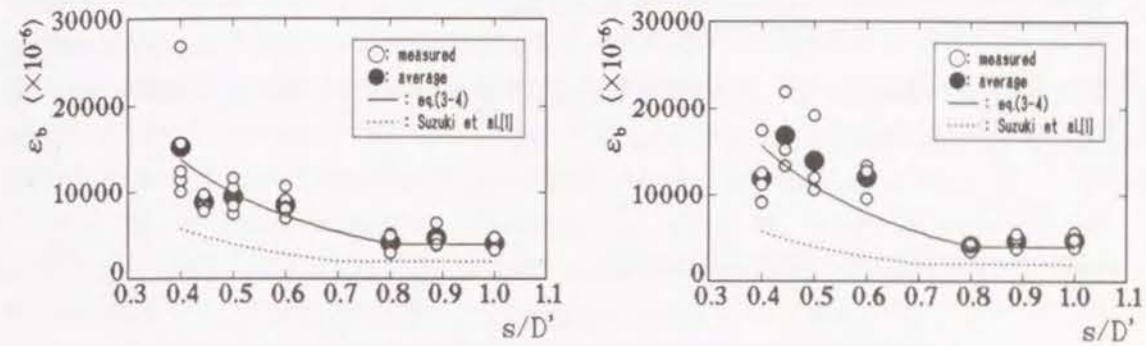

(a) d=10mm (b) d=13mm

Fig.3-14 Relationships between s/D' ratio and ε_b-values

longitudinal bars becomes larger in case of n=3 than n=1. However, the effects of these two variables on the strain at buckling of longitudinal bars are relatively small compared with those of spacing of hoops and diameter of longitudinal bar.

As mentioned above, distinct influences of cover thickness for hoops are not recognized and the difference in cover thickness can be replaced by the size of core concrete confined by a hoop, that is, the minimum leg of a hoop (D'). Therefore, ε_b-value of each specimen is re-plotted versus s/D' as shown in Fig.3-14. In this figure, ε_b-value is almost in inverse proportion to s/D' up to s/D'=0.6, while takes a constant value of approximately 0.004 in the region of s/D'≥0.8. Suzuki et al. [1] indicated that the strain at the buckling of longitudinal bar became almost constant in the region of s/D>0.7. In the case of the specimens tested, this border line exists between s=6cm and s=8cm. From these results, the following equations representing the strain at buckling initiation of longitudinal bars were derived from the regression analysis of tested data.

$$\varepsilon_b=\alpha[(D'/s)-(1.0/0.8)]+0.004 \quad (s/D'<0.8) \tag{3-4a}$$

α=0.00782 for d=10mm and 0.00936 for d=13mm

$$\varepsilon_b=0.004 \quad (s/D'\geq 0.8) \tag{3-4b}$$

The strains at buckling initiation calculated by Eq.(3-4) are also shown ih Fig.3-14 together with those by Eq.(3-2) proposed by Suzuki et al. [1]. The ε_b-values calculated by Eq.(3-4) are more than twice of those by Eq.(3-2). This is mainly because Method II for determining the strain at buckling is more similar to

the method proposed by Koyanagi et al. [3] than that by Suzuki et al. [1]. These facts agree with the report [5] that the strain at buckling derived from the method proposed by Suzuki et al. is approximately 40% of that from the method proposed by Koyanagi et al..

3.5 CONCLUSIONS OF CHAPTER 3

In this chapter, investigations are done on the effective methods to determine the strain at buckling initiation of longitudinal bars in confined RC column specimens. The effects of spacing of hoops, diameter of longitudinal bars, cover thickness and number of intervals having the specified length on the determined strains at buckling are also discussed. The main conclusions obtained are as follows.

(1) Method I utilizing the relationship between the load-longitudinal strain curve of the region where the buckling of longitudinal bars occurs and that of the adjacent unfailed region and Method II using the gradient of load-longitudinal strain curves are considered to be effective for determining the buckling initiation of longitudinal bars in confined concrete based on the test results.

(2) It is desirable that Method III based on the load-longitudinal strain curves obtained by subtracting the P-ε curves of the specimens without longitudinal bars from that of the specimens having longitudinal bars and Method IV based on the relative change in the readings of the strains gauges attached on the longitudinal bars should be used as supplementary to the above methods.

(3) A closer spacing of hoops or a larger diameter of bars tend to cause the buckling mode spanning more than two hoop intervals or the buckling mode accompanied by end translation. The effective buckling length is approximately equal to one-half of the minimum length of cross section although it becomes a little larger in the specimens with a larger diameter of longitudinal bars.

(4) Closer spacings of hoops of $s/D' \leq 0.6$ (s: spacing of hoops, D': minimum leg of a hoop) is desirable in order to avoid premature buckling of longitudinal bars and attain a sufficient amount of inelastic deformability until the initiation of buckling. In case of $s/D' \geq 0.8$, the effect of hoop spacing does not appear and the strain at buckling initiation indicates a constant value of approximately 0.004.

(5) The effect of bar diameter becomes significant when the s/D' ratio is relatively small (in this study, $s/D' \leq 0.6$). In such cases, a larger diameter of longitudinal bars indicates a larger strain at buckling initiation.

(6) The effects of cover thickness for hoops and number of intervals having the specified length on the strain at buckling of longitudinal bars are relatively small compared with those of spacing of hoops and diameter of longitudinal bars.

(7) As far as these tests are concerned, the strain at buckling initiation of longitudinal bars in confined RC column specimens can be represented by the function of s/D' ratio and diameter of longitudinal bars.

REFERENCES OF CHAPTER 3

1) Suzuki, K., Nakatsuka T., Nagata, N. and Inoue, K., "Buckling Behavior of Longitudinal Compressive Reinforcement in Confined Concrete with Circular Spiral Reinforcement," Proc. of the JCI, Vol.9, No.2, pp.151-156, 1987. [in Japanese]
2) Suzuki, K., Nakatsuka, T., Yamaguchi, Y. and Shoda, T., "Buckling Behavior of Compressive Reinforcing Bars in Confined Concrete with Rectangular Transverse Reinforcement," Proc. of JCI Symposium on Design of Reinforcement and Ductility of Concrete Structures, pp.61-68, 1990. [in Japanese]
3) Koyanagi, W., Rokugo, K., Yamamoto, T. and Kondo, Y., "Buckling of Longitudinal Steels in Concrete Subjected to Compressive Load," Proc. of the 44th Annual Conference of the JSCE, Vol.5, pp.502-503, 1989. [in Japanese]
4) Maruyama K., Zhao, W. J. and Shimizu K., "Some Considerations on Instability of Longitudinal Bars in RC Columns," Proc. of JCI Symposium on Design of Reinforcement and Ductility of Concrete Structures, pp.47-60, 1990. [in Japanese]
5) Yoshida, N., Hatanaka, S. and Ageta, H., "Study on Initiation Strain of Buckling of Compressive Steel Bars in RC Columns and Beams," Proc. of the JCI, Vol.14, No.2, pp.331-336, 1992. [in Japanese]
6) Gosain, N. K., Brown, R. H. and Jirsa, J. O., "Shear Requirements for Load Reversals on RC Members," Journal of the Structural Division, ASCE, Vol.103, No.ST7, pp.1461-1476, 1977.
7) Scribner, C. F., "Reinforcement Buckling in Reinforced Concrete Flexural Members," Journal of the ACI, Vol.83, No.6, pp.966-973, 1986.

8) Papia, M. and Russo, G., "Compressive Concrete Strain at Buckling of Longitudinal Reinforcement," Journal of Structural Engineering, ASCE, Vol.115, No.2, pp.382-397, 1989.
9) Papia, M., Russo, G. and Zingone, G., "Instability of Longitudinal Bars in RC Columns," Journal of Structural Engineering, ASCE, Vol.114, No.2, pp.445-461, 1988.
10) Shima, H., Itoh, K., Kitanishi, T. and Mizuguchi, H., "Effect of Hoop Arrangement on Bar Buckling and Ductility of Reinforced Concrete Bridge Piers," Proc. of JCI Symposium on Design of Reinforcement and Ductility of Concrete Structures, pp.33-40, 1990. [in Japanese]
11) Kato, D. and Kanaya, J., "Buckling of Main Bars in Reinforced Concrete Columns," Proc. of JCI Symposium on Design of Reinforcement and Ductility of Concrete Structures, pp.41-46, 1990. [in Japanese]
12) Kato, D. and Kanaya, J., "Buckling Behaviors of Steel Bars in R/C Columns Subjected to Cyclic Loading,", Proc. of the JCI, Vol.13, No.2, pp.369-374, 1991. [in Japanese]
13) Hatanaka, S., Yanagawa, Y. and Yoshida, N., "Buckling Behavior of Reinforcing Bar in Ultimate State of RC Beams," Proc. of the JCI, Vol.13, No.2, pp.275-280, 1991. [in Japanese]
14) Nakamura, H., Niwa, J. and Tanabe, T., "Effect of Buckling of Longitudinal Reinforcement on the Post-Peak Behavior of RC Structure," Proc. of the JCI, Vol.14, No.2, pp.337-342, 1992. [in Japanese]
15) Inoue, S., Miyagawa, T. and Fujii, M., "An Experimental Study on Buckling of Longitudinal Reinforcement in Reinforced Concrete Members," Journal of the Society of Materials Science Japan, Vol.40, No.456, pp.1208-1213, 1991. [in Japanese]
16) Inoue, S., Tsukada, K., Miyagawa, T. and Fujii, M., "Experimental Study on Buckling of Longitudinal Reinforcement in RC Column Specimens," Transactions of the JCI, Vol.13, pp.287-294, 1991.

CHAPTER 4

INELASTIC BEHAVIOR OF PRESTRESSED CONCRETE BEAMS USING CONFINED CONCRETE IN COMPRESSION ZONE OF SECTION

4.1 GENERAL REMARKS

Prestressed concrete (PC) has many advantages compared with reinforced concrete (RC) and has been applied to many kinds of civil engineering structures such as long span bridges, storage or digestion tanks and nuclear reactor vessels, in addition to precast industrial products as sleepers, piles and poles.

Some of the characteristics of prestressed concrete, however, do not always become advantages compared with reinforced concrete. One of disadvantages of prestressed concrete is grouting. In post-tensioned prestressed concrete members, grouting into the ducts is usually done after prestressing so that prestressing steels may be bonded to concrete. However, this grouting procedure may be one of obstacles from the view point of labor-saving and shortening of construction period. In addition, poor grouting causes earlier deterioration of structures due to corrosion of prestressing steels and the quality of grouting has large influence on the durability of prestressed concrete structures.

Another disadvantage is that energy dissipation of prestressed concrete is much less than that of reinforced concrete, although elastic resistance becomes higher and residual deformation at unloading becomes smaller in prestressed concrete compared with reinforced concrete. This property is not favorable in case of large earthquakes under which a large energy dissipation is required because a smaller energy dissipation results in a larger dynamic response during earthquakes.

As a structure which supplements the defects of PC as mentioned above, unbonded prestressed concrete (UPC) and partially prestressed concrete (PPC) have been noticed in recent years.

Unbonded prestressed concrete can omit grouting procedure by using polyethylene sheathed unbonded tendons filled with grease, and restore the loss of prestress due to drying shrinkage and creep of concrete and relaxation of prestressing steels by re-tensioning. On the other hand, partially prestressed concrete has considerable freedom of design compared with RC and PC, and offers

a good solution with regard to control of crack width and deflection. It becomes also possible to change its load-deflection hysteresis loop from a high restoring deformation type as PC to a high energy dissipation type like RC. Therefore, the potential economic and serviceability advantages of PPC are being fully realized in construction practice. However, some disadvantages of UPC under seismic loads were also reported and inelastic deformation properties of PPC under seismic loads have not been made clear. Therefore, it is essential to make clear their fundamental inelastic behavior when subjected to seismic loading for their more extensive structural use.

In this chapter, improvement of inelastic deformation properties of unbonded prestressed concrete and partially prestressed concrete (including ordinary prestressed concrete) by using laterally confined concrete are mainly discussed.

4.2 REVIEW OF PREVIOUS RESEARCH WORKS

4.2.1 Influencing Factors on the Inelastic Behaviors of Prestressed Concrete

In general, inelastic deformability of prestressed concrete members is supposed to be inferior to that of reinforced concrete. In addition, the failure mode of the former becomes more brittle than that of the latter especially in unbonded prestressed concrete, although prestressed concrete shows a higher restoring force with a less residual deformations within the range of elastic deformation. These properties are not favorable from the view point of structural safety under large earthquakes. Therefore, many research works has been done on the improvement of ductility of prestressed concrete.

The main factors which have influences on the ductility of prestressed concrete are as follows.

1. content of longitudinal steel.
2. content of transverse reinforcement.
3. distribution of prestressing steel.
4. amount of prestress (content of non-prestressing steels).
5. cover thickness.
6. bond of prestressing steel.
7. mechanical properties of materials used.

The content of longitudinal steels in the section is usually expressed by steel index (q) defined as below.

$$q=q_p+q_s \tag{4-1}$$

Where,

$$q_p=\frac{A_p f_{py}}{bd_p f'_c}, \qquad q_s=\frac{A_s f_{sy}}{bd_s f'_c} \tag{4-2}$$

q_p: prestressing steel index.
q_s: non-prestressing steel index.
A_p: area of prestressing steel.
A_s: area of non-prestressing steel.
f_{py}: yield strength of prestressing steel.
f_{sy}: yield strength of non-prestressing steel.
d_p: depth of prestressing steel.
d_s: depth of non-prestressing steel.
b: width of cross section.
f'_c: compressive strength of concrete.

In order to ensure sufficient ductility in seismic design, it is desirable to keep the steel index less than 0.2 [1, 2]. Various seismic code provisions [3-5] also provide some limits for the amount of steels in section.

The content of transverse reinforcement has large influences on the ductility of prestressed concrete. The amount of transverse reinforcement is usually expressed by its volumetric ratio (ρ_s) to the volume of confined core concrete. Many seismic codes also indicate the minimum requirement of transverse reinforcement for the members subjected to seismic loads in order to ensure an appropriate amount of ductility. As for the effects of transverse reinforcement for lateral confinement, many research works have been reported [1, 6-10] and the ductility of prestressed concrete members can be improved significantly by arranging an appropriate amount of transverse steel even if they have a large steel index of approximately q=0.4 [11, 12].

The amount of introduced prestress and non-prestressing steel has also large influences on the inelastic behaviors of prestressed concrete members. As the index which represents the degree of prestress and the amount of non-prestressing

steel in the section, mechanical degree of prestress, λ, defined as below can be used.

$$\lambda = \frac{A_p f_{py}}{A_p f_{py} + A_s f_{sy}} \tag{4-3}$$

λ=0 indicates reinforced concrete and λ=1.0 indicates prestressed concrete without non-prestressing steels in the section. In PPC beams, the area surrounded by load-deformation hysteresis loop becomes smaller with increasing the λ-value, resulting in a smaller energy dissipation ability [13-15], especially in a larger deformation level.

Research works which investigated the effects of cover thickness, distribution of prestressing steel and mechanical properties of materials have been also reported [1, 12, 16, 17].

4.2.2 Properties of Unbonded Prestressed Concrete

In unbonded prestressed concrete, the maximum flexural strength is less than that of ordinary bonded prestressed concrete and the ultimate failure mode in the former is more brittle than in the latter, although elastic recovery of deformation is larger in the former than in the latter. This is mainly due to that the stress in prestressing steel at the ultimate state does not usually reach its yield strength in unbonded prestressed concrete because the bond between concrete and prestressing steel does not exist.

For example, JSCE indicates in the Commentary of Standard Specification for Design and Construction of Concrete Structures [18] that the ultimate flexural strength of an unbonded prestressed concrete section should preferably be taken at 70% of that of the equivalent bonded prestressed concrete section in case without special consideration. However, the measured ultimate flexural strengths of unbonded prestressed concrete members are almost in the range of 85-95% of those of equivalent bonded prestressed concrete members [19, 20]. Ultimate flexural strength of an unbonded prestressed concrete section can be calculated strictly by considering the strain compatibility that the strain increment in prestressing steel due to the applied load is equal to the total strain increment in the concrete at the position of prestressing steel summed along with the longitudinal

direction of the member [21]. However, the calculation process of this method is very complicated although the agreement of the results is quite well. Therefore, some simplified method have been proposed based on the experimental data.

Baker [22] proposed the equation which gives the strain in unbonded prestressing steel at the flexural failure of the member by using the strain compatibility factor.

$$\varepsilon_{pu} = \varepsilon_{pe} + \alpha\left(\varepsilon_{ce} + \varepsilon_{cu}\frac{d_p - x_u}{x_u}\right) \tag{4-4}$$

Where,

ε_{pu}: strain in prestressing steel at the flexural failure.
ε_{pe}: strain in prestressing steel due to the effective prestress.
ε_{ce}: strain in concrete at the position of prestressing steel due to the effective prestress.
ε_{cu}: ultimate strain of concrete.
x_u: neutral axis depth.
α: strain compatibility factor.

As for the value of strain compatibility factor, for examples, α=0.1-0.2 by Muguruma et al. [21], 0.4-0.6 for epoxy or asphalt coated unbonded steel by Miyamoto et al. [23] and 0.25 for polyethylene sheathed unbonded steel by Kobayashi et al. [24], are recommended.

On the other hand, Mattock et al. [25] proposed the equation representing the approximate value of the stress in unbonded prestressing steel at the flexural failure by the analysis of the experimental data.

$$f_{ps} = f_{pe} + \frac{1.4 f'_c}{100 p_p} + 700 \tag{4-5}$$

Where,

f_{ps}: stress in prestressing steel at the flexural failure (in kgf/cm^2).
f_{pe}: stress in prestressing steel due to the effective prestress (in kgf/cm^2).
p_p: prestressing steel ratio ($=A_p/bd_p$).

The same approach was done by Warwaruk et al. [26] and these researches

are reflected on various code provisions, for examples, as ACI [4] and AIJ [27].

In general, flexural strengths of unbonded prestressed concrete sections calculated by these simplified methods coincided well with the measured ones.

4.3 INELASTIC BEHAVIOR OF PARTIALLY PRESTRESSED CONCRETE BEAMS [28]

4.3.1 Experimental Procedures

(1) Specimens

Dimensions of the beam specimens are shown in Fig.4-1. All of the tested beams had a 10 x 20cm rectangular cross-section and a total length of 160cm.

Mechanical degree of prestress λ was chosen at two levels of 0.44 and 0.78 for most of tested PPC beams. Conventionally reinforced (λ=0: RC) and fully prestressed (λ=1: PC) beams were also prepared for comparison. These four kinds of beam sections were symmetrically reinforced and designed to have approximately the same ultimate flexural strength among them.

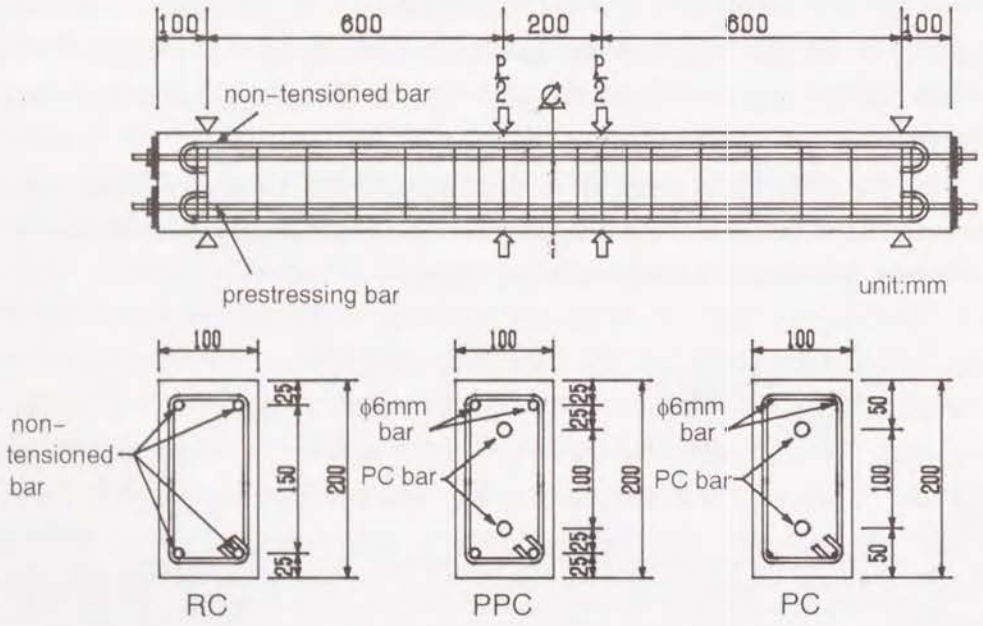

Fig.4-1 Dimensions of Series-A, B and C beams

In addition, supplementary reversed cyclic loading tests were also done on two kinds of unsymmetrically reinforced PPC beams having different λ-values (or ultimate flexural strength) between upper and lower part of section, that is, λ=(upper: 0.44, lower: 0.56) and (0.60, 0.78).

Each pair of two beams with or without ϕ6mm rectangular hoops (f_{syh}=49kgf/mm^2) for lateral confinement, each designated as R-type and N-type, were prepared for two types of reversed cyclic loading. These hoops were arranged at the spacing of s=d/4 (d: effective depth) within an expected plastic hinge region of 50cm length over a mid-span of beam on the basis of the provisions drafted by the New Zealand Concrete Design Code Committee [29]. This value corresponded to the volumetric ratio of lateral confinement of approximately 2.60%. The vertical rectangular stirrups of ϕ6mm were also provided as web reinforcement in the remaining part of span, the amount of which was determined by taking into account the shear resistance of concrete according to the JSCE PC Standard Code [30].

The design compressive strength of concrete was f'_c=400kgf/cm^2 (W/C=53%) throughout the tested beams. A total of 28 beams were tested under three types of loading, that is, Series-A, B and C. Details of beams for each test series are listed in Table 4-1, 4-2 and 4-3, respectively. The prestressing bars arranged in PPC and PC beams were grouted with cement paste of W/C=45% containing an adequate amount of water reducing agent and aluminum powder.

(2) Loading methods

Each beam was hinged at both ends and tested under symmetrical two-points loads with shear span length of 60cm and flexural span length of 20cm as shown in Fig.4-1. Loading patterns were divided into three series as follows.

(a) Series-A (unidirectional cyclic loading)

Series-A tests were done in order to obtain the basic data for the following Series-B and C tests. Loading sequence of Series-A tests is shown schematically in Fig.4-2-(a). The beams were fully unloaded when the load attained the compression fiber strain of mid-span section (ε_c) of 0.001, 0.002, 0.0025, 0.003, the maximum ultimate load (P_u) and also the levels corresponding to the mid-span deflection of δ=20mm (θ=0.029), 25mm (θ=0.036), 30mm (θ=0.043), --- in the falling branch region after P_u, in which θ indicates the rotation angle (θ=2δ/l, l: span length).

(b) Series-B (reversed cyclic loading with one load repetition at each deflection amplitude)

Table 4-1 Details and test results of Series-A beams

Specimens	*1 λ	*2 q	*3 s (cm)	*4 A_s	*5 A_p	*6 σ_p (kgf/cm²)	*7 P_c, (tonf)	*8 P_u (tonf)	*9 P_u' (tonf)	*10 μ
RC-A-N	0	0.184	∞	2-D16	—	—	2.25	9.74	7.64	16.50
PPC1-A-N	0.44	0.231	∞	2-D13	φ9.2-A	44	4.02	9.97	8.13	6.84
PPC2-A-N	0.71	0.252	∞	2-D10	φ13-A	98	4.09	9.47	7.90	3.43
PC-A-N	1.0 (0.86)	0.276	∞	2-φ6	φ13-C	132	5.52	9.00	8.37	2.17

*1) Mechanical degree of prestress. When considering φ6, λ-value of PC-A becomes 0.86.
*2) Steel index.
*3) Spacing of hoops.
*4) Area of non-prestressing reinforcing steel.
D16: A_s=1.986cm², f_{sy}=3700kgf/cm²
D13: A_s=1.267cm², f_{sy}=3800kgf/cm²
D16: A_s=0.713cm², f_{sy}=3600kgf/cm²
D16: A_s=0.283cm², f_{sy}=4900kgf/cm²
*5) Area of prestressing steel.
φ9.2-B: A_p=0.6648cm², f_{py}=11400kgf/cm²
φ13-A: A_p=1.327cm², f_{py}=9400kgf/cm²
φ13-C: A_p=1.327cm², f_{py}=12500kgf/cm²
*6) Introduced prestress.
*7) Measured flexural cracking load.
*8) Measured maximum ultimate load.
*9) Calculated maximum ultimate load.
*10) Ductility factor.

Table 4-2 Details and test results of Series-B beams

Specimens	*1 λ	*2 q	*3 s (cm)	*4 A_s	*5 A_p	*6 σ_p (kgf/cm²)	*7 P_u (tonf)	*8 P_u' (tonf)	*9 μ
RC-B-N	0	0.180	∞	2-D16	—	—	8.66 (8.61)	7.67	5.76 (2.60)
RC-B-R	0	0.180	d/4	2-D16	—	—	9.50 (9.50)	7.67	4.02 (1.84)
PPC1-B-N	0.44	0.231	∞	2-D13	φ9.2-B	49	10.27 (9.56)	8.13	3.52 (5.67)
PPC1-B-R	0.44	0.231	d/4	2-D13	φ9.2-B	48	12.00 (10.44)	8.13	10.00 (7.25)
PPC2-B-N	0.71	0.264	∞	2-D10	φ13-A	91	9.64 (9.13)	8.01	3.83 (4.03)
PPC2-B-R	0.71	0.264	d/4	2-D10	φ13-A	93	9.88 (9.60)	8.01	7.73 (6.33)
PPC3-B-N	0.56 (0.44)	0.303 (0.231)	∞	2-D13	φ13-A (φ9.2-B)	90 (39)	11.56 (9.73)	9.75 (8.13)	2.66 (2.73)
PPC3-B-R	0.56 (0.44)	0.318 (0.243)	d/4	2-D13	φ13-A (φ9.2-B)	98 (40)	10.75 (10.60)	9.65 (8.08)	5.73 (5.73)
PPC4-B-N	0.71 (0.60)	0.264 (0.189)	∞	2-D10	φ13-A (φ9.2-B)	93 (39)	9.75 (7.25)	8.01 (6.25)	2.79 (3.56)
PPC4-B-R	0.71 (0.60)	0.264 (0.189)	d/4	2-D10	φ13-A (φ9.2-B)	89 (40)	9.78 (7.75)	8.01 (6.25)	8.08 (7.50)
PC-B-N	1.0 (0.86)	0.276	∞	2-φ6	φ13-C	111	10.69 (8.81)	8.41	1.53 (2.20)
PC-B-R	1.0 (0.86)	0.276	d/4	2-φ6	φ13-C	115	10.13 (9.13)	8.41	2.09 (3.64)

*1) Mechanical degree of prestress. When considering φ6, λ-value of PC-B becomes 0.86.
The parentheses indicate the values in the negative direction.
*2) Steel index. The parentheses indicate the values in the negative direction.
*3) Spacing of hoops.
*4) Area of non-prestressing reinforcing steel.
D16: A_s=1.986cm², f_{sy}=3700kgf/cm²
D13: A_s=1.267cm², f_{sy}=3800kgf/cm²
D16: A_s=0.713cm², f_{sy}=3600kgf/cm²
D16: A_s=0.283cm², f_{sy}=4900kgf/cm²
*5) Area of prestressing steel.
φ9.2-B: A_p=0.6648cm², f_{py}=11400kgf/cm²
φ13-A: A_p=1.327cm², f_{py}=9400kgf/cm²
φ13-C: A_p=1.327cm², f_{py}=12500kgf/cm²
The parentheses indicate the values in the negative direction.
*6) Introduced prestress. The parentheses indicate the values in the negative direction.
*7) Measured maximum ultimate load. The parentheses indicate the values in the negative direction.
*8) Calculated maximum ultimate load. The parentheses indicate the values in the negative direction.
*9) Ductility factor. The parentheses indicate the values in the negative direction.

Table 4-3 Details and test results of Series-C beams

Specimens	*1 λ	*2 q	*3 s (cm)	*4 A_s	*5 A_p	*6 σ_p (kgf/cm²)	*7 P_u (tonf)	*8 P_u' (tonf)	*9 μ
RC-C-N	0	0.180	∞	2-D16	—	—	8.60 (8.38)	7.67	2.79 (2.77)
RC-C-R	0	0.180	d/4	2-D16	—	—	8.81 (8.31)	7.67	3.57 (5.88)
PPC1-C-N	0.44	0.231	∞	2-D13	φ9.2-A	46	10.31 (9.85)	8.13	2.38 (2.67)
PPC1-C-R	0.44	0.231	d/4	2-D13	φ9.2-A	47	10.49 (9.49)	8.13	4.00 (4.56)
PPC2-C-N	0.71	0.264	∞	2-D10	φ13-A	88	9.64 (8.94)	8.01	1.71 (2.26)
PPC2-C-R	0.71	0.264	d/4	2-D10	φ13-A	92	9.81 (9.19)	8.01	6.94 (5.68)
PPC3-C-N	0.56 (0.44)	0.303 (0.231)	∞	2-D13	φ13-A (φ9.2-B)	100 (38)	12.63 (9.53)	9.75 (8.13)	1.92 (2.84)
PPC3-C-R	0.56 (0.44)	0.318 (0.243)	d/4	2-D13	φ13-A (φ9.2-B)	104 (43)	12.51 (9.63)	9.65 (8.08)	3.64 (4.80)
PPC4-C-N	0.71 (0.60)	0.264 (0.189)	∞	2-D10	φ13-A (φ9.2-B)	91 (35)	11.03 (7.01)	8.01 (6.25)	1.99 (2.76)
PPC4-C-R	0.71 (0.60)	0.264 (0.189)	d/4	2-D10	φ13-A (φ9.2-B)	108 (33)	9.44 (7.51)	8.01 (6.25)	5.24 (6.00)
PC-C-N	1.0 (0.86)	0.276	∞	2-φ6	φ13-C	111	10.44 (8.81)	8.41	1.51 (1.84)
PC-C-R	1.0 (0.86)	0.276	d/4	2-φ6	φ13-C	115	10.38 (9.63)	8.41	1.59 (2.26)

*1) Mechanical degree of prestress. When considering φ6, λ-value of PC-C becomes 0.86.
The parentheses indicate the values in the negative direction.
*2) Steel index. The parentheses indicate the values in the negative direction.
*3) Spacing of hoops.
*4) Area of non-prestressing reinforcing steel.
D16: A_s=1.986cm², f_{sy}=3700kgf/cm²
D13: A_s=1.267cm², f_{sy}=3800kgf/cm²
D16: A_s=0.713cm², f_{sy}=3600kgf/cm²
D16: A_s=0.283cm², f_{sy}=4900kgf/cm²
*5) Area of prestressing steel.
φ9.2-B: A_p=0.6648cm², f_{py}=11400kgf/cm²
φ13-A: A_p=1.327cm², f_{py}=9400kgf/cm²
φ13-C: A_p=1.327cm², f_{py}=12500kgf/cm²
The parentheses indicate the values in the negative direction.
*6) Introduced prestress. The parentheses indicate the values in the negative direction.
*7) Measured maximum ultimate load. The parentheses indicate the values in the negative direction.
*8) Calculated maximum ultimate load. The parentheses indicate the values in the negative direction.
*9) Ductility factor. The parentheses indicate the values in the negative direction.

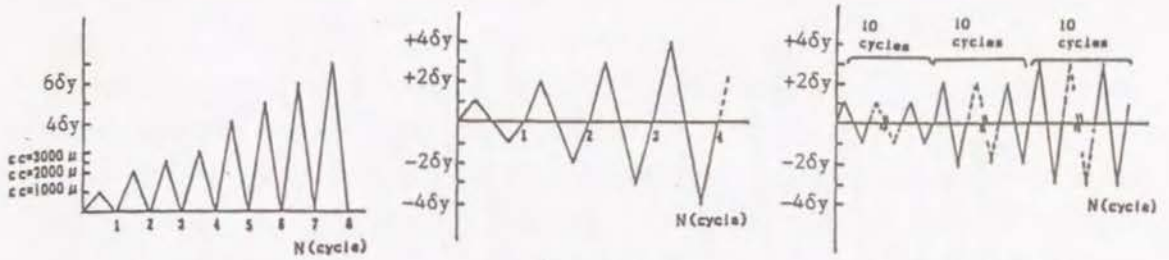

(a) Series-A (b) Series-B (c) Series-C

Fig.4-2 Loading sequences

As shown in Fig.4-2-(b), each one cycle of load reversal was given at gradually increased deflection amplitude of $\delta=\pm\delta_y$ ($\theta=\pm 0.007$), $\pm 2\delta_y$, $\pm 3\delta_y$, --- (δ_y=5mm: chosen in these tests as the mid span deflection at first yielding of RC beams).

(c) Series-C (reversed cyclic loading with ten load repetitions at each deflection amplitude)

As shown in Fig.4-2-(c), reversed cyclic loading with load repetitions of ten cycles was applied at several levels of deflection amplitude of $\delta=\pm\delta_y$ ($\theta=\pm 0.007$), $\pm 2\delta_y$, $\pm 3\delta_y$, ---.

4.3.2 Results of Tests and Discussions

(1) Series-A

All beams in Series-A tests failed ultimately in flexure. In Table 4-1 are shown their measured flexural cracking loads (P_{cr}) and maximum ultimate loads (P_u) together with the calculated ultimate one (P_u'). P_u' is calculated by the conventional ultimate strength theory using rectangular stress block equal to 0.85 times of cylinder concrete strength (f'_c) and yield strength of steels (f_{sy}, f_{py}). Ductility factor (μ) in Table 4-1 was defined in the term of two mid-span deflections at $0.9P_u$ on the ascending and falling branch curves given by envelope of the load - deflection hysteresis.

Flexural cracking strength is clearly found to increase with increasing λ-value, when reinforced to have approximately the same maximum ultimate strength.

Fig.4-3 shows the measured load - deflection (P - δ) hysteresis of Series-A beams together with each theoretical P - δ envelope curve, which was calculated

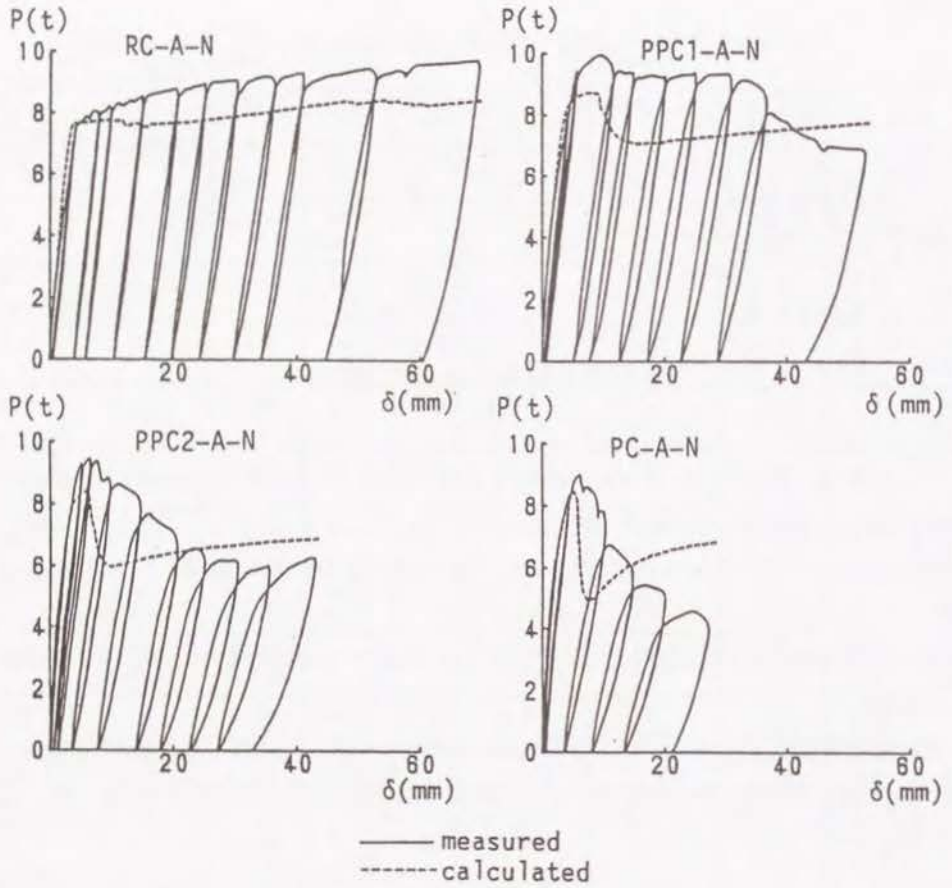

Fig.4–3 Load – deflection hysteresis loops (Series–A)

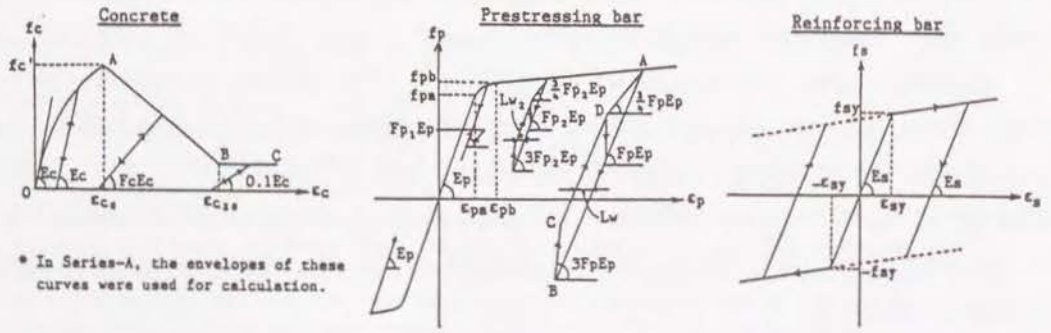

Fig.4–4 Modified stress – strain relationships of constitutive materials

by modifying the stress – strain relationships of constitutive materials proposed by Park et al. [1, 31] as illustrated in Fig.4–4. As seen in Fig.4–3 and Table 4–1, beam ductility decreases with increasing λ–value. Theoretical P–δ envelope curve of each beam coincides well with each measured one.

On the other hand, the elastic recoveries are compared among four tested beams in Fig.4–5, which are expressed by restoring index (α) as defined in the term of ratio of restoring mid–span deflection at full unloading to total one. Elastic recovery of RC beams is considerably smaller within the range of $\theta \leq 0.03$. On the other hand, even in PPC beams having a relatively small λ–value of 0.44, the index α is well in excess of 0.9 before the maximum ultimate load ($\theta < 0.01$). Within the falling branch region after that, however, α–value commences to decrease rapidly irrespective of the magnitude of λ.

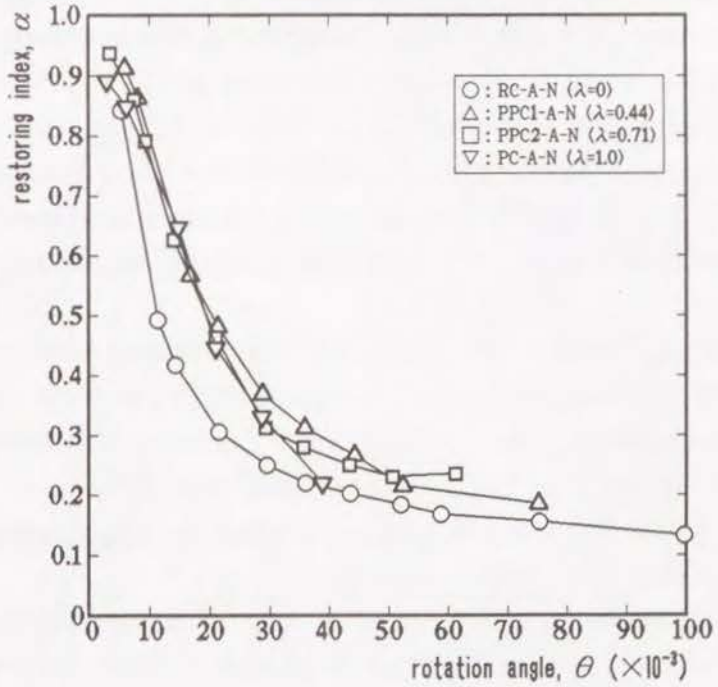

Fig.4–5 Elastic recovery expressed by restoring index (Series–A)

(2) Series-B

(a) Ultimate strength and failure mode

All of PPC beams as well as PC ones failed ultimately in flexure under reversed cyclic loading as done in Series-B tests. On the other hand, RC beams showed brittle shear failure due to significant reduction in effectiveness of concrete shear resistance mechanism after the formation of X-shaped diagonal shear cracks at $\delta=\pm 4\delta_y$, although these failed in flexure in a more ductile manner under unidirectional loading.

In Table 4-2 are shown the measured maximum ultimate loads (P_u) together with theoretical ones (P_u') estimated by the same method as done for Series-A beams. It is indicated in Table 4-2 that the measured maximum ultimate load of any beam including RC beams is well in excess of the theoretical one even under the reversed cyclic loading.

(b) Deformation property

Fig.4-6 shows the measured load - deflection (P - δ) hysteresis of Series-B beams together with the theoretical P - δ envelope curves obtained by the same method as applied for Series-A and also the measured P - δ envelope curve of each corresponding Series-A beam. And then, in Fig.4-7 are shown some examples of the moment - curvature (M - ϕ) hysteresis loops measured within the maximum moment span together with the theoretical ones calculated on the basis of stress - strain relationships of constitutive materials as already illustrated in Fig.4-4.

Load carrying capacity of N-type beams without lateral confinement reduces rapidly once the cyclic load exceeded P_u. This strength reduction becomes more remarkable in the beams having a higher λ-value. However, it is clearly indicated in Table 4-2 and Fig.4-6 that the ductility of PPC and PC beams which failed ultimately in flexure can be improved remarkably by using laterally confined concrete at the compression zone of section.

Comparing the measured P - δ envelopes of corresponding two beams between Series-B and Series-A tests, the reduction in load carrying capacity is found to commence somewhat earlier in the former than in the latter.

In RC beams, a significant pinching effect in P - δ hysteresis loops is observed due to the extensive diagonal shear cracks at about $\delta=\pm 6\delta_y$ ($\theta=\pm 0.043$), although stable before $\delta=\pm 5\delta_y$ ($\theta=\pm 0.036$).

As shown in Fig.4-7, the M - ϕ hysteresis loops for any type of PPC beams can be well estimated by the above mentioned analysis.

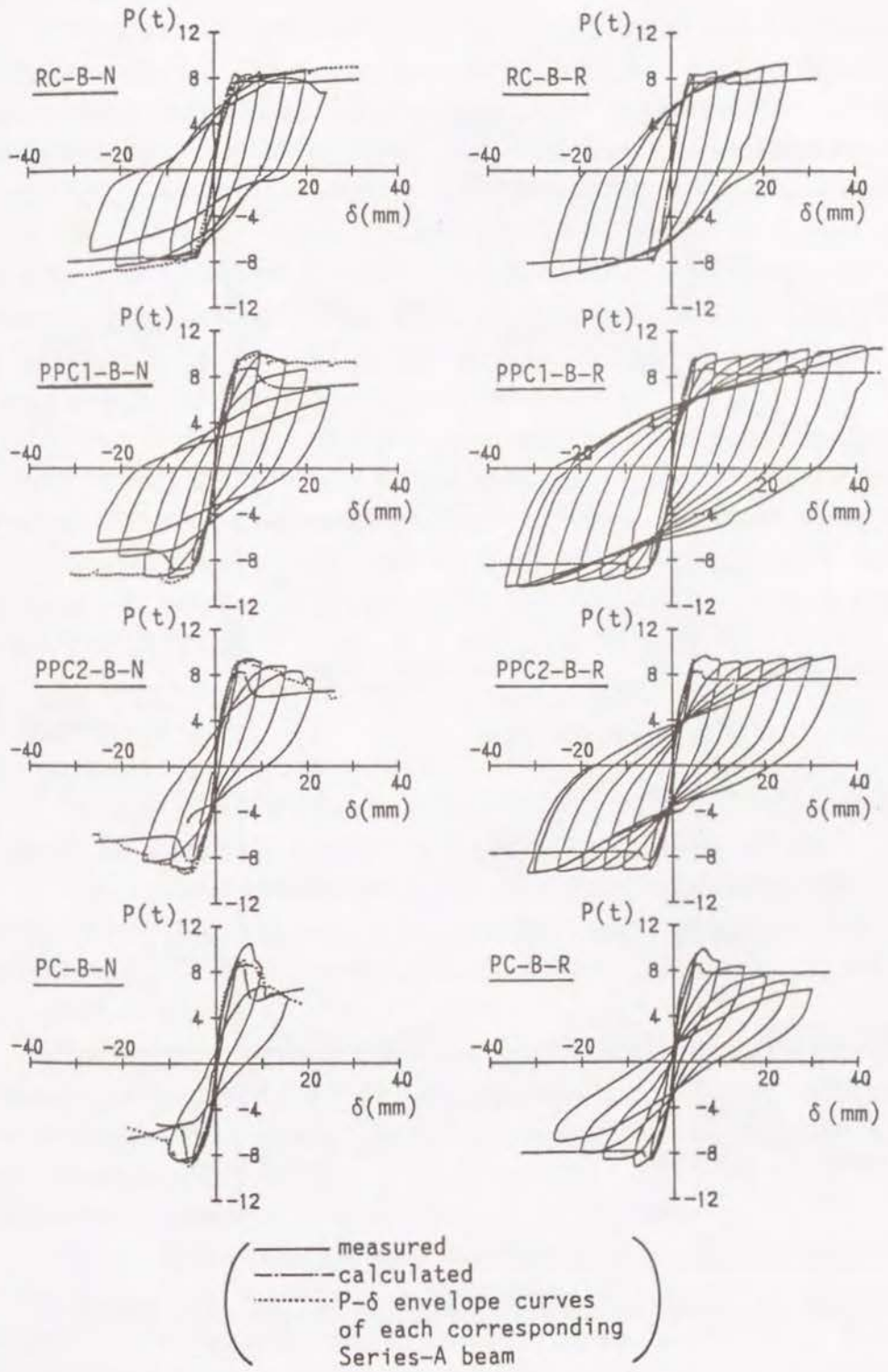

Fig.4-6 Load - deflection hysteresis loops (Series-B)

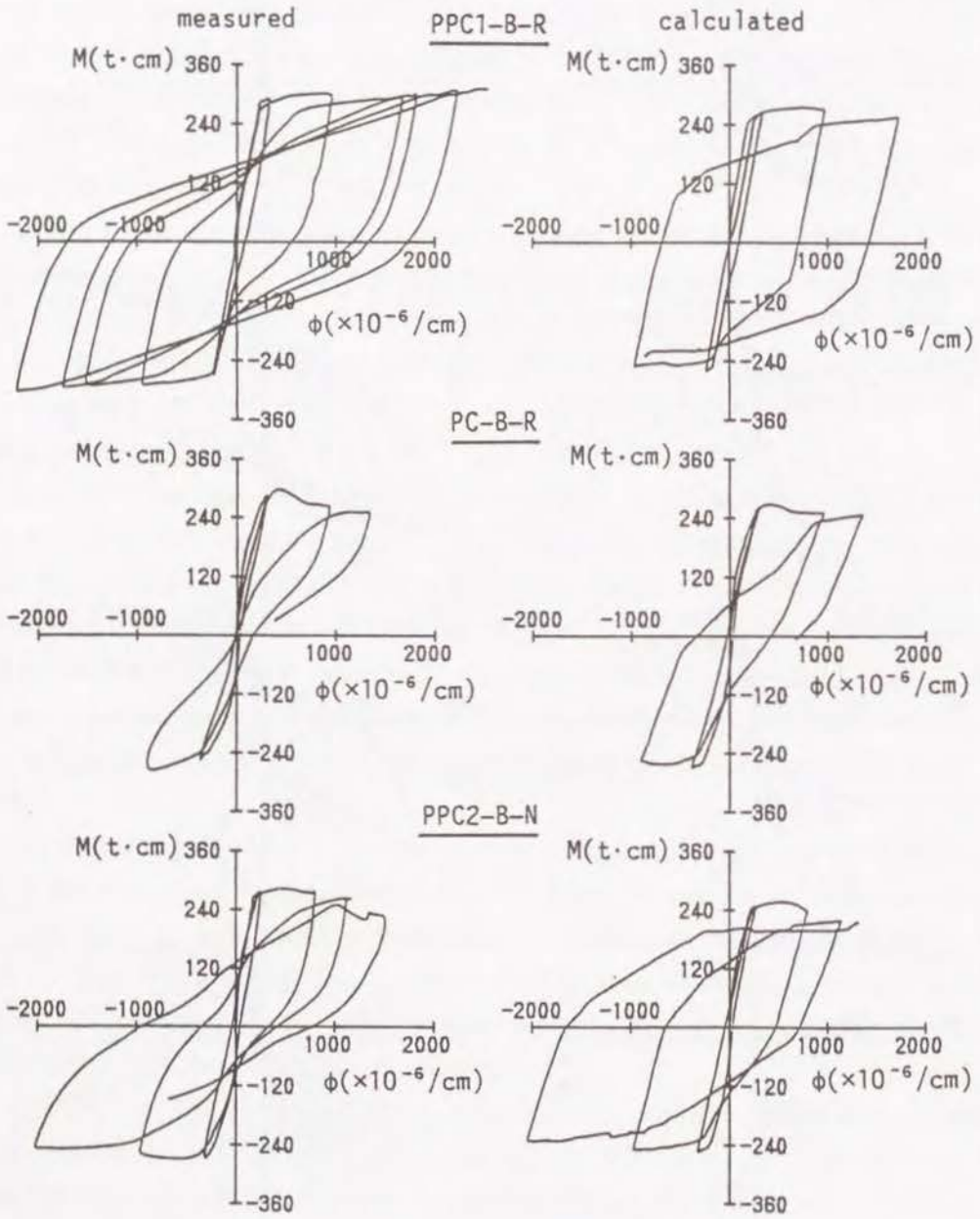

Fig.4-7 Examples of moment - curvature hysteresis loops (Series-B)

(c) Equivalent coefficient of damping

The equivalent coefficients of damping (h_{eq}) obtained from the measured P-δ hysteresis loops of Series-B beams are shown in Fig.4-8. The h_{eq}-value increases with increase in the deflection amplitude or rotation angle (θ). When compared at the same θ-value of θ<0.021, the h_{eq}-value of RC beam is considerably larger than that of PPC beam, but commences to decrease due to pinching effect after $\theta \geq 0.021$. It can be observed in PPC and PC beams that the h_{eq}-value of N-type tends to increase more rapidly with increase in θ-value and to be higher than that of R-type. However, a significant difference cannot be recognized in the h_{eq}-values between RC beams of N-type and R-type because of the extensive shear cracks irrespective of beam types.

Comparing the h_{eq}-value of unsymmetrically reinforced PPC beam with that of symmetrically reinforced one, both of which had the same mechanical degree of prestress (λ) or steel index (q) in one side of section, as shown in Fig.4-9, the former is somewhat smaller than the latter when another side of section is reinforced with higher λ or q-value (PPC3 vs PPC1), while larger in the opposite case (PPC4 vs PPC2).

(3) Series-C

(a) Ultimate strength and failure mode

All of PPC and PC beams failed in flexure, although RC beams failed in shear at load reversals of $\delta = \pm 6\delta_y$ ($\theta = \pm 0.043$) as well as Series-B tests.

It is indicated in Table 4-3 that an attainable negative maximum ultimate load of Series-C beams tends to be somewhat small compared with that of each corresponding Series-B beam, although any one was well in excess of the theoretical value.

The results of Series-B and Series-C tests confirmed that the introduction of prestress of about 50kgf/cm^2 to the beam, as done in the tested PPC beams of λ=0.44, is very effective for preventing the degradation of concrete shear resistance under reversed cyclic loading.

(b) Deformation property

Fig.4-10 shows the measured load - deflection (P - δ) hysteresis of Series-C beams. And then, Fig.4-11 shows the strength reduction (P/P_{max}: average value for positive and negative sides) with repeated cycles, in which P_{max} denotes the maximum load at each deflection amplitude. It is indicated in Fig.4-10 and Fig.4-11 that the reduction in strength after 10 cycles of load reversals, for instance at

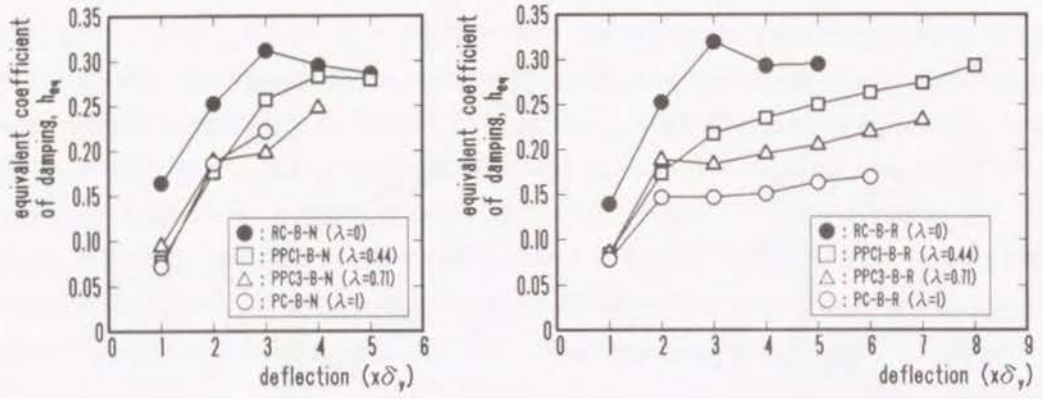

Fig.4-8 Equivalent coefficient of damping (Series-B, Effect of λ)

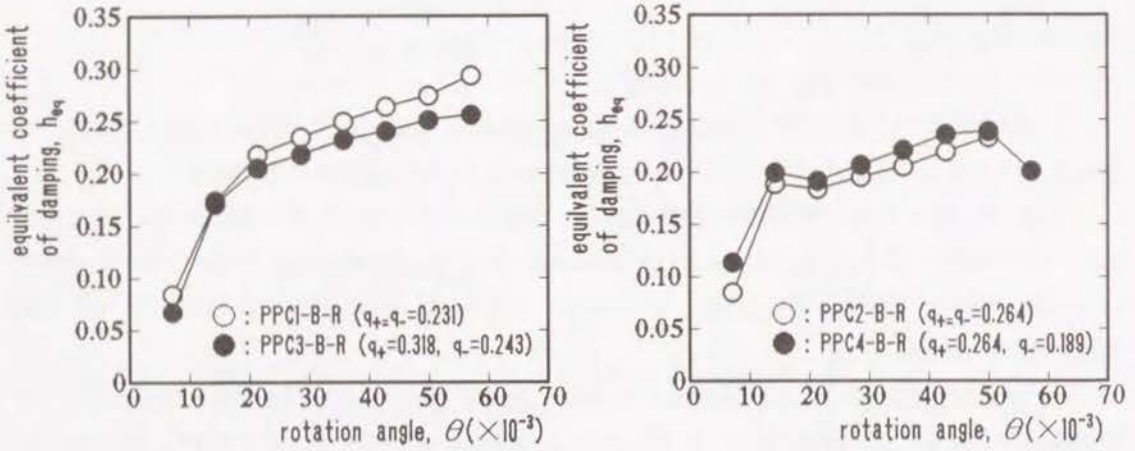

Fig.4-9 Comparison of h_{eq} between unsymmetrically and symmetrically reinforced beams (Series-B)

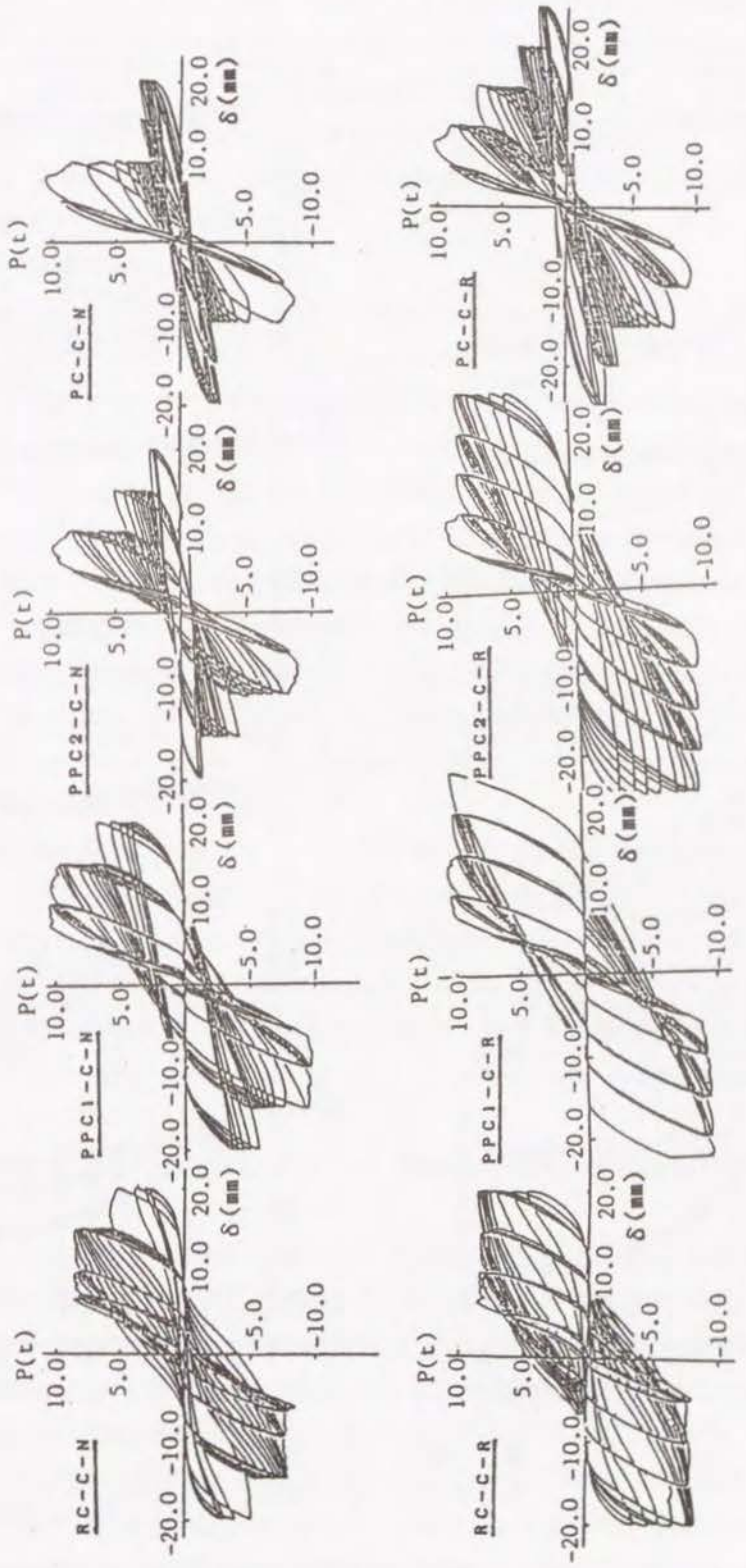

Fig.4-10 Load - deflection hysteresis loops (Series-C)

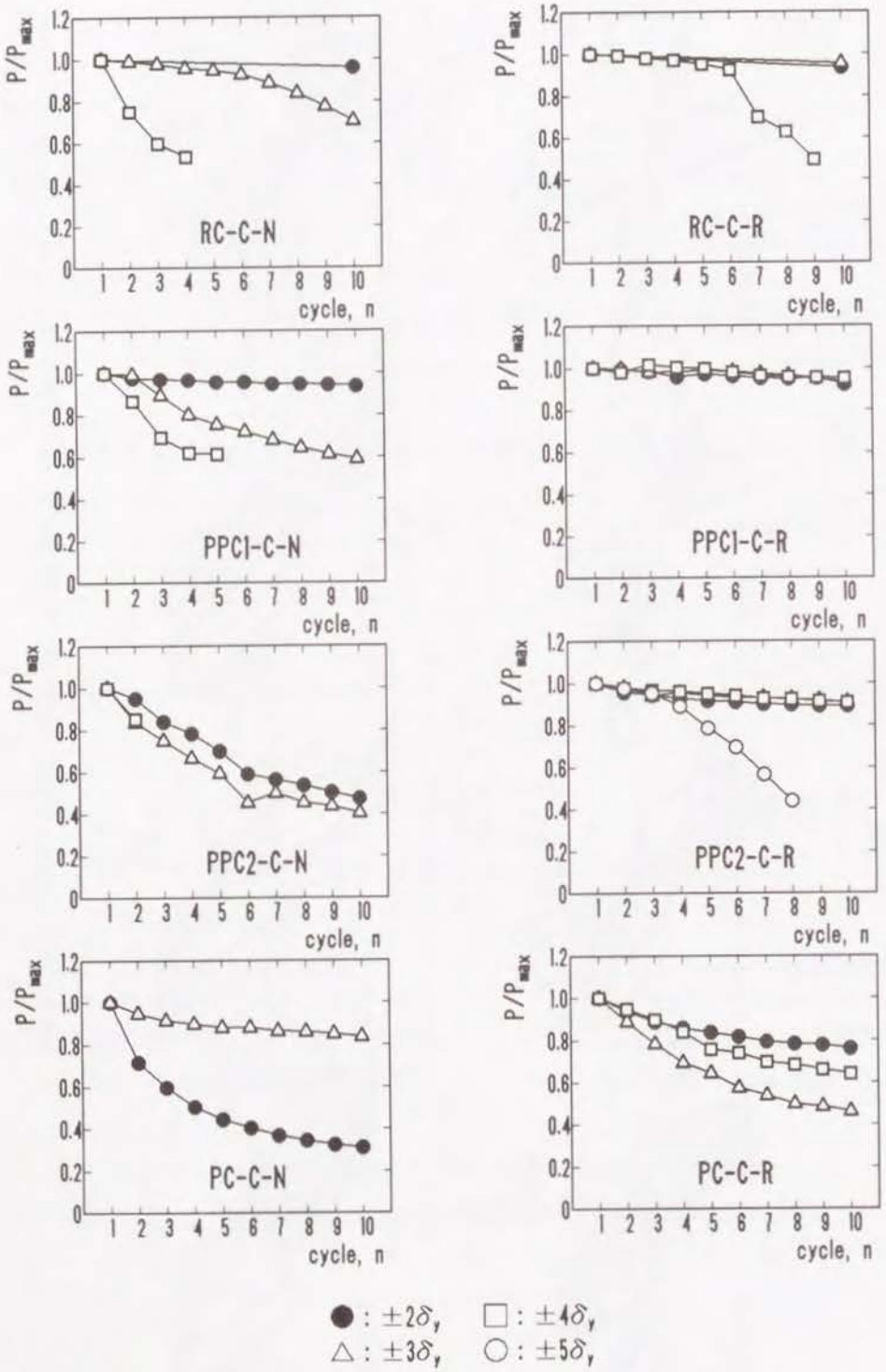

Fig.4-11 Strength reduction with repeated cycles (Sereis-C)

$\delta=\pm 4\delta_y$, is only less than 10% in all of PPC beams with lateral confinement. However, remarkable strength deterioration with increased number of load reversals at $\delta=\pm 3\delta_y$ is observed in PC beams due to progressive crushing and spalling of concrete even if lateral confinement is arranged.

Similar tendency is recognized at $\delta=\pm 4\delta_y$ in RC beams due to the development of X-shaped cracks.

(c) Equivalent coefficient of damping

The relations between equivalent coefficients of damping (h_{eq}) and repeated cycles are shown in Fig.4-12. The h_{eq}-value of PPC and PC beams decreases somewhat abruptly at the second cycle of relatively small deflection amplitude of $\delta=\pm 2\delta_y$, but any marked change of h_{eq}-value can not be observed up to the tenth cycle after the third cycle. On the other hand, at larger deflection amplitudes of $\delta\geq\pm 4\delta_y$, the h_{eq}-value of these beams tends to increase with repeated cycles at a constant deflection amplitude, while that of RC beams decreases rather rapidly because of the pinching effect caused by the gradual development of shear cracks with repeated cycles. It is also found in Fig.4-12 that the h_{eq}-value increases with decrease in λ-value when $\delta\leq\pm 3\delta_y$, but that h_{eq} of RC beams decreases rapidly with repeated cycles when $\delta>\pm 3\delta_y$, resulting in a somewhat small value compared with both of PPC and PC beams.

As typically shown in Fig.4-13, the same tendency as observed in Series-B tests can be recognized as for the difference of h_{eq}-values between unsymmetrically and symmetrically reinforced PPC beams. And also, any remarkable difference can not be found in the change of h_{eq}-value with repeated cycles at a given deflection amplitude between these two types of beams.

4.3.3 Summary of the Results on Partially Prestressed Concrete Beams

(1) All of tested PPC beams of $\lambda\geq 0.44$ as well as PC beams failed ultimately in flexure. On the other hand, RC beams showed brittle shear failure due to significant reduction in effectiveness of concrete shear resistance mechanism after the formation of extensive X-shaped diagonal cracks under reversed cyclic loading at $\delta=\pm 4\delta_y$, although these failed in flexure under unidirectional loading.

(2) Loss in strength after ten cycles of load reversals, for instance at $\pm 4\delta_y$ is only less than 10% in all of PPC beams with lateral confinement. However remarkable strength deterioration with increased number of load reversals at $\delta=\pm 3\delta_y$ is

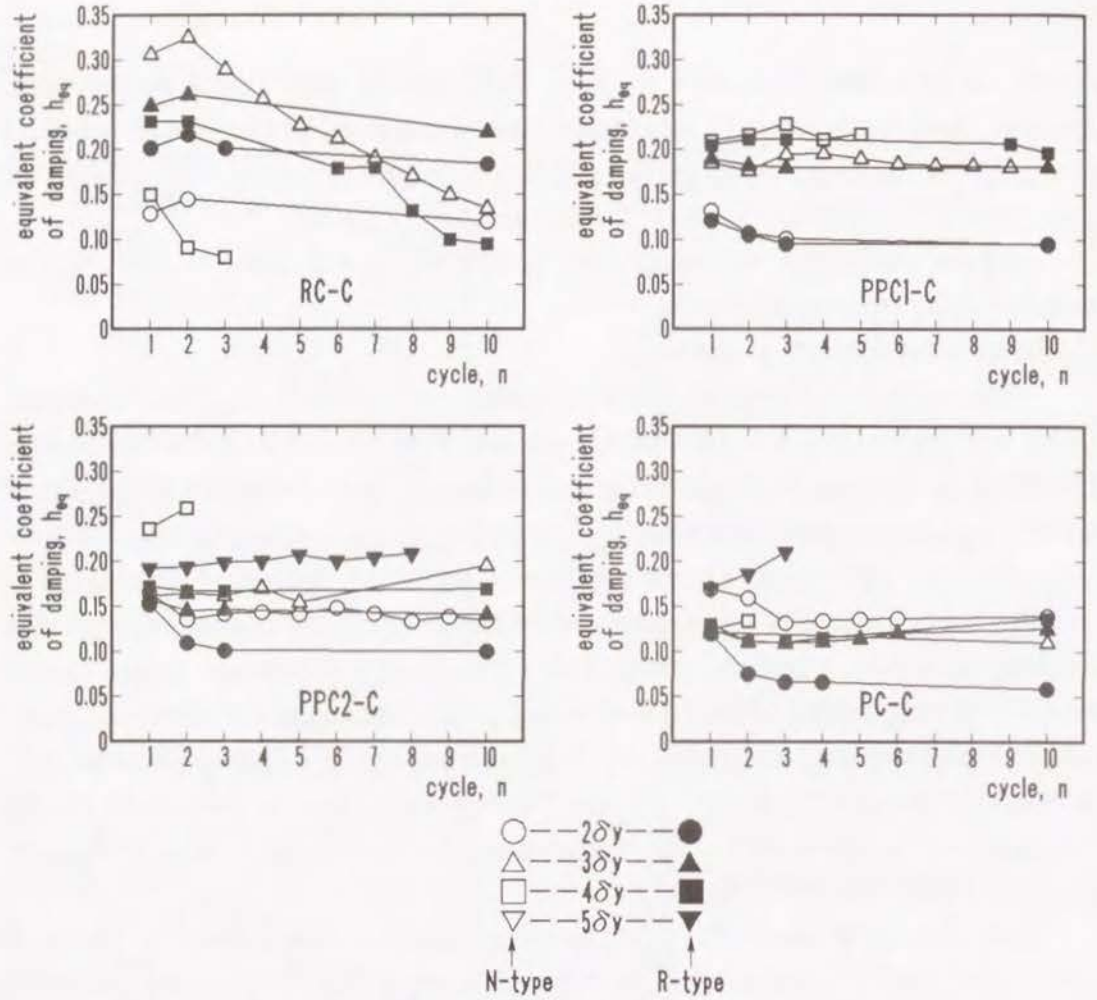

(a) Effect of applied deflection amplitude

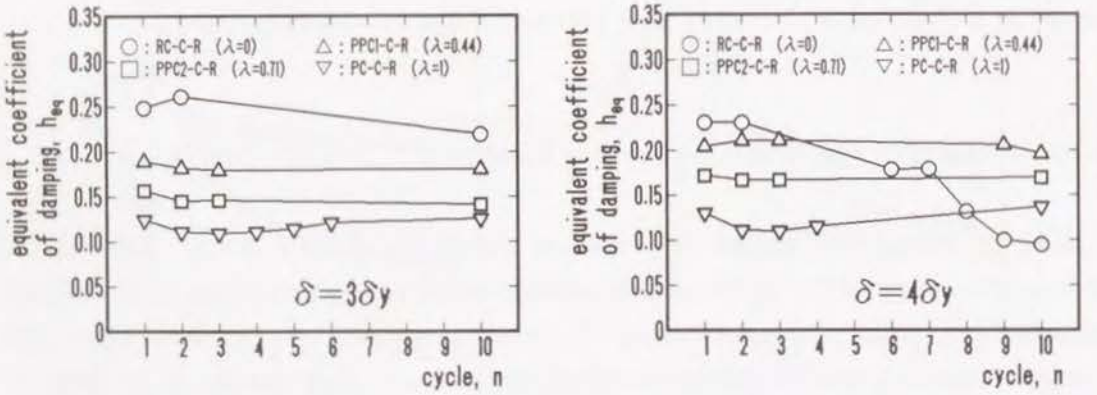

(b) Effect of λ

Fig.4-12 Changes of h_{eq} with repeated cycles (Series-C)

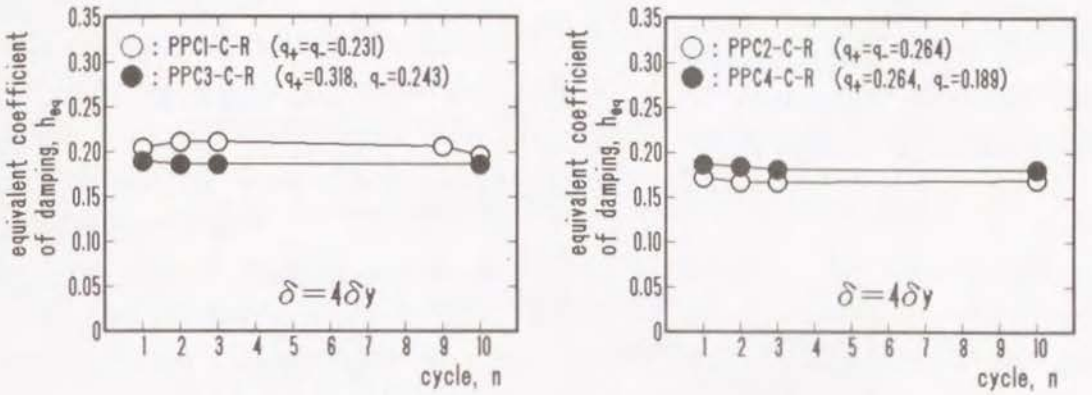

Fig.4-13 Comparison of h_{eq} between unsymmetrically and symmetrically reinforced beams (Series-C)

observed in PC beams due to progressive crushing and spalling of concrete even if lateral confinement is arranged, and similar tendency is recognized at $\delta = 4\delta_y$ in RC beams due to significant development of X-shaped diagonal cracks.

(3) Equivalent coefficient of damping as well as dissipated energy is significantly affected not only by beam types (mechanical degree of prestress, spacing of hoops) but also by reversed cyclic loading conditions (deflection amplitude, repeated cycles).

(4) Moment - curvature hysteresis loops for any types of PPC beams can be well estimated by taking into account the stress - strain relationship of constitutive materials and effect of lateral confinement.

(5) The results of these fundamental tests implies that the inelastic behaviors of PPC beam under reversed cyclic loading as experienced with earthquake action is favorable in comparison with RC or PC beam.

4.4 INELASTIC BEHAVIOR OF UNBONDED PRESTRESSED CONCRETE BEAMS [32, 33]

4.4.1 Experimental Procedures

All of the tested beams were of a rectangular section of width (b) x full depth (h) = 10 x 20cm and a total length of 160cm. Test programs consist of two series, that is, Series-D and Series-E, and the details of each test series are as follows.

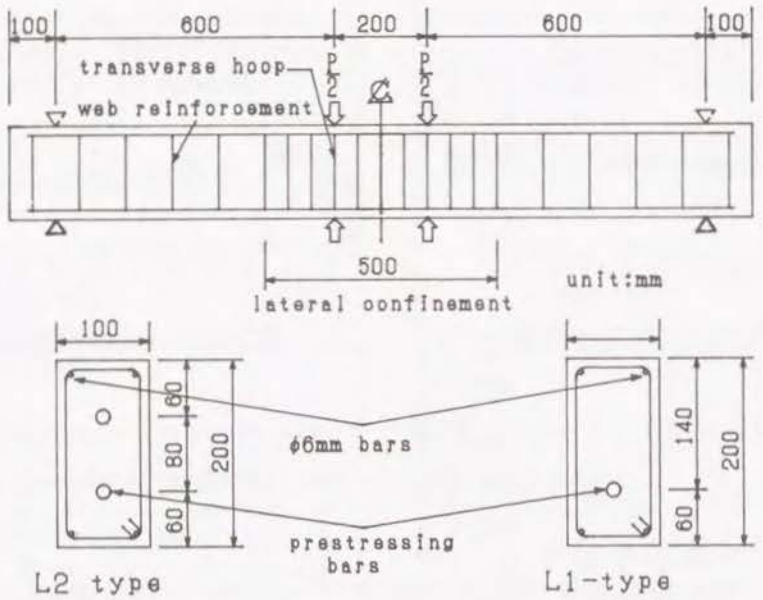

Fig.4-14 Dimensions of Series-D beams

(1) Series-D

(a) Specimens

In this series, unbonded prestressed concrete beams without grouting of cement paste were used together with the corresponding bonded ones. In these beams, prestressing bars were used for prestressing steel. The details of the cross section of these beams are shown in Fig.4-14. A half number of Series-D beams, subjected to reversed loading, were uniformly prestressed, whereas the remaining half number of beams, which were subjected to unidirectional loading, were non-uniformly prestressed with one prestressing bar.

The main test variables are as follows.

a) prestressing steel index (q): 0.133, 0.216 and 0.241.

b) spacing of hoops for lateral confinement (s): ∞, d/2 and d/4. These corresponded to the volumetric ratio of ρ_s=0%, 1.39% and 2.78%, respectively.

Concrete of f'_c=450kgf/cm^2 (W/C=44%) was used in all of Series-D beams. The ϕ6mm hoops of f_{sy}=49kgf/mm^2 were arranged at the prescribed spacings within 50cm length over a mid-span, which covered the plastic hinge zone. In order to prevent the premature shear failure, web reinforcement of ϕ6mm vertical stirrups were provided in the remaining parts of the span. The amount of web reinforcement

was determined based on the JSCE PC Code [30], in which the shear carried by concrete (V_c) was taken into account in contrast to the New Zealand Code [3] and FIP Recommendation [34] which assume V_c to be zero for reversed cyclic loading because of reduction in the effectiveness of the concrete shear resistance mechanism. The details of Series-D beams are listed in Table 4-4.

(b) Loading methods

A total of 12 simply supported beams were tested under symmetrical two points load with a/d_p ratio of 4.3. Two patterns of cyclic loadings with or without load reversals were adopted. The former type of loading corresponds to L2 and the latter to L1 in Table 4-4.

In L1 type of loading, the beams were fully unloaded at each repetition when the load attained the compression fiber strains of mid-span section (ε_c) of 0.001, 0.002, (0.0025), 0.003, the maximum ultimate (P_u) and also some levels on the falling branch of load - mid-span deflection curve. On the other hand, in the beams of L2 type of loading, in which hoops were arranged at the spacing of s=d/4, each mid-span deflection amplitude was kept nearly equal in the positive and negative directions. Each amplitude corresponded to ε_c of 0.001, 0.002, (0.0025), 0.003 and P_u, on the positive run and some levels on the falling branch curve.

(2) Series-E

(a) Specimens

In Series-E, unbonded prestressed concrete beams with polyethylene sheathed 7-ply unbonded prestressing strand filled with grease were used together with the corresponding bonded beams. The details of the cross section and the anchorage are shown in Fig.4-15. The adopted test variables are as follows.

i) prestressing steel index (q): 0.18 and 0.26.

ii) spacing of hoops for lateral confinement (s): ∞ and d/4. These values correspond to ρ_s=0% and 2.43%, respectively.

The design compressive strength of concrete was 550kgf/cm^2, and the hoops and vertical stirrups were arranged in the same manner as Series-D beams.

One pair of beams, unbonded and bonded, were prepared for each test variable. The details of Series-E beams are shown in Table 4-5.

(b) Loading methods

In total, 16 simply supported beams were tested under symmetrical two points load with a/d_p ratio of 3.75. Loading patterns similar to those used in Series-D were adopted. In reversed cyclic loading, however, unloading was done at the

Table 4-4 Details and test results of Series-D beams

Specimens	*1 Loading Type	*2 Bonded or Unbonded	*3 q	*4 s (cm)	*5 A_p	*6 σ_p (kgf/cm²)	*7 P_{cr} (tonf)	*8 P_u (tonf)	*9 P_u' (tonf)	*10 μ
D-1	L1	U	0.216	∞	φ13-B	110	4.00	7.70	7.24	7.5
D-2		B				113	4.40	7.80	8.58	7.7
D-3		U		d/2		113	4.00	7.26	7.21	12.2
D-4		B				114	3.60	8.00	8.58	>9.5
D-5		U		d/4		85	3.60	7.33	7.33	>12.9
D-6		B				116	4.00	8.58	8.58	>12.7
D-7	L2	U	0.133	d/4	φ11-B	78	3.50 (3.20)	7.20 (5.80)	5.67	5.7
D-8		B				74	3.60 (3.60)	7.30 (6.70)	6.95	12.0
D-9		U	0.216		φ13-B	102	3.60 (3.60)	7.60 (6.22)	7.29	8.6
D-10		B				103	3.20 (3.20)	8.20 (7.74)	8.58	11.4
D-11		U	0.241		φ17-A	121	5.10 (5.10)	9.08 (8.20)	9.42	>9.2
D-12		B				138	5.20 (4.80)	10.33 (9.28)	10.67	9.1

*1) L1: Unidirectional loading, L2: Reversed cyclic loading.
*2) U: Unbonded, B: Bonded.
*3) Steel index.
*4) Spacing of hoops.
*5) Area of prestressing steel.
φ11-B: A_p=0.9503cm², f_{py}=11200kgf/cm²
φ13-B: A_p=1.327cm², f_{py}=11000kgf/cm²
φ17-A: A_p=2.27cm², f_{py}=8500kgf/cm²
*6) Introduced prestress.
*7) Measured flexural cracking load. The parentheses indicate the values in the negative direction.
*8) Measured maximum ultimate load. The parentheses indicate the values in the negative direction.
*9) Calculated maximum ultimate load.
*10) Ductility factor in the positive direction.

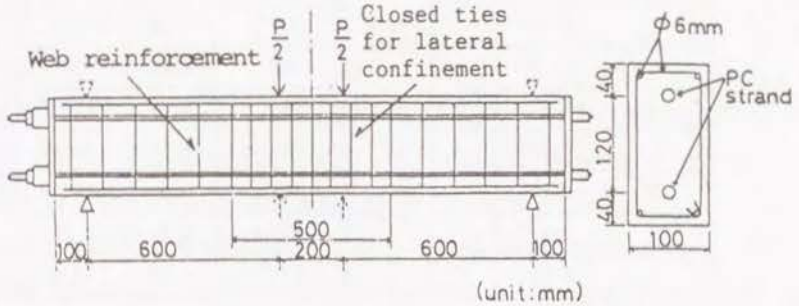

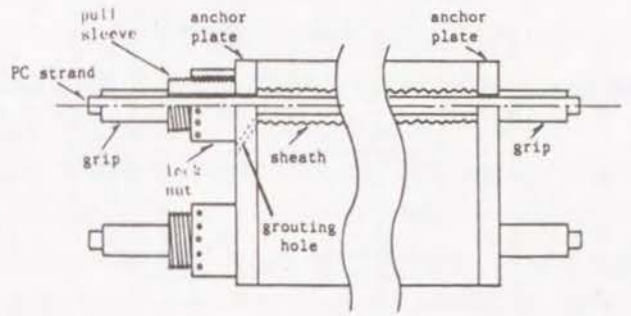

Fig.4-15 Dimensions of Series-E beams and details of its anchorage zone

Table 4-5 Details and test results of Series-E beams

Specimens	*1 Loading Type	*2 Bonded or Unbonded	*3 q	*4 s (cm)	*5 A_p	*6 σ_p (kgf/cm²)	*7 P_{cr} (tonf)	*8 P_u (tonf)	*9 P_u' (tonf)	*10 μ
E-1	L1	U	0.186	∞	7-ply 12.4mm	121	4.50	8.66	8.09	3.7
E-2		B	0.154			121	4.30	10.10	9.34	3.3
E-3		U	0.186	d/4		109	4.50	8.07	7.59	>15.8
E-4		B	0.167			113	5.00	10.46	9.28	>8.6
E-5		U	0.269	∞	7-ply 15.2mm	163	6.00	10.17	9.88	3.6
E-6		B	0.243			164	5.50	12.38	12.17	2.5
E-7		U	0.271	d/4		175	4.50	9.48	10.31	7.7
E-8		B	0.247			171	6.00	12.60	12.15	>9.3
E-9	L2	U	0.186	∞	7-ply 12.4mm	109	3.00 (3.00)	8.21 (7.87)	7.59	4.1
E-10		B	0.152			112	5.00 (4.00)	8.75 (8.43)	9.35	5.6
E-11		U	0.186	d/4		117	5.00 (3.00)	7.59 (7.51)	7.92	>9.2
E-12		B	0.167			109	5.50 (5.00)	10.39 (9.66)	9.28	>5.2
E-13		U	0.269	∞	7-ply 15.2mm	159	5.00 (4.00)	8.98 (8.37)	9.72	3.7
E-14		B	0.243			168	6.50 (6.00)	12.40 (10.59)	11.97	2.9
E-15		U	0.271	d/4		161	5.50 (4.50)	8.74 (9.20)	9.79	4.5
E-16		B	0.247			165	6.10 (5.00)	11.63 (11.61)	12.31	>5.7

*1) L1: unidirectional loading, L2: Reversed cyclic loading.
*2) U: Unbonded, B: Bonded.
*3) Steel index.
*4) Spacing of hoops.
*5) Area of prestressing steel.
7-ply 12.4mm: A_p=0.9203cm², f_{py}=17200kgf/cm²
7-ply 15.2mm: A_p=1.385cm², f_{py}=16600kgf/cm²
*6) Introduced prestress.
*7) Measured flexural cracking load. The parentheses indicate the values in the negative direction.
*8) Measured maximum ultimate load. The parentheses indicate the values in the negative direction.
*9) Calculated maximum ultimate load.
*10) Ductility factor in the positive direction.

deflection amplitudes corresponding to ε_c=0.002, maximum ultimate load and the rotation angle of $\theta \fallingdotseq 0.029$.

4.4.2 Results of Tests and Discussions

(1) Series-D

(a) Load carrying capacities

In all of the beams, the first flexural cracking occurred when ε_c on the initial positive run was less than 0.001, and the negative flexural cracking strength was almost equal to the positive one as shown in Table 4-4.

The unbonded beam (B7), having a low steel index of q=0.133 and narrow hoop spacing of s=d/4, failed finally by rupture of prestressing steel at extremely large mid-span deflection of approximately 40mm. The final failure in the other beams were caused by crushing of concrete without rupture of prestressing steel.

In Table 4-4 are shown the measured maximum ultimate loads (P_u) together with the calculated ones (P_u'). P_u' of the unbonded beams were calculated by using Eq.(4-5) proposed by Mattock et al.. As indicated in Table 4-4, P_u of the unbonded beam is less than that of a comparable bonded beam, irrespective of the loading types. However, its reduction ratio is at most 15%.

The measured ultimate loads of unbonded beams coincide well with the calculated ones by assuming the rectangular stress block equal to $0.85f'_c$ of concrete and the stress in prestressing steel at the ultimate state (f_{ps}) derived from Eq.(4-5). Even after subjected to high intensity reversed cyclic loading, the ultimate flexural strength of unbonded beams scarcely reduced compared with the calculated value except for the beam D-11 with the largest q-value.

The significant shear cracks did not occur up to failure in all of the beams. This suggests that the requirement for web reinforcement as provided in the JSCE PC Code [30] may be conservative for the post-tensioned beam, whether it is bonded or unbonded, which is subjected to load reversals well into the inelastic range.

It is indicated in Fig.4-16 that the ratio of negative maximum load to positive one (P^-/P^+) at each repeated cycle of the same deflection amplitude tends to be smaller in the unbonded beams in the region of rotation angle $\theta \geqq 0.010$ than the bonded ones. This result suggests that the flexural rigidity in the negative loading run of unbonded beams can be more remarkably reduced by the previous positive

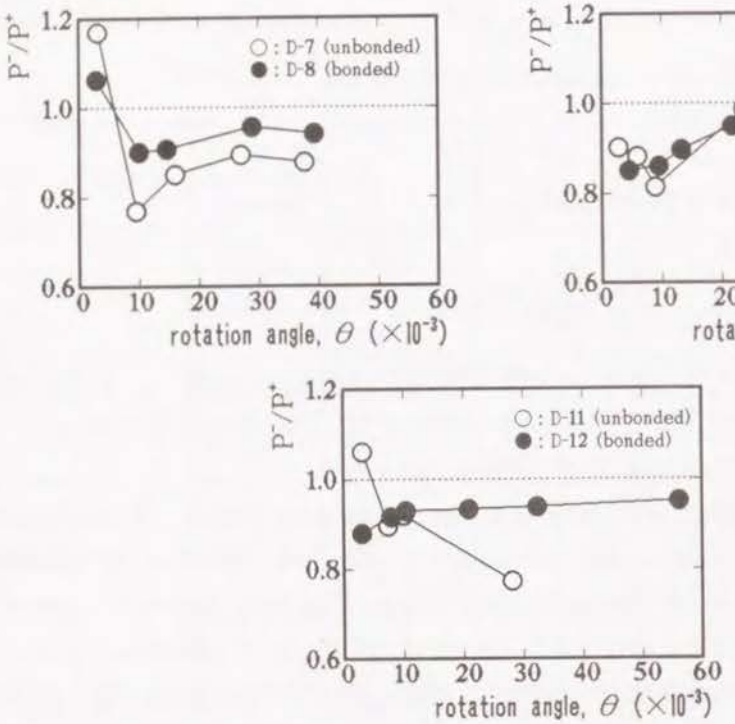

Fig.4-16 Ratio of negative attainable load (P^-) to positive one (P^+) at each cycle (L2 Type of Series-D)

run compared with bonded beams.

(b) Elastic recovery

In Fig.4-17 are shown some examples of elastic recovery on unloading, being expressed by restoring index (α) as defined before. The unbonded beams show that, up to failure somewhat marked elastic recovery in comparison with the bonded ones, especially in the range of $\theta \geq 0.030$.

(c) Equivalent coefficient of damping

In Fig.4-18 are shown the equivalent coefficients of damping (h_{eq}) under reversed cyclic loading (L2-type). Except for the case of q=0.133, in which the h_{eq}-values of unbonded beam is considerably larger than those of bonded one, h_{eq}-values are not so much different between unbonded and bonded beams. This is mainly due to the debonding of prestressing steel aggravated by high intensity load reversals [35], and confirms the previous results of tests that the energy absorption for grouted bars was only 10 to 20% greater than ungrouted bars [36].

On the other hand, h_{eq}-values of unbonded beams are affected by q-values, that is, h_{eq}-value at the same rotation angle tends to be smaller with increase in q-

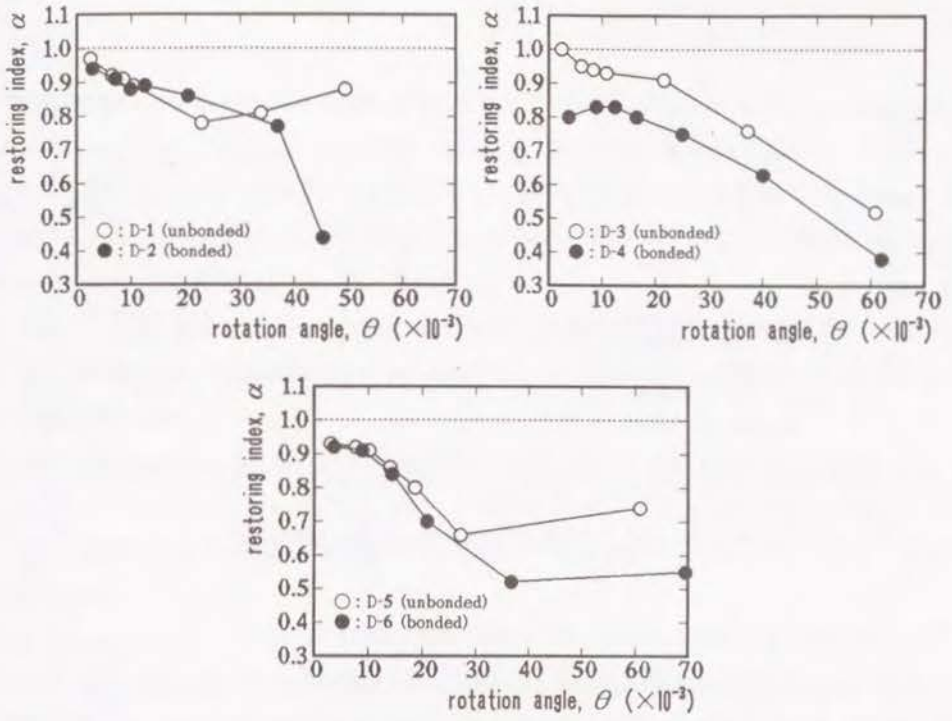

Fig.4-17 Elastic recovery expressed by restoring index (L1 Type of Series-D)

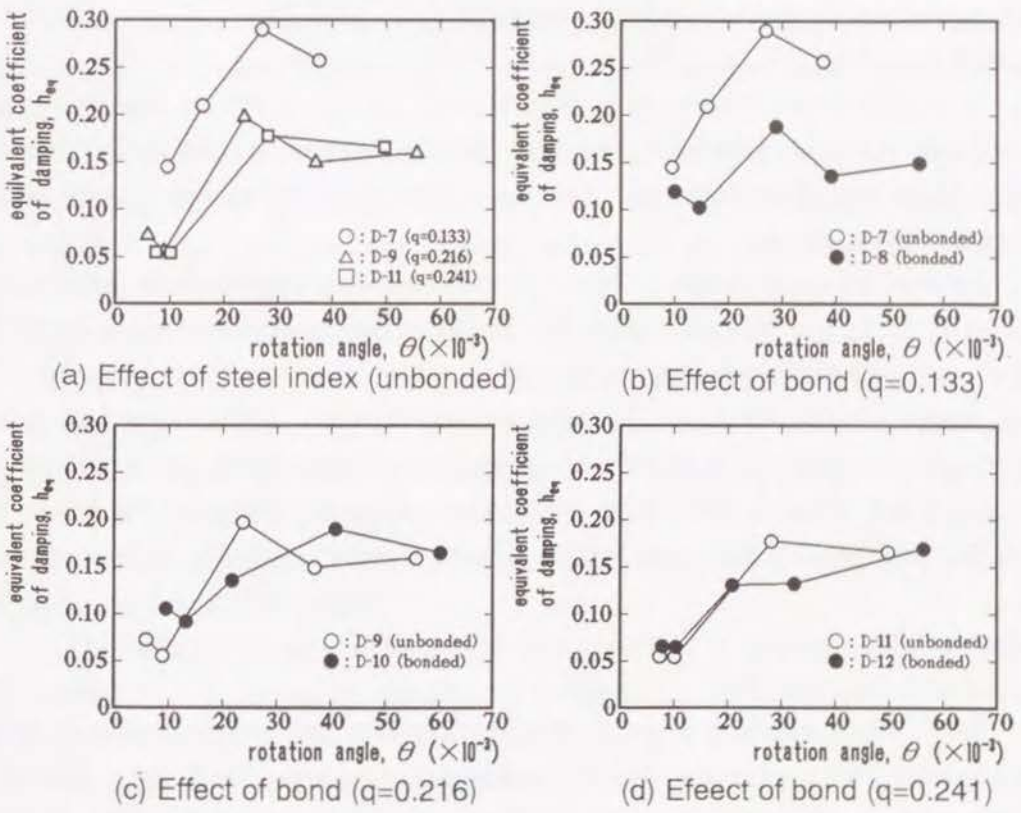

(a) Effect of steel index (unbonded)

(b) Effect of bond (q=0.133)

(c) Effect of bond (q=0.216)

(d) Efeect of bond (q=0.241)

Fig.4-18 Equivalent coefficient of damping (L2 Type of Series-D)

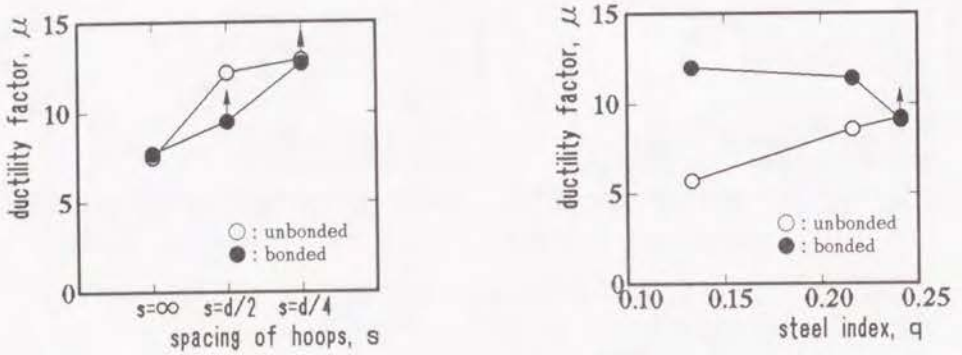

(a) Effect of hoop spacing (L1 Type) (b) Effect of steel index (L2 Type)

Fig.4–19 Ductility factors (Series–D)

value. This tendency is also observed in bonded beams [9].

As far as Series–D tests are concerned, the value of h_{eq} at the maximum ultimate load, irrespective of spacing of tie and existence of grouting, is approximately 0.15 for q=0.2 which may be considered appropriate as the upper limit in seismic design of prestressed elements.

(d) Ductility factors

In Fig.4–19 are shown the ductility factors μ which is defined in term of the ratio of two mid–span deflections at 0.8 P_u on the ascending and falling branch curves given by the envelope of load – deflection hysteresis loops under unidirectional loading.

As can be clearly seen in Fig.4–19, the unbonded beams show almost the same ductility as the bonded ones under unidirectional loading and the ductility of both of unbonded and bonded beams can be remarkably improved by arranging lateral hoops closely, for example, at the spacing of s=d/4. Under reversed cyclic loading, on the other hand, ductility of unbonded beams tends to be smaller than that of bonded ones in the range of smaller q–values, especially at q=0.133. However this difference becomes smaller with increase in q–value.

(2) Series–E

(a) Load carrying capacities

The flexural cracking strength of the beams with high prestress of q=0.26 is approximately 25% higher than that of corresponding beams of q=0.18 as indicated in Table 4–5. In almost all of the Series–E beams, the negative flexural cracking strength is about 20% lower than the positive one. This result is somewhat different

from that observed in Series–D beams. This is mainly due to that the flexural cracks generated during the first positive loading extended significantly because the deflection amplitude at the first positive run was relatively large compared with that in Series–D, resulting in considerable reduction of section rigidity when subjected to subsequent negative loading.

Significant shear cracks did not occur up to failure and all of the beams failed ultimately in flexure accompanied by crushing of concrete within mid–span as seen in Series–D beams.

As indicated in Table 4–5, the measured maximum ultimate loads (P_u) of the unbonded beams are lower by about 20% than those of the bonded beams, although this reduction ratio is at most 15% in Series–D beams without grouting of cement paste.

(b) Elastic recovery

In Fig.4–20 are shown the typical P – δ hysteresis loops. Some examples of elastic recovery on unloading are shown in Fig.4–21, which are expressed by restoring index (α) as defined previously.

The index, α, decreases with increasing applied deflection amplitude, but are well in excess of approximately 0.8 in all of the beams even when unloaded at P_u (θ≅0.015).

The value of α, within the falling branch region, is considerably higher in the beam having a close spacing of hoops (s=d/4) than that in the beam without lateral confinement. The unbonded beams show almost the same elastic recovery as that observed in the bonded ones.

(3) Equivalent coefficients of damping

In Fig.4–22 are shown the equivalent coefficients of damping (h_{eq}). The coefficient, h_{eq}, increases with increasing applied deflection amplitude. The value of h_{eq} is equal to approximately 0.05 at the loading level of ε_c=0.002 (θ≅0.008), and then 0.15 at P_u (θ≅0.015) irrespective of test variables. Moreover, h_{eq} is larger in the beams without lateral confinement than in those with lateral confinement within the falling branch region (θ>0.020).

The effect of prestressing steel index and bond for prestressing strands on the coefficient, h_{eq}, cannot be significantly noticed.

(d) Ductility factors

In Table 4–5 are listed the deflection ductility factor (μ). It can be clearly observed in Table 4–5 that the ductility of prestressed beams are considerably improved by arranging the hoops closely, for instance, s=d/4, and this effect is more

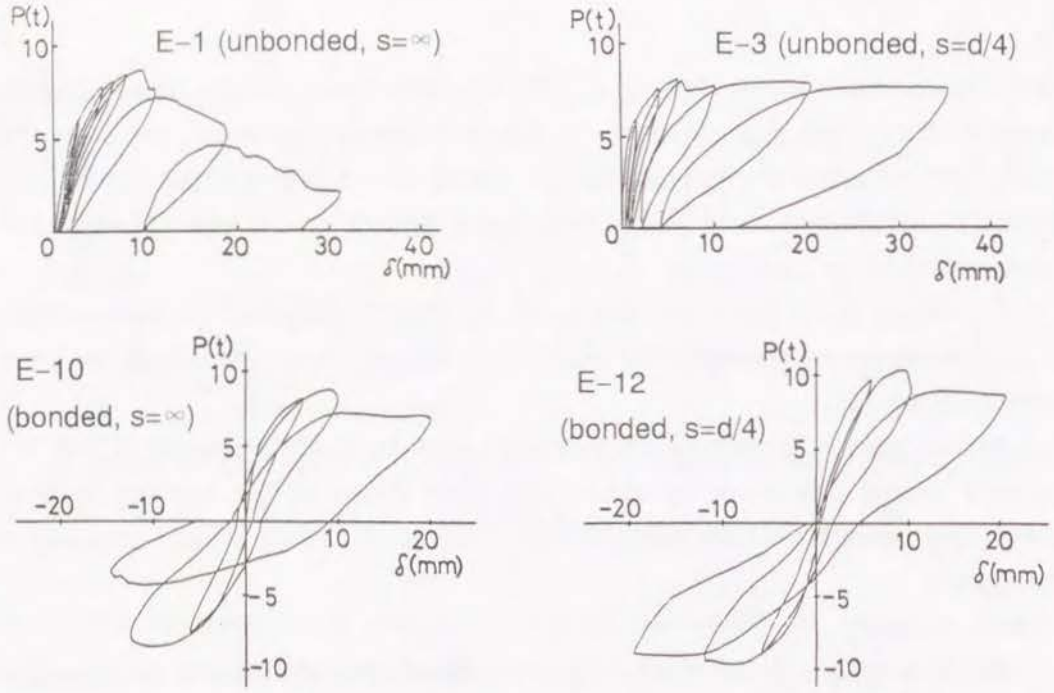

Fig.4-20 Typical load-deflection hysteresis loops (Series-E)

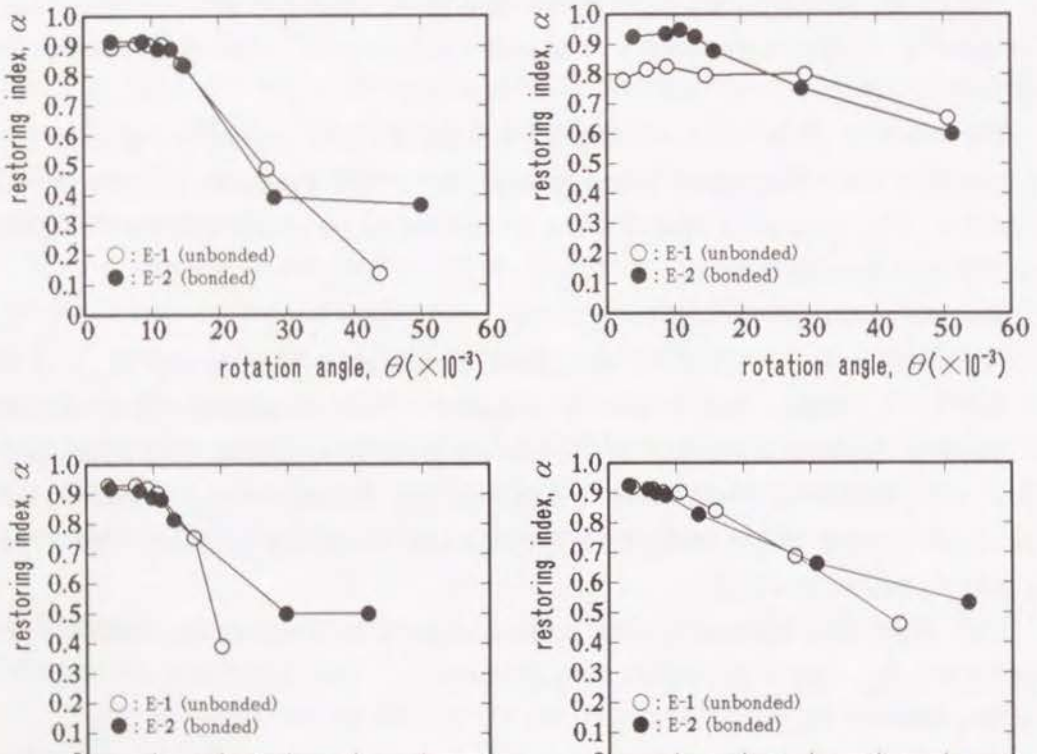

Fig.4-21 Elastic recovery expressed by restoring index (L1 Type of Series-E)

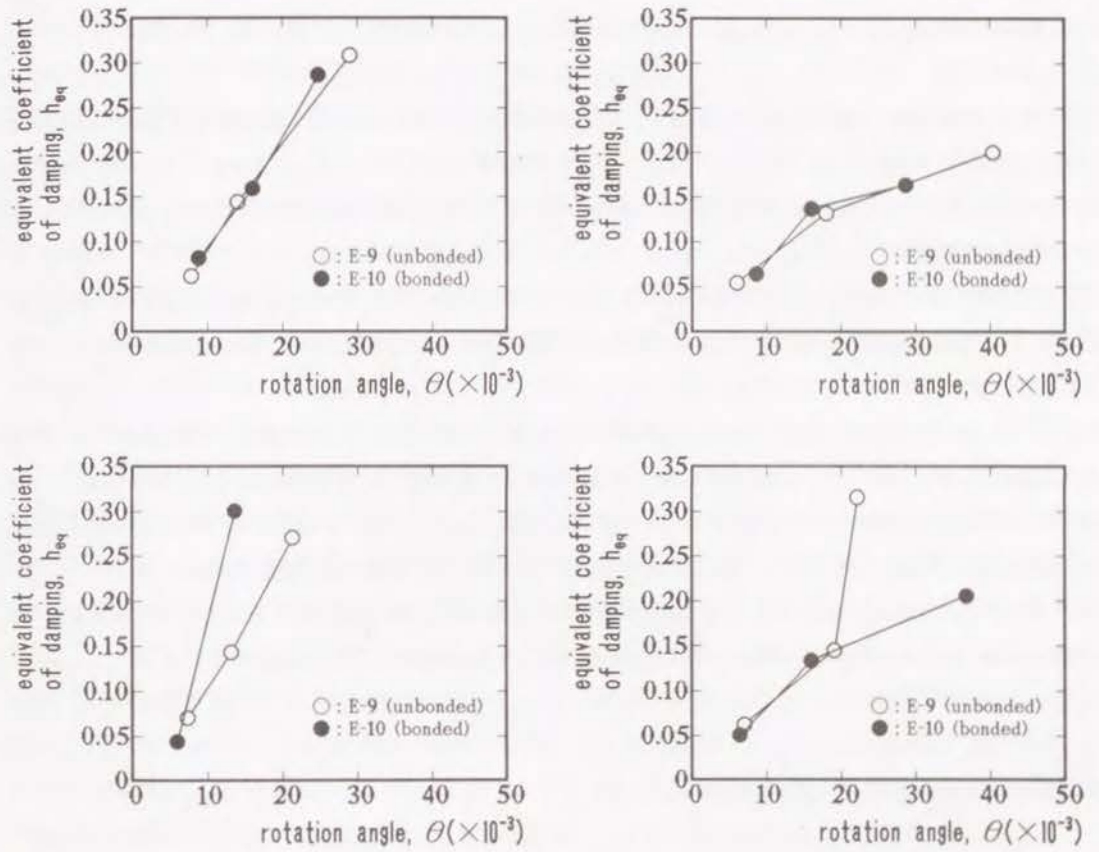

Fig.4-22 Equivalent coefficient of damping (L2 Type of Series-E)

remarkable in unbonded beams.

4.4.3 Summary of the Results on Unbonded Prestressed Concrete Beams

(1) The maximum ultimate load, P_u, of unbonded beams with grease-filled type of prestressing strand is approximately 20% lower than that of bonded ones, while this reduction ratio is at most 15% in case of the unbonded beams without grouting of cement paste.
(2) Elastic recovery of prestressed beams can be in excess of, at least, 0.8 even when unloaded at P_u, and that is somewhat higher in the unbonded beams than the bonded ones.
(3) The equivalent coefficient of damping, h_{eq}, at the maximum ultimate load is approximately 0.15 irrespective of hoop spacing and existence of bond for prestressing steel. Within the falling branch region, however, the value of h_{eq} is considerably affected by the spacing of hoops for lateral confinement.
(4) A closer spacing of lateral confinement, for example, s=d/4 is very effective for improving the deflection ductility, especially, in unbonded beams.

4.5 CONCLUSIONS OF CHAPTER 4

In this chapter, inelastic behavior of partially prestressed concrete beams and unbonded prestressed concrete beams are discussed by focusing mainly on the effect of transverse hoops for lateral confinement on their inelastic deformation properties. The main conclusions obtained are as follows.

(1) All of the tested partially prestressed concrete beams ($\lambda \geq 0.44$) including unbonded prestressed ones failed ultimately in flexure even when subjected to reversed cyclic loading well into the inelastic range. Reinforced concrete beams, on the other hand, failed ultimately in shear under reversed cyclic loading due to the significant reduction in shear resistance of concrete after the formation of X-shaped diagonal cracks which appeared at $\delta = \pm 4\delta_y$, although these failed in flexure under unidirectional loading. These facts suggest that even a small amount of introduced prestress is very effective in order to restrain the reduction in shear resistance of concrete under reversed cyclic loading.

(2) Ultimate flexural strength of unbonded prestressed concrete beams is smaller than that of corresponding bonded ones. However, its reduction ratio is at most 15% in case of no grout type and about 20% in case of grease filled type, although the specification of JSCE considers the reduction ratio to be 30%. Ultimate flexural strength of unbonded prestressed concrete beams can be well estimated by assuming the stress in prestressing steel at the ultimate state as, for example, Eq.(4-5).
(3) Elastic recovery of partially prestressed concrete beams before the maximum ultimate load is well in excess of 0.8 even when the introduced prestress is relatively small (λ=0.44). Elastic recovery of unbonded prestressed concrete beams is almost equal to or somewhat larger than that of corresponding bonded ones. Closer arrangement of hoops is effective for improving elastic recovery even within the falling branch region after the maximum ultimate load.
(4) Equivalent coefficient of damping as well as energy dissipation of partially prestressed concrete beams including reinforced and prestressed concrete ones tends to decrease with increasing mechanical degree of prestress, although that of RC beams begins to decrease at a smaller deflection amplitude compared with PPC and PC ones because of the pinching effect in load - deflection hysteresis loops due to the extensive diagonal cracks. On the other hand, equivalent coefficient of damping of unbonded prestressed concrete beams is almost equal to that of corresponding bonded ones, and its value at the maximum ultimate load is approximately 0.15 irrespective of the existence of transverse hoops.
(5) Ductility of prestressed concrete beams including partially prestressed and unbonded prestressed ones can be improved significantly by arranging transverse hoops in the compression zone of section for lateral confinement at the spacing of, for example, 1/4 of effective depth. However, the results of these fundamental tests suggest that the inelastic behavior of partially prestressed concrete beam under reversed cyclic loading as expected during earthquake action is more favorable than that of reinforced concrete and prestressed concrete beam.

REFERENCES OF CHAPTER 4

1) Thompson, K. J. and Park, R., "Ductility of Prestressed and Partially Prestressed Concrete Beam Sections", PCI Journal, Vol.25, No.2, pp.46-70, 1980.

2) Okamoto, S., "Seismic Safety of Prestressed Concrete Structures," Journal of Japan Prestressed Concrete Engineering Association, Vol.21, No.4, pp.38-54, 1979. [in Japanese]
3) Standards Association of New Zealand, "Code of Practice for the Design of Concrete Structures (NZS 3101)," Part1, 1982.
4) ACI Committee 318, "Building Code Requirements for Reinforced Concrete (ACI 318-89)," 1989.
5) Architectural Institute of Japan, "Recommendations for Design and Construction of Partially Prestressed Concrete (Class III of Prestressed Concrete) Structures," 1989. [in Japanese]
6) Okamoto, S., "Experimental Study on the Ductility of Partially Prestressed Concrete Beams," Proc. of FIP Symposium, Part2, 1980.
7) Suzuki, K., Nakatsuka, T., Hiramatsu, K. and Nagata, S., "High Ductile Behavior of Partially Prestressed Concrete Beams with Confined Concrete in the Compression Zone," Proc. of JCI 7th Conference, pp.485-488, 1985. [in Japanese]
8) Park, R. and Thompson K. J., "Behavior of Prestressed, Partially Prestressed and Reinforced Concrete Interior Beam-Column Assemblies under Cyclic Loading: Test Results of Units 1 to 7," Research Report, Dept. of Civil Engineering, University of Canterbury, New Zealand, 1974.
9) Okada, K., Kobayashi, K., Inoue, S. and Inoue, S., "Studies on Performances of Prestressed Concrete Beams under Cyclic flexure in Post-Elastic Range," Proc. of the 26th Japan Congress on Materials Research, pp.169-174, 1983.
10) Muguruma, H., Watanabe, F., Tanaka, H. and Katsuda, S., "Improving the Ductility of Prestressed Concrete Beam by Using the High Yield Strength Hoop Reinforcement," Proc. of JCI 2nd Conference, pp.377-380, 1980. [in Japanese]
11) Fujii, M., Agawa, T., Hongo, T. and Miyahara, K., "Improvement of Ductility of Overreinforced Concrete Beams by Transversely Confining Reinforcement," Proc. of JSCE, No.348/V-1, pp.77-86, 1984. [in Japanese]
12) Inoue, S., Hattori, A., Miyagawa, T., Fujii, M. and Kobayashi, K., "Application of Rectangular Hoop as Lateral Confinement for Concrete Beam Members," CAJ Proceedings of Cement & Concrete, No.43, pp.340-345, 1989.
13) Muguruma, H., Watanabe, F., Fukai, S. and Nasu, T., "Fundamental Study on the Behavior of Class 3 Partially Prestressed Concrete Beam," Proc. of JCI 2nd Conference, pp.381-384, 1980. [in Japanese]

14) Inoue, S., Kobayashi, K. and Katsuno, Y., "Inelastic Deformation Properties of Partially Prestressed Concrete Beams under Reversed Cyclic Loading," Proc. of the 42nd Annual Conference of the JSCE, Vol.5, pp.232-233, 1987. [in Japanese]
15) Inoue, S., Takahashi, K., Igo, Y., Miyagawa, T. and Fujii, M., "Effects of Various Factors on the Accumulated Dissipated Energy of Concrete Beams under Reversed Cyclic Loading," Proc. of the 45th Annual Conference of the JSCE, Vol.5, pp.674-675, 1990. [in Japanese]
16) Muguruma, H., Watanabe, F., Ogura, M. and Kontani, O., "On the Class 3 Prestressed Concrete Members with High Strength Concrete," Proc. of JCI 5th Conference, pp.449-452, 1983. [in Japanese]
17) Okada, K., Kobayashi, K. and Inoue, S., "Inelastic Behaviors of Post-Tensioned Prestressed Beams with High-Strength Concrete under High-Intensity Reversed Cyclic Loading," Proc. of International Symposium on Fundamental Theory of Reinforced and Prestressed Concrete, Nanjing, Vol.2, pp.847-854, 1986.
18) Japan Society of Civil Engineers, "Standard Specification for Design and Construction of Concrete Structures," Part 1 [Design], 1991. [in Japanese]
19) Okada, K., Kobayashi, K., Kojima, T. and Hatamura, H., "Studies on Basic Properties of Unbonded Prestressed Concrete Beams," Journal of Japan Prestressed Concrete Engineering Association, Vol.24, No.3, pp.15-23, 1982. [in Japanese]
20) Oishi, T., "The Loading Test of Prestressed Concrete Model Beams with Unbonded Tendons," Journal of Prestressed Concrete, Japan, Vol.27, No.1, pp.91-109, 1985. [in Japanese]
21) Muguruma, H., Watanabe, F. and Nishiyama, M., "Flexural Strength of Unbonded Prestressed Concrete Members," Journal of Prestressed Concrete, Japan, Vol.26, No.1, pp.10-16, 1984. [in Japanese]
22) Baker, A. L. L., "A Plastic Theory of Design for Ordinary Reinforced and Prestressed Concrete Including Moment Redistribution in Continuous Members," Magazine of Concrete Research, Vol.1, No.2, pp.57-6, 1949.
23) Miyamoto, Y. and Iwasaki, I., "Ultimate Flexural Strength of Prestressed Concrete Beams," Railway Technical Research Report, No.836, pp.1-25, 1973. [in Japanese]
24) Kobayashi, K. and Nieda, T., "Flexural Behavior of Unbonded Prestressed Concrete Beams with Lateral Confinement by Rectangular Hoops," Proc. of

the JCI, Vol.14, No.2, pp.565-570, 1992. [in Japanese]
25) Mattock, A. H., Yamazaki, J. and Kattula, B. T., "Comparative Study of Prestressed Concrete Beams with and without Bond," Journal of the ACI, Vol.68, No.2, pp.116-125, 1971.
26) Warwaruk, J., Sozen, M. and Siess, C. P., "Strength and Behavior in Flexure of Prestressed Concrete Beams," Bulletin No.464, Engineering Experiment Station, University of Illinois, 1962.
27) Architectural Institute of Japan, "Standard for Structural Design and Construction of Prestressed Concrete Structures," 1987. [in Japanese]
28) Kobayashi, K., Inoue, S. and Matsumoto, T., "Inelastic Behavior of Partially Prestressed Concrete under Reversed Cyclic Loading," Proc. of the 5th Canadian Conference on Earthquake Engineering, Ottawa, pp.841-848, 1987.
29) New Zealand Concrete Design Code Committee, "Proposed Provisions for New Zealand Concrete Design Code, Chapter 22: Prestressed Concrete Members - Additional Seismic Requirements", 1976.
30) Japan Society of Civil Engineers, "Standard Code for Prestressed Concrete", 1978. [in Japanese]
31) Blakeley, R. W. G. and Park, R., "Prestressed Concrete Sections with Cyclic Flexure", Journal of the Structural Division, ASCE, Vol.99, No.ST8, pp.1717-1742, 1973.
32) Okada, K., Kobayashi, K. and Inoue, S., "Inelastic Performance of Prestressed Concrete Beams under Cyclic Flexure," Proc. of the 8th World Conference on Earthquake Engineering, San Francisco, Vol.VI, pp.709-716, 1984.
33) Okada, K., Kobayashi, K., Miyagawa, T. and Inoue, S., "Inelastic Behaviors of Post-Tensioned Prestressed Concrete Beams," Review of the 38th General Meeting of CAJ, pp.386-389, 1984.
34) FIP, "Report of the FIP Commission on Seismic Structures," Proc. of the 7th Congress of the FIP, New York, 1974.
35) Blakeley, R. W. G and Park, R.: Seismic Resistance of Prestressed Concrete Beam-Column Assemblies, Journal of the ACI, Vol.68, No.9, 1971.
36) Kvitsaridze, O. I, et al.: Experimental Study of Prestressed Reinforced Concrete Elements of Antiseismic Buildings, Proc. the 6th World Conference on Earthquake Engineering, New Delhi, 1977.

CHAPTER 5

ENERGY DISSIPATION OF PARTIALLY PRESTRESSED CONCRETE BEAMS AND THEIR DAMAGE EVALUATION BASED ON DISSIPATED ENERGY

5.1 GENERAL REMARKS

Safety of concrete structures under earthquake loads is usually examined by means of deformation ductility of constituent members under unidirectional monotonous loads. Under reversed cyclic loads as experienced during earthquakes, however, ductility of concrete members is significantly reduced compared with that under monotonous loads. This implies that the damage of concrete members is accumulated during cyclic load reversals and that the degree of seismic damage of concrete structures is closely related to the hysteretic energy dissipation properties of their constituent members. From this viewpoint, some damage index considering both reduction in load carrying capacity due to load repetitions and hysteretic dissipated energy have been proposed in recent years [1, 2].

However, energy dissipation properties of concrete members, which are very important when considering response and hysteretic damping of concrete structures during earthquakes, are affected by many factors, and their effects have not been made clear in quantitative sense. Therefore, it is necessary to make clear the effects of various factors quantitatively on the energy dissipation of constituent members of concrete structures in order to evaluate structural damage during earthquakes.

As indicated in Chapter 4, partially prestressed concrete shows better inelastic deformation properties and ductility under reversed cyclic loading as experienced during earthquakes compared with those of reinforced concrete and fully prestressed concrete. However, its energy dissipation properties have not been so much dealt with in conjunction with seismic damage compared with reinforced concrete.

In this chapter, the effects of various factors on the accumulation process of dissipated energy in partially prestressed concrete beams are discussed and a damage index based on the hysteretic dissipated energy is proposed. Energy

dissipation of reinforced concrete beams, which tends to fail in shear under reversed cyclic loading, is discussed in the next chapter.

5.2 REVIEW OF PREVIOUS RESEARCH WORKS

5.2.1 Energy Dissipation of Partially Prestressed Concrete Beams

As indicated in Chapter 4, inelastic behavior of partially prestressed concrete including energy dissipation properties is influenced largely by the magnitude of introduced prestress. In a qualitative sense, some research works on the energy dissipation of partially prestressed concrete members have been reported.

Muguruma et al.[3] indicated that the area surrounded by each hysteresis loop became smaller with increasing magnitude of introduced prestress, resulting in smaller equivalent coefficient of damping especially at larger applied deflection amplitudes.

Oishi [4] reported that the load – deflection hysteresis loops of partially prestressed concrete beam with λ=0.5 was more similar to that of reinforced concrete one than that of prestressed concrete one.

The author [5] also reported that the energy dissipation at the same deflection amplitude decreased with increasing value of mechanical degree of prestress, and that the effects of transverse hoops on the energy dissipation were not remarkable before the deflection amplitude of approximately $4\delta_y$ (δ_y: yield deflection) although became significant after that deflection amplitude.

Another researches dealing with the energy dissipation of partially prestressed concrete, for examples Ref.[6, 7], have been reported. However, their results was almost the same as mentioned above and the effects of test variables were not made clear in a quantitative sense.

5.2.2 Index for Evaluating Hysteretic Damage

As mentioned previously, seismic damage of concrete members is usually evaluated by the ratio of the maximum deformation under earthquake to the ultimate deformation under monotonous loading. In recent years, however, new damage indexes considering the hysteretic damage accumulation due to load repetitions

have been proposed.

Park et al. [1] proposed the damage index based on the statistical analysis of many experimental data on reinforced concrete members, which is expressed as a linear function of the maximum deformation and the effect of repeated cyclic loading.

$$D=\frac{\delta_m}{\delta_u}+\frac{\beta}{Q_y\delta_u}\int dE \qquad (5-1)$$

Where,

D: damage index.

δ_M: maximum deformation under earthquake.

δ_u: ultimate deformation under monotonous loading.

Q_y: calculated yield strength.

dE: incremental absorbed hysteretic energy.

β: non–negative parameter expressing the strength degradation per cycle.

Under elastic response, the value of D should be zero, that is, D=0 means no damage. On the other hand, $D \geq 1.0$ signifies complete collapse or total damage.

The calibration of this proposed damage index was done by using the data of reinforced concrete buildings which were damaged during past earthquakes [8]. In that report, the relationship between calculated damage index and observed seismic damage was indicated, for examples, $D \leq 0.4$ means repairable damage and $D>0.4$ means unrepairable.

On the other hand, Chung et al. [2] proposed another new damage index which combines a modified Miner's hypothesis with damage modifiers that reflect the effect of loading history (cf. Fig.5–1).

$$D_e=\sum_i(\alpha_i^+\frac{n_i^+}{N_i^+}+\alpha_i^-\frac{n_i^-}{N_i^-}) \qquad (5-2)$$

Where,

i: indicator of displacement or curvature level.

$N_i=\dfrac{M_i-M_{fi}}{\Delta M_i}$: number of cycles to cause failure at curvature level i.

M_i: moment at curvature level i.

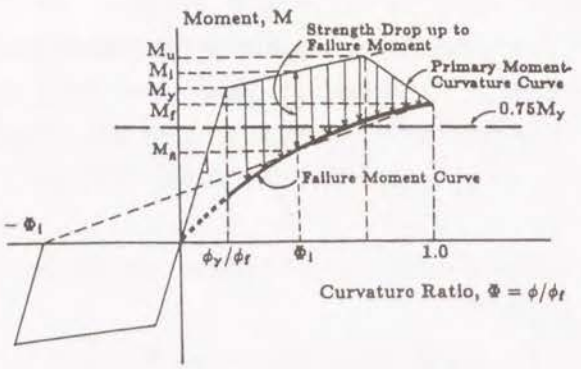

Fig.5-1 Definition of failure by Chung et al. [2]

M_{fi}: failure moment for given curvature level ϕ_i.
ΔM_i: strength drop due to one load cycle at curvature level i.
n_i: number of cycles actually applied at curvature level i.
α_i: damage modifier.
+ and −: indicators of loading sense.

They also examined the accuracy of their proposed model by using many experimental results and indicated that the proposed model could simulate hysteretic response of reinforced concrete members.

Another index for evaluating the damage of reinforced concrete members, called damage function based on the maximum response and accumulated damage theory due to low cycle fatigue, was also proposed by Stephens et al. [9].

5.3 EXPERIMENTAL PROCEDURES [5, 10~15]

5.3.1 Specimens

Specimens used for loading tests were partially prestressed concrete simple beams including fully prestressed concrete ones with a rectangular cross section of b x h = 10 x 20cm (b:width, h:full depth of section) and a total length of 160cm. As shown in Fig.5-2, they were symmetrically reinforced with prestressing bars and non-prestressing deformed bars. All of these specimens were post-tensioned and grouted with cement paste of W/C=45%. They were provided with φ6mm vertical

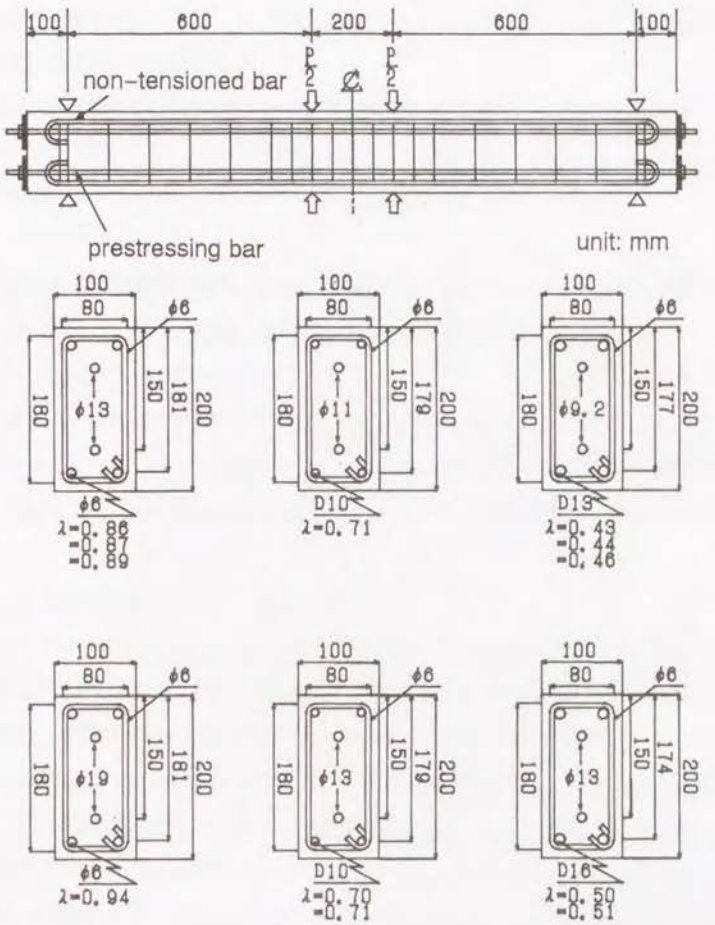

Fig.5-2 Dimensions of specimens and details of cross section

stirrups (f_{sy}=49kgf/mm^2) as web reinforcement in order to prevent premature shear failure in accordance with JSCE Standard Specification for Design and Construction of Reinforced Concrete Structures [16].

5.3.2 Test Variables

As the factors having influences on energy dissipation properties, the following five test variables were selected.

(1) Volumetric ratio of transverse hoops (ρ_s)

As transverse reinforcement arranged within the potential plastic hinge

region, ϕ6mm hoops (f_{syh}=49kgf/cm^2) were used. ρ_s is defined as below.

$$\rho_s = \frac{\text{volume of one transverse hoop}}{\text{volume of core concrete confined by one transverse hoop}} \times 100\ (\%) \qquad (5\text{-}3)$$

In principle, four levels of ρ_s-value, that is, 0%, 0.63%, 1.25% and 2.50%, were adopted here. However, the actual values ranged from 0% to 2.80% in the tested specimens.

(2) Mechanical degree of prestress (λ)

Mechanical degree of prestress is defined as below.

$$\lambda = \frac{A_p f_{py}}{A_p f_{py} + A_s f_{sy}} \qquad (5\text{-}4)$$

Where,

A_p: area of prestressing steel.
A_s: area of non-tensioned deformed bar.
f_{py}: yield strength of prestressing steel.
f_{sy}: yield strength of non-tensioned deformed bar.

As the value of λ, three levels, that is, 0.4, 0.7 and 1.0 were selected. λ=1.0 means fully prestressed concrete. However, this value becomes somewhat smaller considering ϕ6mm mild bars used for set up of hoops and stirrups. The value of λ is also affected by the actual yield strength of prestressing steels and non-tensioned deformed bars. Therefore, the actual λ-values ranged from 0.43 to 0.94 in the tested beams.

(3) Steel index (q)

Steel index is defined as Eq.(5-5).

$$q = q_p + q_s = \frac{A_p f_{py}}{b d_p f'_c} + \frac{A_s f_{sy}}{b d_s f'_c} \qquad (5\text{-}5)$$

Where,

b: width of cross section.
d_p: effective depth of prestressing steel.
d_s: effective depth of non-tensioned deformed bar.
f'_c: compressive strength of concrete.

In the tested beams, the actual q-values ranged from 0.216 to 0.445.

(4) Compressive strength of concrete (f'_c)

In almost all the specimens, design compressive strength of concrete was chosen as 400kgf/cm^2. In some specimens, however, high strength concrete of f'_c=800kgf/cm^2 was used in order to investigate the effect of concrete strength.

(5) Shear span - effective depth ratio (a/d)

Many of the specimens were tested under symmetrical two-point load with shear span length of 60cm and flexural span length of 20cm. This corresponds to the shear span - effective depth ratio of approximately 3.5. However, in order to investigate the effect of shear span - effective depth ratio, another levels of a/d ratio, that is, approximately 2.9 (shear span length: 50cm, flexural span length: 40cm) and 2.3 (shear span length: 40cm, flexural span length: 40cm) were also adopted. In this case, effective depth d is defined as the depth of combined gravity center of prestressing steel and non-tensioned deformed bars. Therefore, the actual a/d ratio of the specimens moved from 2.33 to 3.77.

5.3.3 Loading Histories

It is indicated that loading histories have large influences on the energy dissipation properties of reinforced concrete members [17]. Therefore, four different loading histories were applied to the specimens and the effects of the above test variables under different loading histories were investigated. Details of each loading history are as follows.

(1) Series-A

Series-A is gradually increased reversed cyclic loading with one load reversals at each deflection amplitude. In this series, the applied deflection

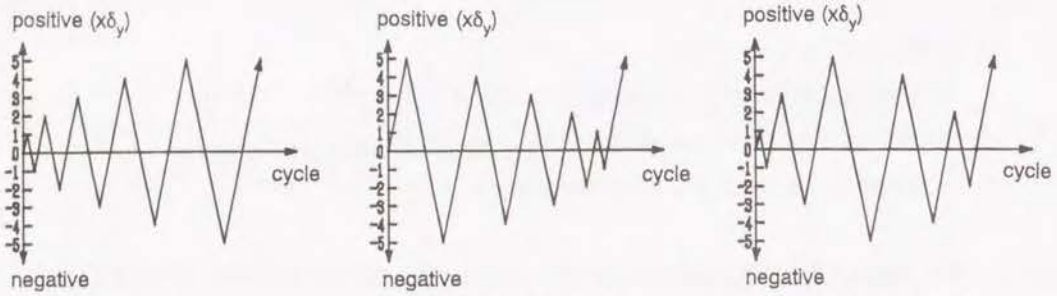

(a) Series–A (b) Series–B (c) Series–C

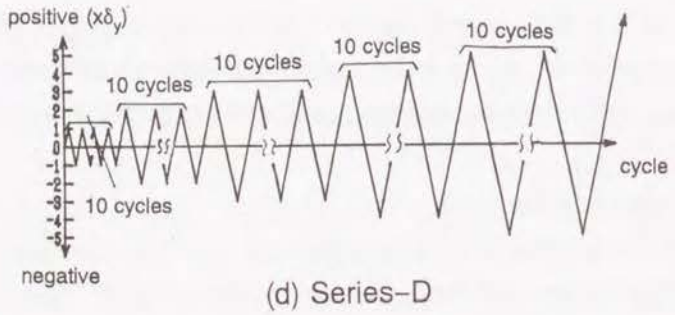

(d) Series–D

Fig.5–3 Applied loading histories

amplitude was gradually increased such as $\pm\delta_y$, $\pm2\delta_y$, $\pm3\delta_y$, --- up to the deflection amplitude where the load carrying capacity was reduced to 80% of the maximum load (δ_u).

(2) Series–B

Series–B is gradually decreased reversed cyclic loading with one load reversals at each deflection amplitude, in which the applied deflection amplitude was gradually decreased from $\pm\delta_u$ to $\pm\delta_y$. The sum of the applied deflection amplitude was adjusted to be equal to that of Series–A.

(3) Series–C

Series–C is the mixed type loading of Series–A and B, in which the applied deflection amplitude was firstly gradually increased up to $\pm\delta_u$ and then gradually decreased. The sum of the applied deflection amplitude of Series–C was also equal to that of Series–A.

(4) Series–D

Series–D is gradually increased reversed cyclic loading with ten load reversals at each deflection amplitude. This series was done in order to investigate the reduction of dissipated energy at the same deflection amplitude due to load repetition.

These loading histories are shown schematically in Fig.5–3. After the prescribed loading sequences, all the beams were subjected to some additional loading cycles until failure.

5.4 RESULTS OF TESTS AND DISCUSSIONS [5, 10–15]

5.4.1 Definition of the Ultimate State and Non–dimensional Dissipated Energy

It is necessary to define the ultimate state of members if the seismic damage of concrete structures is to be evaluated. In this chapter, the ultimate state of a member is defined as the point at which the load carrying capacity is reduced to 80% of the maximum load.

Dissipated energy at each deflection amplitude (E_d) is expressed by the area surrounded by each loop of load – deflection hysteresis. Among the beams with approximately the same flexural strength of section under the same loading condition, the values of E_d can be compared directly with one another. Dissipated energy itself, however, indicates significantly different values under different loading conditions even if the section is the same. Therefore, non–dimensional dissipated energy at each deflection amplitude (E_d') is defined in this study as follows,

$$E_d' = \frac{E_d}{P_{ycal}\delta_{ycal}} \tag{5–6}$$

where, P_{ycal} and δ_{ycal} are the calculated yield load and yield deflection of each beam, respectively, in order to eliminate the effect of difference in the maximum load carrying capacity among the beams.

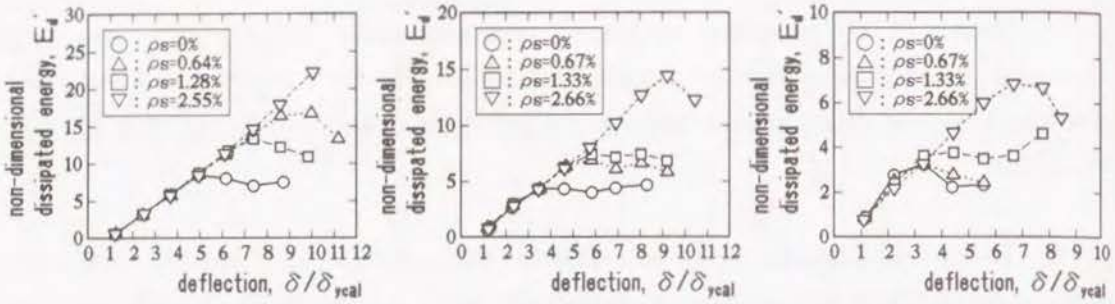

(a) λ=0.43 (b) λ=0.70 (c) λ=0.89

Fig.5-4 Effects of ρ_s on E_d'-value of Series-A beams

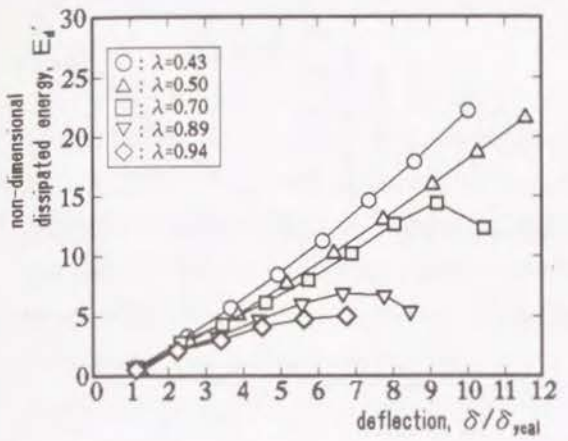

Fig.5-5 Effects of λ on E_d'-value of Series-A beams (ρ_s≅2.5%)

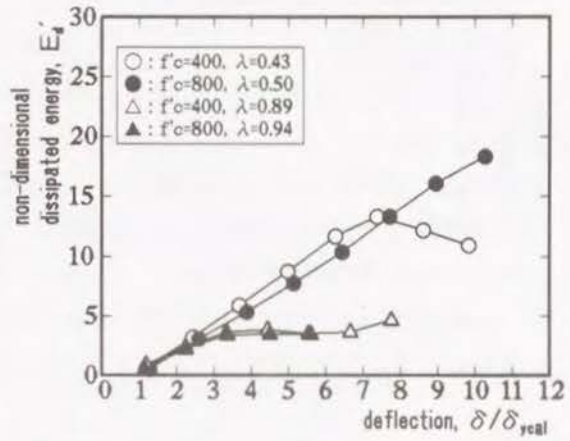

Fig.5-6 Effects of f'_c on E_d'-value of Series-A beams (ρ_s≅1.25%)

5.4.2 Effects of Test Variables on the Energy Dissipation of Series-A Beams

(1) Effects of volumetric ratio of transverse hoops (ρ_s)

Fig.5-4 shows the effects of volumetric ratio of transverse hoops (ρ_s) on the energy dissipation of Series-A beams, in which the horizontal axis indicates non-dimensional applied deflection amplitude (δ/δ_{ycal}) and the vertical axis shows non-dimensional dissipated energy (E_d') at each deflection amplitude.

As seen in Fig.5-4, E_d'-value increases almost linearly with increasing applied deflection amplitude within the range in which the applied deformation is relatively small and its increasing ratio is almost the same irrespective of the ρ_s-value if the other test variables are the same. E_d'-value of the beam with a smaller ρ_s-value, however, stops increasing or commences to decrease at a smaller deflection amplitude. This is due to that the beam with a smaller ρ_s-value showed a remarkable strength degradation at smaller deflection amplitude, resulting in a lower energy dissipation after that. In other words, the point from which the E_d'-value does not increase linearly can be related to a remarkable strength reduction point, that is, the ultimate state of a beam.

(2) Effects of mechanical degree of prestress (λ)

Fig.5-5 shows the effects of mechanical degree of prestress (λ) on E_d'-values.

As seen in this figure, the E_d'-value at the same deflection amplitude becomes smaller with increasing λ-value. This is due to that, as previously reported, the area surrounded by each hysteresis loop becomes smaller with increasing λ-value. It is also indicated that the deflection amplitude at which the E_d'-value stops increasing is smaller in the beam with a larger λ-value. This suggests that improving effect of energy dissipation by transverse hoops is affected by mechanical degree of prestress.

(3) Effects of compressive strength of concrete (f'_c)

Fig.5-6 shows the E_d'-values of the beams with different compressive strength of concrete.

The E_d-value of the beam of f'_c=400kgf/cm^2 is somewhat larger than that of the beam of f'_c=800kgf/cm^2 compared at the same deflection amplitude. However, the λ-value of the former is 0.43 and somewhat smaller than that of the latter, that is, 0.50. Therefore, considering the difference of λ-values of these two beams, the effect of compressive strength of concrete is supposed to be smaller compared with those of volumetric ratio of transverse hoops and mechanical degree of prestress.

(4) Effects of steel index (q)

In Fig.5-7 is shown an example of the E_d'-values of the beams with different steel index, that is, q=0.257 and 0.434.

As indicated in this figure, the E_d'-values of these two beams at the same deflection amplitude are almost equal. Therefore, the effects of steel index on the

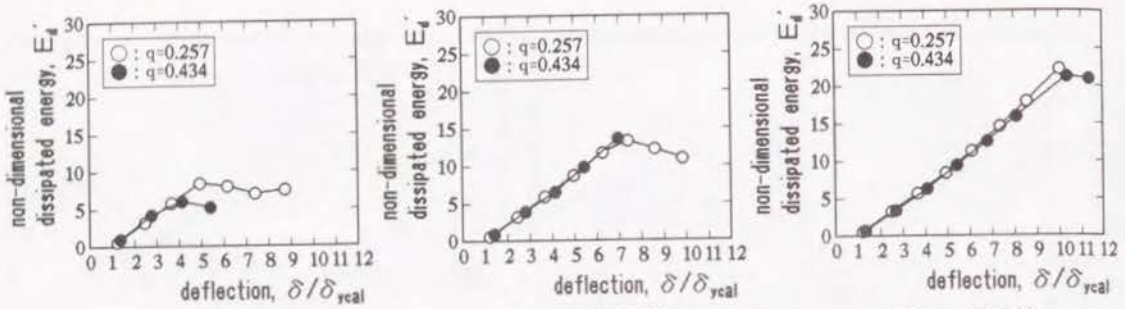

(a) ρ_s=0% (b) ρ_s≅1.25% (c) ρ_s≅2.5%

Fig.5-7 Effects of q on E_d'-value of Series-A beams (λ≅0.45)

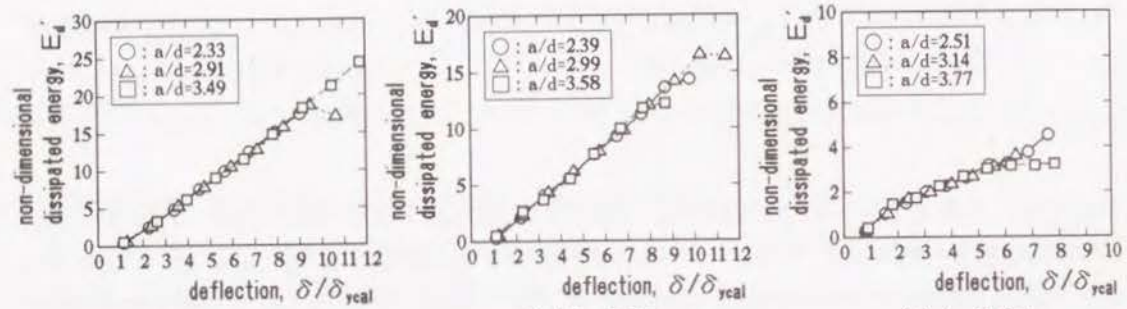

(a) λ=0.46 (b) λ=0.71 (c) λ=0.87

Fig.5-8 Effects of a/d on E_d'-value of Series-A beams (ρ_s=2.43%)

non-dimensional dissipated energy can be considered to be negligible if the other test variables are the same.

(5) Effects of shear span – effective depth ratio (a/d)

In Fig 5-8 are shown the E_d'-values of the beams loaded under different a/d ratios.

As indicated in Fig.5-8, the E_d'-value at the same non-dimensional deflection amplitude is almost the same irrespective of the a/d ratio. This result implies that the effects of a/d ratio on the non-dimensional dissipated energy is small if the beams are designed to fail in flexure even when loaded under a smaller a/d ratio within the range of 2.33-3.77 adopted in these tests.

5.4.3 Energy Dissipation Properties under Different Loading Histories

From the results of Series-A tests, it can be observed that the effects of compressive strength of concrete, steel index and shear span effective ratio on the accumulation process of non-dimensional dissipated energy are relatively small compared with those of volumetric ratio of lateral confinement and mechanical degree of prestress. Therefore, the accumulation process of non-dimensional dissipated energy until the ultimate state under different loading histories is discussed here mainly in the light of the effects of mechanical degree of prestress and volumetric ratio of lateral confinement.

(1) Series-A

In Fig.5-9 are shown some examples of load – deflection (P-δ) hysteresis loops of Series-A beams, and in Fig.5-10 are shown the relationships between non-dimensional dissipated energy (E_d') and normalized applied deflection amplitude (δ/δ_{ycal}) of Series-A beams, in which the calculated values derived from the regression analysis as mentioned below are also indicated.

As previously mentioned, E_d'-value of each Series-A beam increases almost linearly with increasing applied deflection amplitude up to the ultimate state. This is mainly because larger energy is required for the occurrence of new cracks and their extension, debonding between steel and concrete, elongation of steels at the cracks, and so on than that required at previous cycle under the gradually increased applied deflection amplitude. Considering this result, the relationship between E_d' and δ/δ_{ycal} can be expressed by a linear function as shown below.

$$E_d' = \alpha\left(\frac{\delta}{\delta_{ycal}}\right)+\beta \qquad (\delta \geq \delta_{ycal}) \tag{5-7}$$

The relationships between coefficients α, β and λ are shown in Fig.5-11-(a) and (b), respectively. As indicated in these figures, coefficients α and β in Eq.(5-7) are supposed to be in linear function of λ although some scattering of data is observed and can be expressed by Eq.(5-8) from the regression analysis of test data.

$$\alpha=-2.43\lambda+3.25, \qquad \beta=4.17\lambda-4.15 \qquad (0.43 \geq \lambda \geq 0.94) \tag{5-8}$$

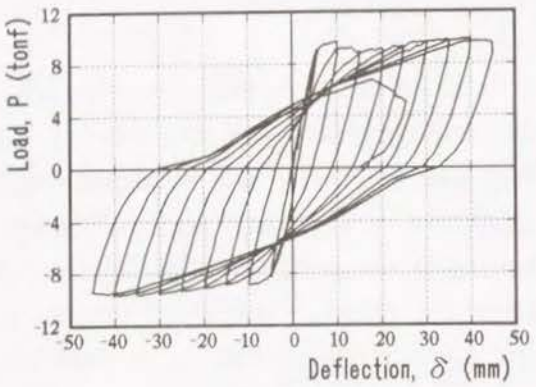

(a) λ=0.46

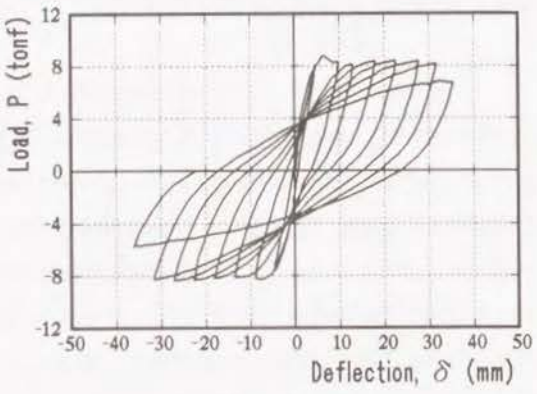

(b) λ=0.71

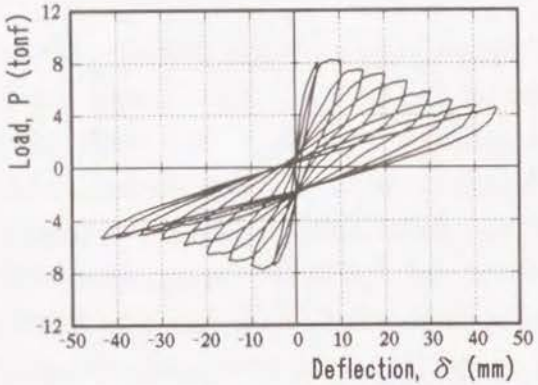

(c) λ=0.87

Fig.5-9 Examples of load – deflection hysteresis loops of Series-A beams (ρ_s=2.43%)

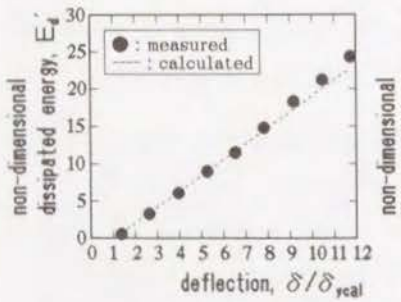

(a) λ=0.46

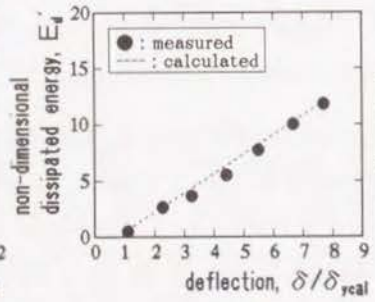

(b) λ=0.71

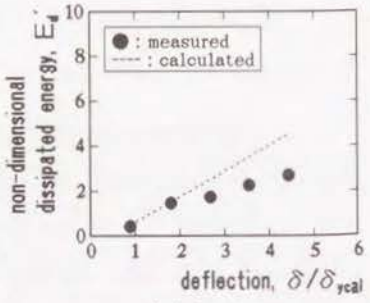

(c) λ=0.87

Fig.5-10 Examples of relationship between E_d' and δ/δ_{ycal} of Series-A beams (ρ_s=2.43%)

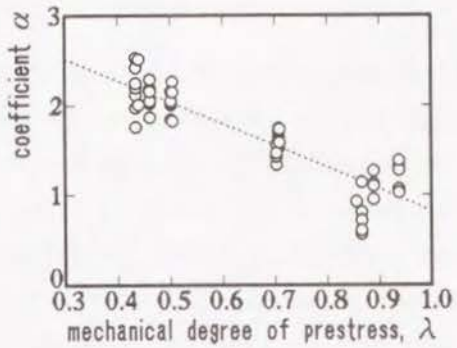

(a) coefficient α

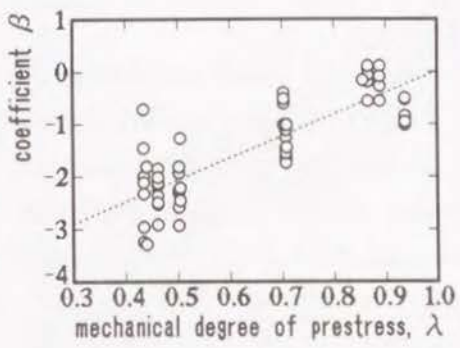

(b) coefficient β

Fig.5-11 Relationships between coefficients α, β and λ

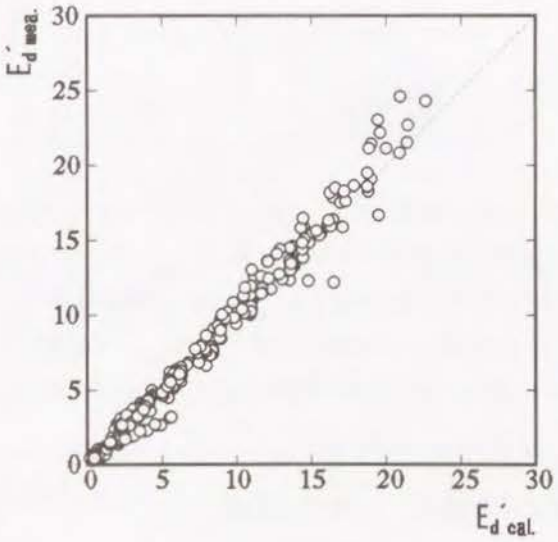

Fig.5-12 Relationship between measured and calculated E_d'-values of Series-A beams

ρ_s-value scarcely affects the values of the coefficients α, β although the deflection amplitude at the ultimate state (δ_u) is dependent on the ρ_s-value.

Fig.5-12 shows the relationship between measured and calculated E_d'-values at each deflection amplitude for a total of 66 Series-A beams. As indicated in Fig.5-10 and Fig.5-12, the calculated values derived from Eq.(5-7) and Eq.(5-8) coincide well with the measured values. In some beams with larger λ-values, however, difference between measured and calculated E_d'-values tends to become larger in the range of larger deflection amplitudes near the ultimate state due to the instability of dissipated energy.

(2) Series-B

Fig.5-13 shows some examples of P-δ hysteresis loops of Series-B beams and in Fig.5-14 are shown the relationships between E_d' and δ/δ_{ycal} of Series-B beams together with the calculated ones. In Series-B, E_d'-value is found to decrease almost quadratically when the applied deflection amplitude is gradually decreased from $\pm\delta_u$. This is because new cracks did not occur in the deflection amplitudes smaller than δ_u under gradually decreased applied deflection amplitudes, resulting in smaller dissipated energy than that of corresponding Series-A beam compared at the same deflection amplitude. Therefore, the relationship between E_d' and δ/δ_{ycal} can be set as Eq.(5-9).

$$E_d' = \gamma\left(\frac{\delta}{\delta_{ycal}}\right)^2 \qquad (\delta \geq \delta_{ycal}) \tag{5-9}$$

The value of the coefficient γ is affected by λ-value and the maximum deflection amplitude applied at the first cycle (δ_{max}). Fig.5-15 shows the relationship between the coefficient γ and $\delta_{max}/\delta_{ycal}$. As indicated in this figure, γ-value decreases almost in inverse proportion of $\delta_{max}/\delta_{ycal}$. As for the beams tested, the equations below were obtained from regression analysis of experimental data.

$$\gamma = 1.494\left(\frac{\delta_{ycal}}{\delta_{max}}\right) + 0.083 \qquad (\text{for } \lambda = 0.46) \tag{5-10}$$

$$\gamma = 1.488\left(\frac{\delta_{ycal}}{\delta_{max}}\right) + 0.038 \qquad (\text{for } \lambda = 0.71) \tag{5-11}$$

$$\gamma = 0.879\left(\frac{\delta_{ycal}}{\delta_{max}}\right) + 0.036 \qquad (\text{for } \lambda = 0.87) \tag{5-12}$$

Fig.5-16 shows the comparison of the calculated E_d'-values at each deflection amplitude, which were derived from Eq.(5-9)~(5-12) for a total of 19 Series-B beams, with the measured ones. As seen in this figure, the calculated E_d'-values coincide well with the measured one although scattering of data is somewhat larger compared with the case of Series-A. As indicated in Fig.5-14, the

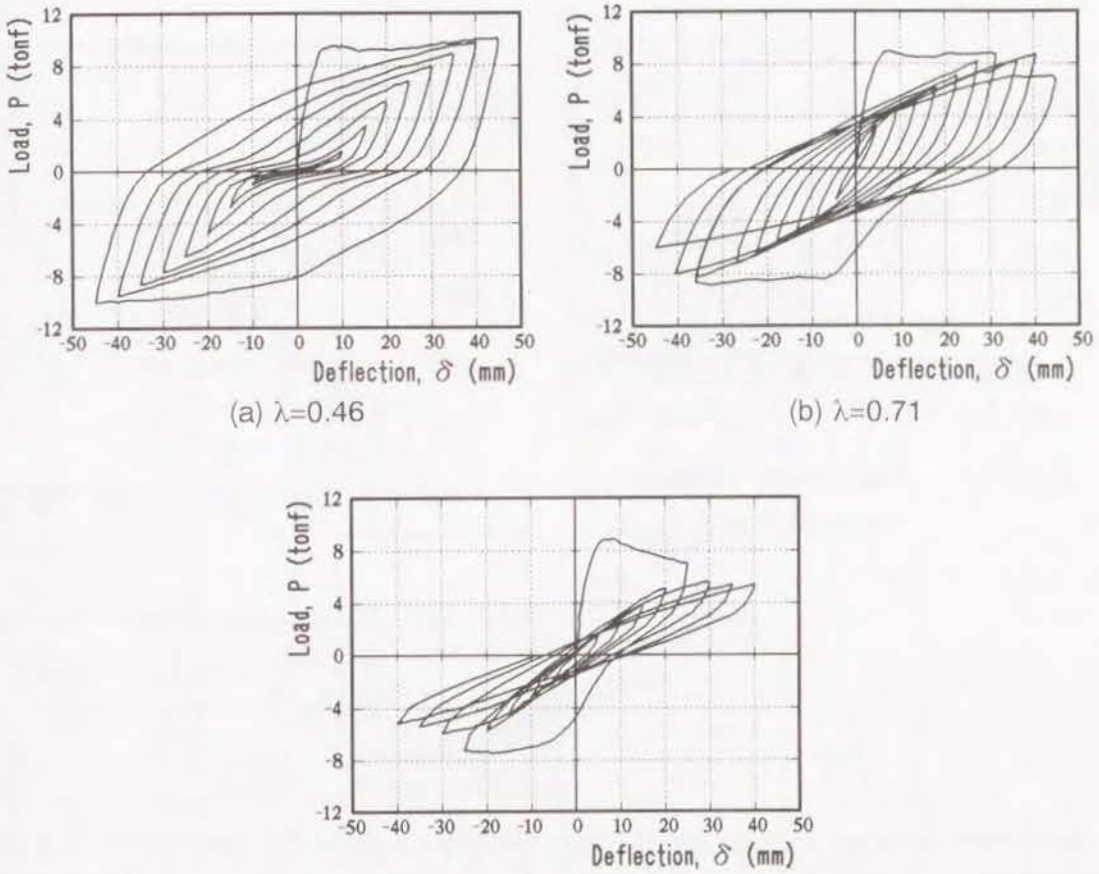

(a) λ=0.46 (b) λ=0.71

(c) λ=0.87

Fig.5-13 Examples of load - deflection hysteresis loops of Series-B beams (ρ_s=2.43%)

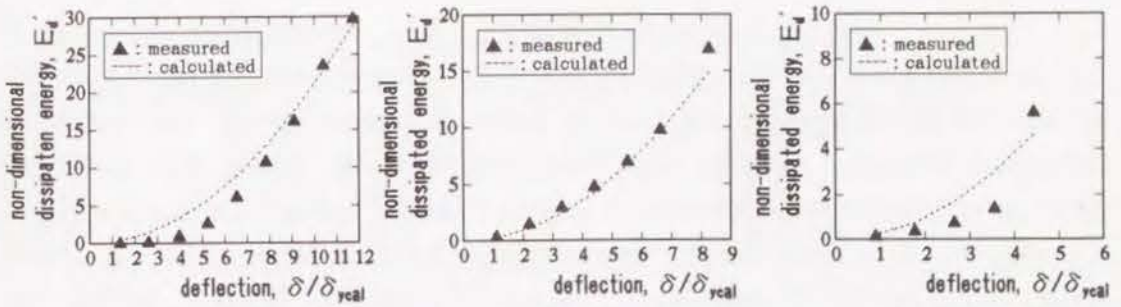

(a) λ=0.46 (b) λ=0.71 (c) λ=0.87

Fig.5-14 Examples of relationship between E_d' and δ/δ_{ycal} of Series-B beams (ρ_s=2.43%)

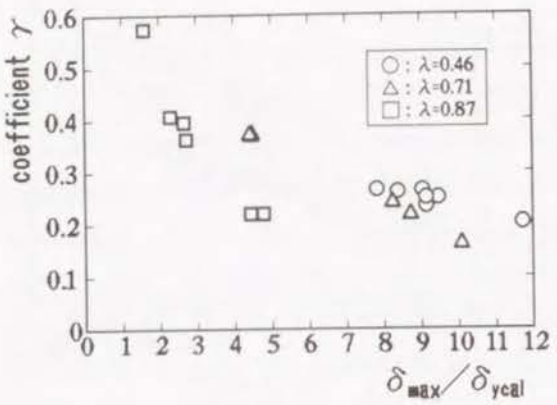

Fig.5-15 Relationship between coefficient γ and $\delta_{max}/\delta_{ycal}$

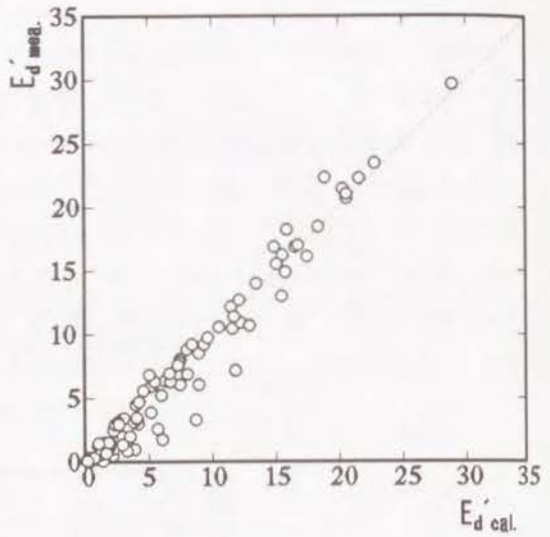

Fig.5-16 Relationship between measured and calculated E_d'-values of Series-B beams

agreement between the calculated and measured values of the beams with λ=0.87 is not so good compared with the cases of λ=0.46 and 0.71. This is mainly due to that the relative reduction ratio in E_d'-values from the first cycle to the second one tends to become larger with increasing λ-values, while the quadratic reduction process is assumed in the calculation irrespective of λ-values.

(3) Series-C

Fig.5-17 and Fig.5-18 show P-δ and E_d'-δ/δ_{ycal} relationships of Series-C beams, respectively. As indicated in Fig.5-18, E_d'-value of Series-C beams shows almost the same behavior as seen in Series-A beams during the deflection increasing process. On the other hand, the behavior during the deflection decreasing process resembles that of Series-B beams. In Fig.5-19 are compared the calculated E_d'-values with the measured ones for the 9 Series-C beams. These values coincide well with each other. Therefore, E_d'-value of Series-C beams can be expressed by the linear function of δ/δ_{ycal} within the deflection increasing region and by the quadratic function of δ/δ_{ycal} within the deflection decreasing region.

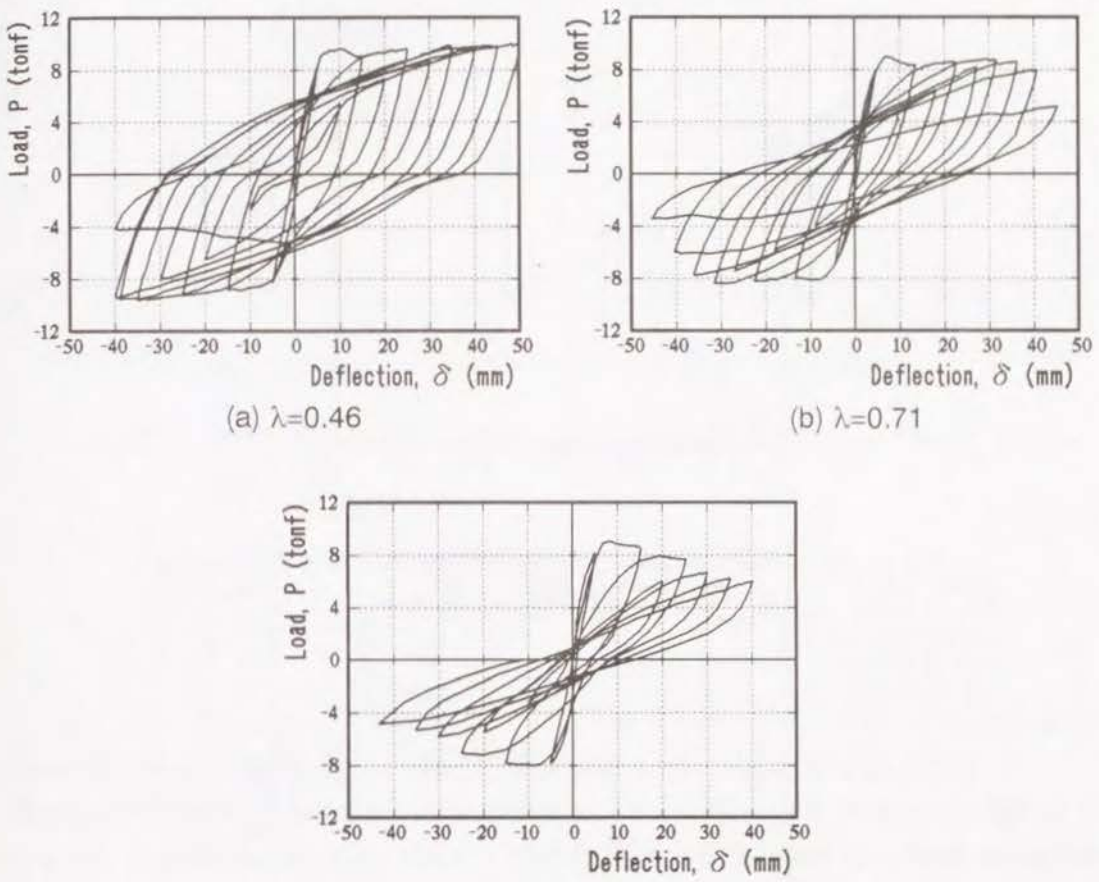

(a) λ=0.46 (b) λ=0.71

(c) λ=0.87

Fig.5-17 Examples of load - deflection hysteresis loops of Series-C beams (ρ_s=2.43%)

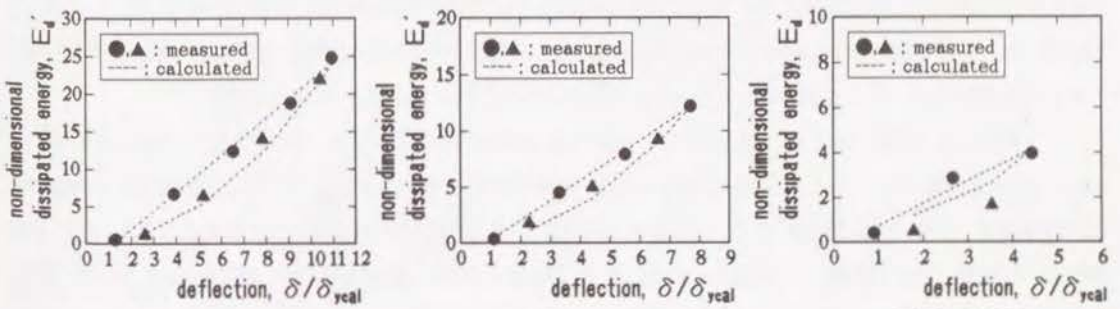

(a) λ=0.46 (b) λ=0.71 (c) λ=0.87

Fig.5-18 Examples of relationship between E_d' and δ/δ_{ycal} of Series-C beams (ρ_s=2.43%)

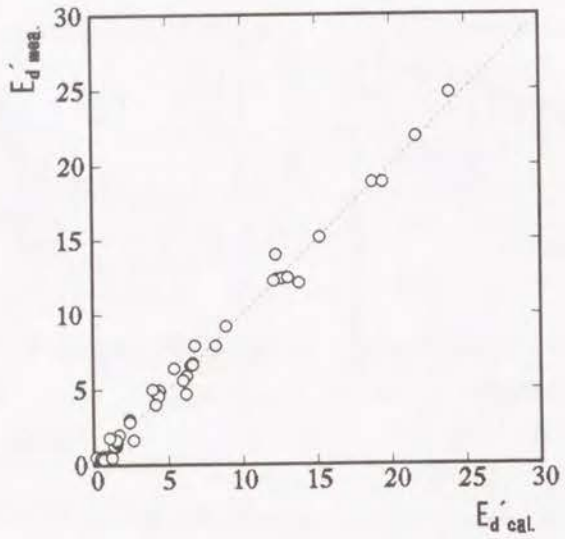

Fig.5-19 Relationship between measured and calculated E_d'-values of Series-C beams

(4) Series-D

In Fig.5-20 are shown some examples of load - deflection hysteresis loops of Series-D beams. Fig.5-21 shows an example of the ratio of non-dimensional dissipated energy at the n-th cycle ($E_d'(D(n))$) of each deflection amplitude to that at the first cycle ($E_d'(D(1))$). Fig.5-22 also shows the ratio of non-dimensional dissipated energy at the first cycle of each deflection amplitude of Series-D beams ($E_d'(D(1))$) to that of corresponding Series-A beams at the same deflection amplitude ($E_d'(A)$).

As shown in Fig.5-21, E_d'-value at the same deflection amplitude decreases with increasing number of load repetition. At the deflection amplitude of δ_y, E_d'-value at the second cycle is reduced to 60~80% of that at the first cycle. After ten load repetitions, E_d'-value becomes 40~60% of that at the first cycle.

Almost the same tendency can be observed at the deflection amplitude of $2\delta_y$, although the reduction ratio after ten load repetitions is somewhat smaller compared with the case of δ_y. At the deflection amplitudes of more than $3\delta_y$, on the other hand, the reduction property in E_d'-values is somewhat different from that observed at δ_y and $2\delta_y$, in that the reduction in E_d'-value from the first cycle to the second one is very small and the total reduction ratio after ten load repetitions is at most 10%.

The mechanism of these facts is supposed to be that the energy required to

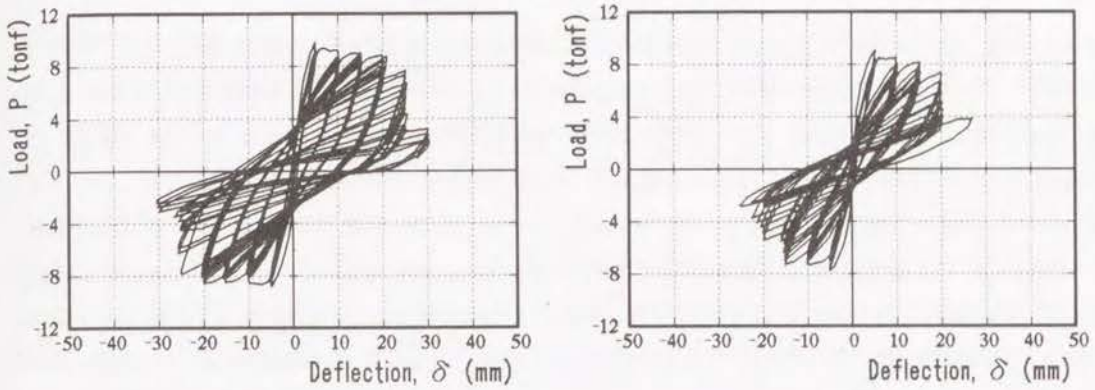

(a) λ=0.70 (b) λ=0.89

Fig.5-20 Examples of load - deflection hysteresis loops of Series-D beams (ρ_s≅2.5%)

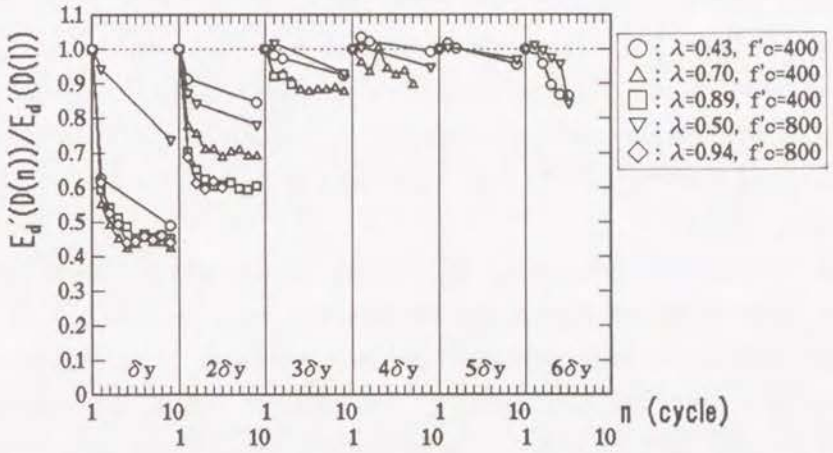

Fig.5-21 Changes of $E_d'(D(n))/E_d'(D(1))$ with repeated cycles (ρ_s≅2.5%)

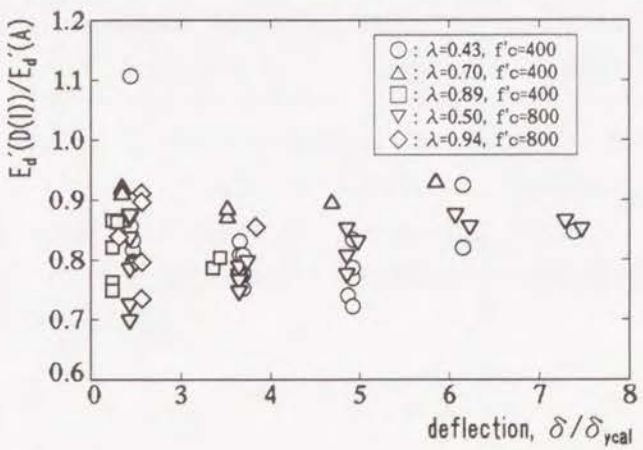

Fig.5-22 Relationship between $E_d'(D(1))/E_d'(A)$ and δ/δ_{ycal}

cause the same deformation after the second cycle is small compared with that at the first cycle at smaller deflection amplitudes of less than $2\delta_y$ because there are few extensive cracks at this stage and constituent materials are in the state of slightly beyond their elastic range. At the deflection amplitudes of more than $3\delta_y$, on the other hand, larger energy is required even after the second cycle because crushing of concrete and debonding between concrete and steels are accelerated by the repeated cycles, and energy is also dissipated by the friction at the interface of extensive cracks, resulting in a smaller decreasing ratio of dissipated energy due to load repetitions. At the deflection amplitude near the ultimate state, for example, $6\delta_y$, E_d'-value begins to decrease remarkably with repeated cycles.

At the deflection amplitudes of more than $2\delta_y$ up to the ultimate state, E_d'-value of Series-D beams at the first cycle of each deflection amplitude is reduced to 70-90% of that of corresponding Series-A beams at the same deflection amplitude. This implies that the energy dissipated at a certain deflection amplitude is influenced by the preceding load repetitions at smaller deflection amplitudes.

From the above mentioned results, E_d-values of the beams subjected to reversed cyclic loading with 10 load repetitions at each deflection amplitude can be estimated as below.

As mentioned previously, E_d'-values at the same deflection amplitude decrease with repeated cycles and its reduction ratio is affected by the applied deflection amplitude and repeated cycles. Therefore, it is assumed that the reduction ratio from the first cycle to the second one is the largest and then becomes smaller and constant from the second cycle to the tenth one. It is also assumed that E_d'-value of Series-D beams at the first cycle of each deflection amplitude is reduced compared with that of corresponding Series-A beams with only one load repetition at each deflection amplitude. These reduction ratios were decided based on the experimental data of Series-D beams.

(a) In case of $\delta=\delta_y$

$$E_d'(D(1))=E_d'(A) \tag{5-13}$$

$$E_d'(D(n))=0.7E_d'(D(1))-\frac{0.2}{8}(n-2) \qquad (2\leq n\leq 10) \tag{5-14}$$

(b) In case of $\delta=2\delta_y$

$$E_d'(D(1))=0.83E_d'(A) \tag{5-15}$$

$$E_d'(D(n))=0.8E_d'(D(1))-\frac{0.1}{8}(n-2) \qquad (2\leq n\leq 10) \tag{5-16}$$

(c) In case of $\delta\geq 3\delta_y$

$$E_d'(D(1))=0.83E_d'(A) \tag{5-17}$$

$$E_d'(D(n))=0.95E_d'(D(1))-\frac{0.05}{8}(n-2) \qquad (2\leq n\leq 10) \tag{5-18}$$

Where,

$E_d'(D(1))$: non-dimensional dissipated energy at the first cycle of each deflection amplitude.

$E_d'(D(n))$: non-dimensional dissipated energy at the n-th cycle of each deflection amplitude.

$E_d'(A)$: non-dimensional dissipated energy of corresponding Series-A beam calculated from Eq.(5-7) and Eq.(5-8) at the same deflection amplitude.

n: repeated cycles.

Fig.5-23 shows the comparison of the calculated E_d-values with the measured ones. In Fig.5-24 are also shown the relationship between the measured and calculated E_d'-values for totally 29 Series-D beams at all deflection amplitudes and repeated cycles.

As shown in Fig.5-23, calculated E_d'-values coincide well with the measured ones within the range of $\delta\leq 3\delta_y$, while tend to underestimate the measured values at the deflection amplitude of more than 4δ. This is mainly due to that E_d'-values of corresponding Series-A beam calculated from Eq.(5-7) and Eq.(5-8) tend to be underestimated at larger deflection amplitudes as indicated in Fig.5-10. However, the difference between measured and calculated E_d'-values are relatively small as shown in Fig.5-24 and E_d'-values of Series-D beams can be well estimated by the above mentioned method.

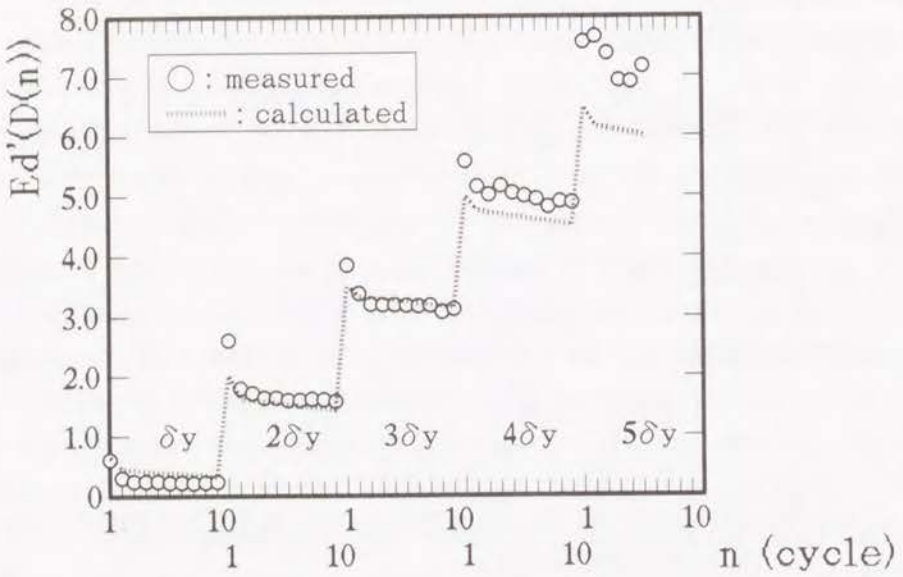

Fig.5-23 Example of changes of measured and calculated E_d'-value (λ=0.70, ρ_s=2.66%)

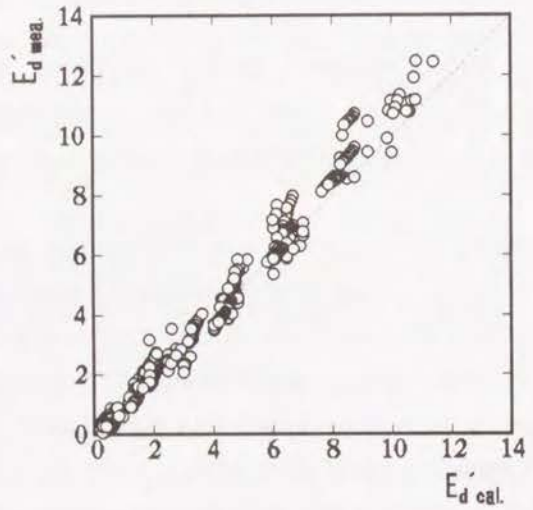

Fig.5-24 Relationship between measured and calculated E_d'-values of Series-D beams

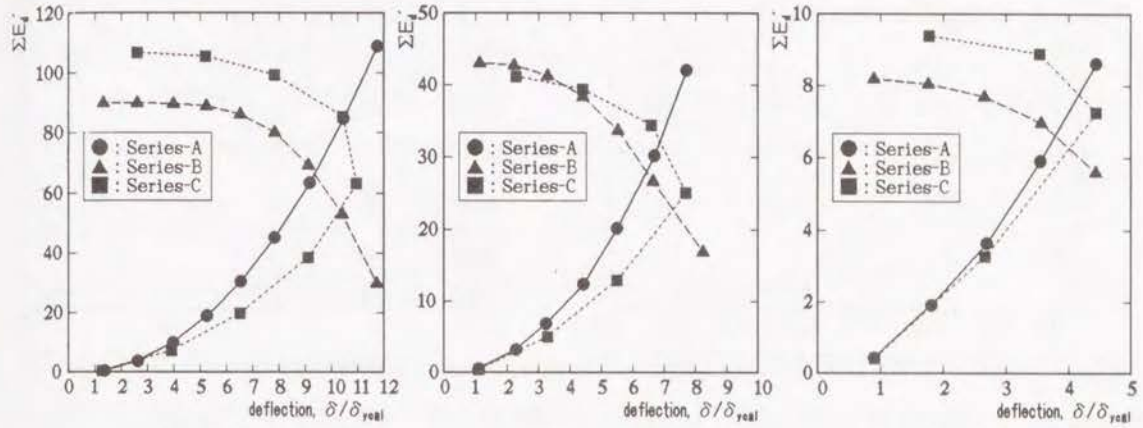

(a) λ=0.46 (b) λ=0.71 (c) λ=0.87

Fig.5-25 Effects of loading histories on $\Sigma E_d'$ (ρ_s=2.43%)

5.4.4 Accumulation Behavior of Non-dimensional Dissipated Energy

Fig.5-25 shows the effect of loading histories on the accumulation process of non-dimensional dissipated energy until the ultimate state.

The effect of loading histories on the non-dimensional total dissipated energy until the ultimate state ($\Sigma E_{d\,ult.}'$) is different according to λ-value. In case of λ=0.46, the value of $\Sigma E_{d\,ult.}'$ becomes approximately 15% smaller under gradually decreased cyclic loading as Series-B test than that under gradually increased one as Series-A. In Series-B tests, a relatively large deflection amplitude was applied at the first cycle of loading. Therefore, large diagonal cracks were extended at the first cycle in the beams with smaller prestress, for example, λ=0.46. These cracks remained open even at unloading, resulting in the pinching effect in P-δ hysteresis loop and reduction in dissipated energy. While in the beams with higher λ-values (λ=0.71 and 0.87), remarkable differences according to the loading histories cannot be observed. In these cases, significant diagonal cracks did not occur even at a large deflection amplitude and restoring performance of cracks was well due to the effectiveness of higher introduced prestress. From these results, the effect of loading histories on the accumulation behavior of dissipated energy in partially prestressed concrete beams is supposed to become smaller with increasing λ-value.

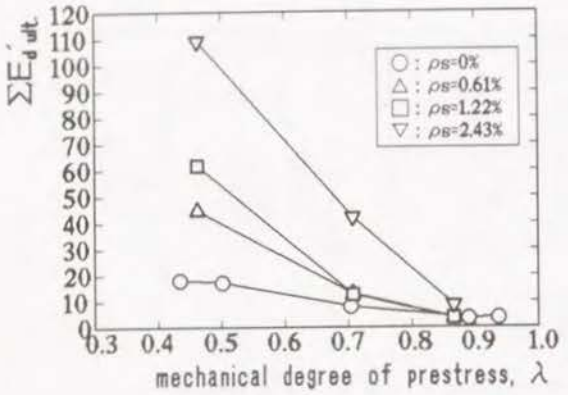

Fig.5-26 Effects of λ on $\Sigma E_{d\,ult.}'$-value (Series-A)

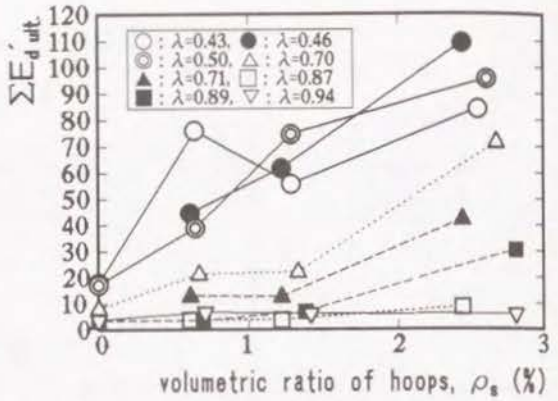

Fig.5-27 Effects of ρ_s on $\Sigma E_{d\,ult.}'$-value (Series-A)

5.4.5 Non-dimensional Total Dissipated Energy until the Ultimate State

In Fig.5-26 and Fig.5-27 are shown the effects of mechanical degree of prestress (λ) and volumetric ratio of transverse hoops (ρ_s) on the non-dimensional total dissipated energy until the ultimate state ($\Sigma E_{d\,ult.}'$) in Series-A beams, respectively. The value of $\Sigma E_{d\,ult.}'$ decreases with increasing λ-value and can be assumed to be almost in inverse proportion to λ-values when ρ_s-value is constant. On the other hand, $\Sigma E_{d\,ult.}'$-value increases with increasing ρ_s-value, and quadratic function can be assumed between $\Sigma E_{d\,ult.}'$ and ρ_s under a constant λ-value. It is also found that the effectiveness of transverse hoops on the improvement of energy dissipation properties is dependent on λ-value. From these results, $\Sigma E_{d\,ult.}'$-value can be expressed by Eq.(5-19).

$$\Sigma E_{d\,ult.}' = a\rho_s^2 + b\left(\frac{1}{\lambda}\right) + c\left(\frac{\rho_s^2}{\lambda}\right) + d \qquad (5\text{-}19)$$

The values of the coefficients, a, b, c and d should be estimated separately for Series-A beams and Series-D beams, respectively, because $\Sigma E_{d\,ult.}'$-values of Series-D beams are substantially different from those of Series-A beams due to ten load repetitions at each deflection amplitude, resulting in larger $\Sigma E_{d\,ult.}'$-values. On the other hand, the values of these coefficients estimated for Series-A beams are supposed to be applicable to Series-B and Series-C beams because the total dissipated energy until the ultimate state is not remarkably different among Series-

A, B and C beams although $\Sigma E_{d\,ult.}'$-value of Series-B beam is a little smaller compared with that of Series-A and Series-C beam.

As for the coefficients, a, b, c and d, for Series-A beams, the following values were obtained from the regression analysis of test results.

a=-5.52, b=32.48, c=7.44, d=-35.20
(Standard deviation of $\Sigma E_{d\,ult.}'$ was 13.52.)

On the other hand, the values of these coefficients for Series-D beams were estimated as below from experimental data.

a=-29.39, b=45.69, c=30.28, d=-46.44
(Standard deviation of $\Sigma E_{d\,ult.}'$ was 24.01.)

Each calculated value of the non-dimensional total dissipated energy until the ultimate state obtained from Eq.(5-19) ($\Sigma E_{d\,ult.(cal)}'$) is indicated together with the measured one ($\Sigma E_{d\,ult.(mea)}'$) in Fig.5-28 and Fig.5-29 for Series-A and Series-D beams, respectively. As seen in these figures, $\Sigma E_{d\,ult.}'$-values are supposed to be estimated to a certain extent. However, the difference between the measured and the calculated $\Sigma E_{d\,ult.}'$-values is relatively large in Series-A beams as indicated in the value of standard deviation of 13.52. This is mainly due to that only the effects of volumetric ratio of transverse hoops and mechanical degree of prestress are considered in the calculation processes and also that the ultimate state defined in this study does not always represent the real ultimate state of each specimen.

On the other hand, in Fig.5-30-(a)-(d) are shown the relationship between $\Sigma E_{d\,ult.(mea)}'$-values and $\Sigma(E_{d\,cal}')_{ult.}$-values of Series-A, B, C and D beams respectively, in which the $\Sigma(E_{d\,cal}')_{ult.}$ is expressed by the sum of the calculated E_d'-value ($E_{d\,cal}'$) at each deflection amplitude derived from Eq.(5-7)-Eq.(5-18) up to the ultimate state of each specimens. In these cases, $\Sigma(E_{d\,cal}')_{ult.}$-values coincide very well with the corresponding $\Sigma E_{d\,ult.(mea)}'$-values. This implies that non-dimensional total dissipated energy until the ultimate state can be well estimated by using Eq.(5-7)-Eq.(5-18) if the loading history until the ultimate state is given.

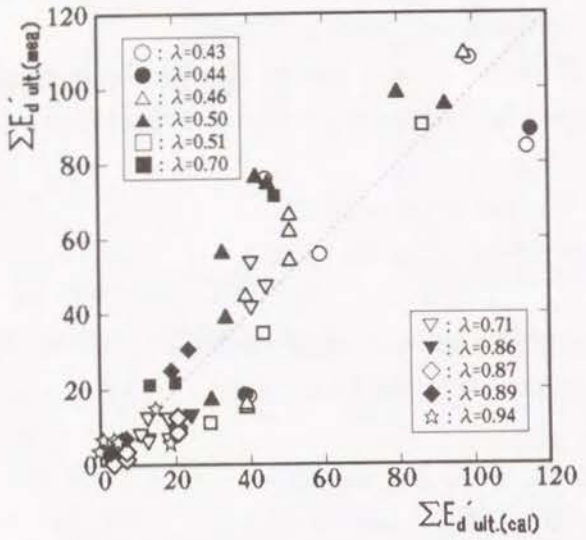

Fig.5-28 Comparison between $\Sigma E'_{d\ ult.(mea)}$-values and $\Sigma E'_{d\ ult.(cal)}$-values (Series-A)

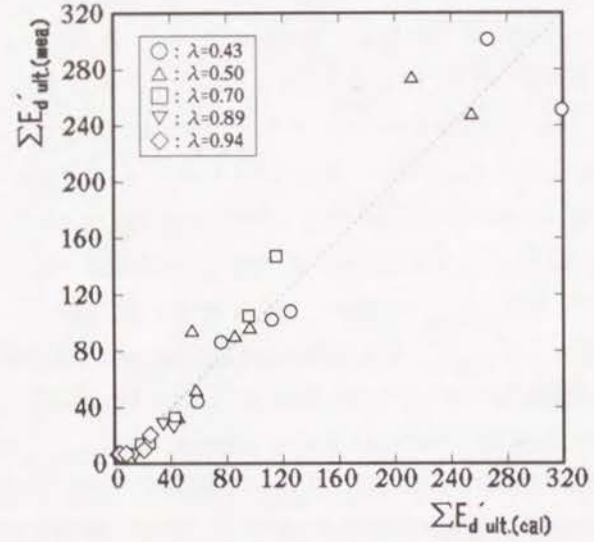

Fig.5-29 Comparison between $\Sigma E'_{d\ ult.(mea)}$-values and $\Sigma E'_{d\ ult.(cal)}$-values (Series-D)

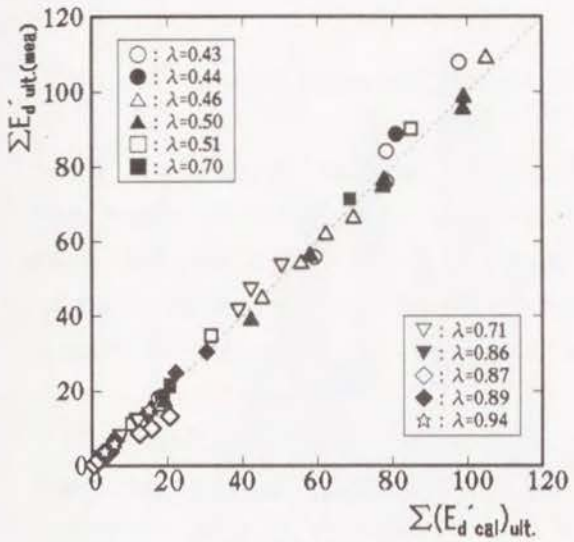

(a) Series-A

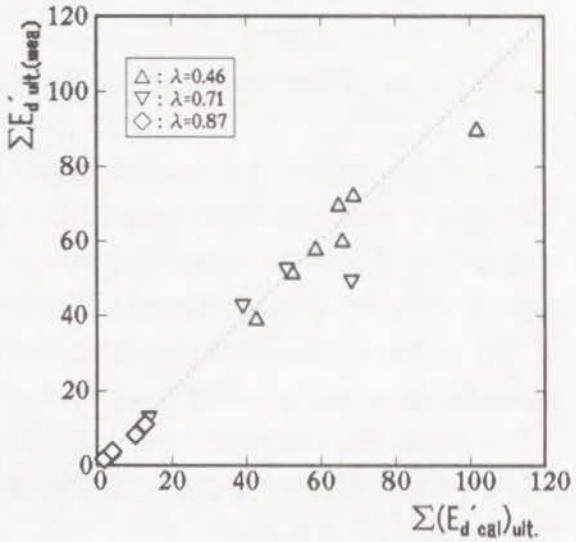

(b) Series-B

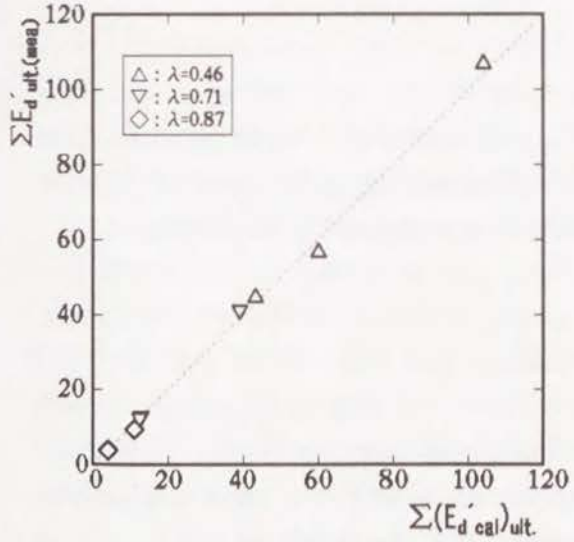

(c) Series-C

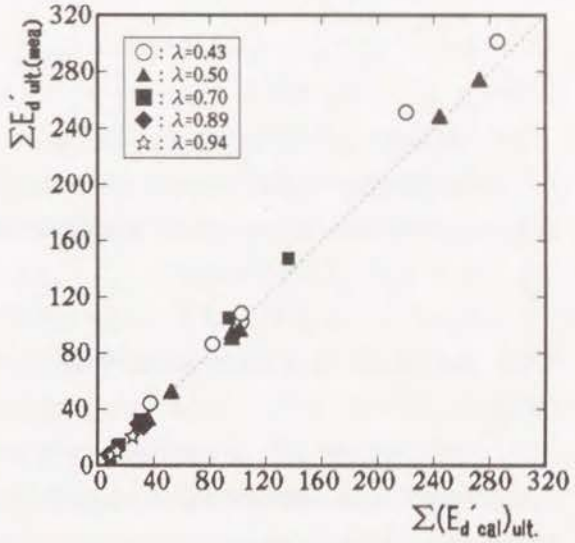

(d) Series-D

Fig.5-30 Comparison between $\Sigma E'_{d\ ult.(mea)}$-values and $\Sigma(E'_{d\ cal})_{ult.}$-values

5.5 DAMAGE EVALUATION BASED ON HYSTERETIC DISSIPATED ENERGY [15, 18]

5.5.1 Concept of Damage Index Based on Hysteretic Dissipated Energy

If the degree of seismic damage of concrete structures or members under earthquake loads can be expressed numerically, it will be a criterion for repair and strengthening of damaged concrete structures or members. As for the index representing the seismic damage, for example, damage index proposed by Park et al. [1] is well known. Here is discussed the possibility of the evaluation of seismic damage based on hysteretic dissipated energy.

Here, the damage index (DI) in this study is defined as Eq.(5-20). DI=0 represents no damage and DI=1.0 means that a member reaches its ultimate state, for example in this study, when the load carrying capacity at given deflection amplitude reduces to 80% of the maximum ultimate load.

$$DI = \frac{\Sigma E_d'}{\Sigma E_{d\,ult.}'} \qquad (5\text{-}20)$$

Where, $\Sigma E_{d\,ult.}'$ is the non-dimensional total energy which can be dissipated by a member until the ultimate state under a given loading history, and $\Sigma E_d'$ is the accumulated non-dimensional energy dissipated actually during the loading.

5.5.2 Application to Experimental Results

$\Sigma E_d'$-value of a member can be calculated from its load - deflection hysteresis loops obtained during loading sequence. Even in the case without P-δ hysteresis loops, it can be calculated from Eq.(5-7)-Eq.(5-18) if the history of applied deflection amplitude is given, for example, by response analysis. As for the value of $\Sigma E_{d\,ult.}'$, on the other hand, it is very difficult to estimate a true and accurate value of each member because $\Sigma E_{d\,ult.}'$-value of a member is affected by too many factors and will be different according to the applied loading histories as mentioned previously. However, the approximate value of DI can be obtained if the $\Sigma E_{d\,ult.}'$-value of a member can be estimated with a certain accuracy.

Considering that the $\Sigma E_{d\,ult.}'$-values of Series-B and Series-C beams are

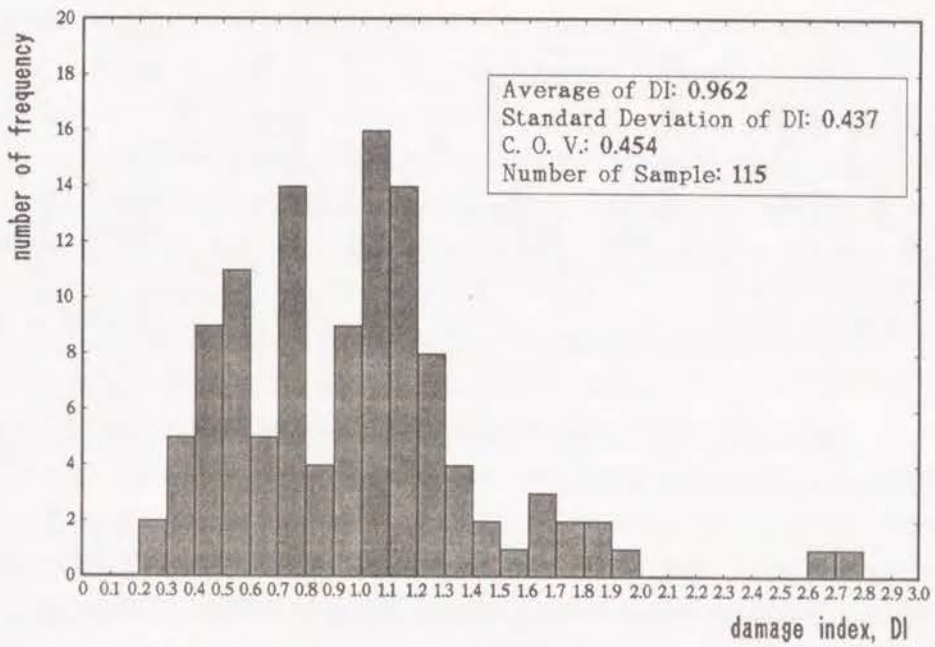

Fig.5-31 Statistics of DI at the ultimate state

almost equal to those of Series-A ones, $\Sigma E_{d\,ult.(cal)}'$-values obtained from Eq.(5-19) for Series-A beams can replace the real $\Sigma E_{d\,ult.}'$-values of Series-A, B and C beams. As for Series-D beams, on the other hand, $\Sigma E_{d\,ult.(cal)}'$-values obtained from Eq.(5-19) by using different values of coefficients from Series-A should be used.

DI-value for each beam at the respective ultimate state was calculated by using Eq.(5-20) by replacing $\Sigma E_{d\,ult.}'$ with $\Sigma E_{d\,ult.(cal)}'$ obtained from Eq.(5-19). In Fig.5-31 are shown the results. As shown in this figure, a high degree of scattering (C.O.V.=0.454) in DI-value at the ultimate state is observed, which is almost the same or somewhat smaller compared with that observed in Park's Damage Index (C.O.V≅0.5) [1]. This is mainly due to the high uncertainty in the definition of the ultimate state under reversed cyclic loading and in the effects of test variables.

In Fig.5-32 are shown some examples of the changes of DI during loading tests. In Series-A, the degree of damage is small at an early stage of loading and the increasing ratio of the accumulated damage becomes larger with increasing applied deflection amplitude. In Series-B, on the other hand, the beams are damaged significantly by the first cycle. After that, however, the increasing ratio of the accumulated damage becomes smaller. In Series-D beams, damage is accumulated by ten load repetitions at each deflection amplitude, resulting in reaching its ultimate state at a smaller deflection amplitude compared with the

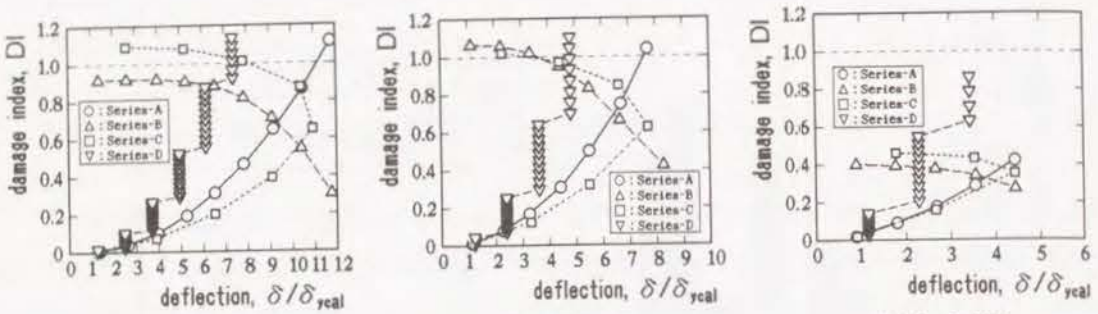

(a) λ≅0.46 (b) λ≅0.71 (c) λ≅0.87

Fig.5-32 Examples of changes of DI (ρ_s≅2.5%)

corresponding Series-A beam. In case of the beams with λ=0.87, DI-value does not reach 1.0 even at the end of loading. This is due to that the value of $\Sigma E'_{d\,ult\,(cal)}$ calculated by Eq.(5-19) may be larger than the actual value.

As previously mentioned, non-dimensional total dissipated energy until the ultimate state is affected by not only the test variables adopted in this study but also some other factors. Therefore, further investigations on the energy dissipation properties should be necessary in order to establish the evaluation method for seismic damage of concrete structures based on hysteretic dissipated energy.

5.6 CONCLUSIONS OF CHAPTER 5

In this chapter, the effects of various test variables on the energy dissipation properties of partially prestressed concrete beams including ordinary prestressed concrete ones are investigated. In addition, an example of damage index based on hysteretic dissipated energy is proposed based on the experimental results. Main conclusions obtained in this chapter are as follows.

(1) Energy dissipation properties of partially prestressed concrete beams are affected mainly by volumetric ratio of transverse hoops and mechanical degree of prestress. The effects of compressive strength of concrete, longitudinal steel index and shear span effective depth ratio are relatively small compared with those of volumetric ratio of transverse hoops and mechanical degree of prestress.

(2) Non-dimensional dissipated energy, which is normalized by the product of

calculated yield load and yield deflection, of partially prestressed concrete beams is also influenced by the applied loading histories. The value of non-dimensional dissipated energy at each deflection amplitude can be expressed by a linear function of the applied deflection amplitude within the deflection increasing process, and by a quadratic one within the deflection decreasing process. The value of the coefficients in these functions are dependent mainly on the value of mechanical degree of prestress.

(3) Non-dimensional dissipated energy at the same deflection amplitude decreases with repeated cycles. Its decreasing ratio is affected by the applied deflection amplitude and number of repeated cycles.

(4) Non-dimensional dissipated energy of partially prestressed concrete beams at any deflection amplitude before the ultimate state can be well estimated by the methods indicated in this chapter.

(5) The value of non-dimensional total dissipated energy until the ultimate state is almost equal if the sum of the applied deflection amplitude is the same, although it tends to be somewhat smaller in case of smaller mechanical degree of prestress under gradually decreased deflection type loading as Series-B.

(6) Non-dimensional total dissipated energy until the ultimate state of partially prestressed concrete beams increases with increasing volumetric ratio of transverse hoops, while it decreases with increasing mechanical degree of prestress. Non-dimensional total dissipated energy until the ultimate state can be estimated to a certain extent by a function of mechanical degree of prestress and volumetric ratio of transverse hoops.

(7) Degree of damage of partially prestressed concrete beams under reversed cyclic loading can be expressed quantitatively by the damage index based on the hysteretic dissipated energy as indicated in this study. However, further investigations on the accumulation process of dissipated energy are necessary for more accurate evaluation of seismic damage of concrete structures.

REFERENCES OF CHAPTER 5

1) Park, Y. J. and Ang, A. H-S., "Mechanistic Seismic Damage Model for Reinforced Concrete," Journal of Structural Engineering, ASCE, Vol.111, No.4, pp.722-739, 1985.

2) Chung, Y. S., Meyer, C. and Shinozuka, M., "Modeling of Concrete Damage,"

ACI Structural Journal, Vol.88, No.3, pp.259-271, 1989.

3) Muguruma, H., Watanabe, F., Fukai, S. and Nasu, T., "Fundamental Study on the Behavior of Class 3 Partially Prestressed Concrete Beam," Proc. of JCI 2nd Conference, pp.381-384, 1980. [in Japanese]

4) Oishi, R., "Fundamental Study on the Flexural Behaviors of Class III Prestressed Concrete Beams," Master Thesis of Kyoto University, 1980. [in Japanese]

5) Inoue, S., Kobayashi, K. and Katsuno, Y., "Inelastic Deformation Properties of Partially Prestressed Concrete Beams under Reversed Cyclic Loading," Proc. of the 42nd Annual Conference of the JSCE, Vol.5, pp.232-233, 1987. [in Japanese]

6) Suzuki, K., Nakatsuka, T., Hiramatsu, K. and Nagata, S., "High Ductile Behavior of Partially Prestressed Concrete Beams with Confined Concrete in the Compression Zone," Proc. of JCI 7th Conference, pp.485-488, 1985. [in Japanese]

7) Thompson, K. J. and Park, R., "Seismic Response of Partially Prestressed Concrete," Journal of the Structural Division, ASCE, Vol.106, No.ST8, pp.1755-1775, 1980.

8) Park, Y. J., Ang, A. H-S. and Wen, Y. K., "Seismic Damage Analysis of Reinforced Concrete Buildings," Journal of Structural Engineering, ASCE, Vol.111, No.4, pp.740-757, 1985.

9) Stephens, J. E. and Yao, J. T. P., "Damage Assessment Using Response Measurements," Journal of Structural Engineering, ASCE, Vol.113, No.4, pp.787-801, 1987.

10) Kobayashi, K., Inoue, S. and Matsumoto, T., "Inelastic Behavior of Partially Prestressed Concrete under Reversed Cyclic Loading," Proc. of the 5th Canadian Conference on Earthquake Engineering, Ottawa, pp.841-848, 1987.

11) Igo, Y., Inoue, S., Kobayashi, K. and Fujii, M., "Load Carrying Capacity of Partially Prestressed Concrete Members under Reversed Cyclic Loading, "Proc. of the 43rd Annual Conference of the JSCE, Vol.5, pp.610-611, 1988. [in Japanese]

12) Inoue, S., Hattori, T., Miyagawa, T., Fujii, M. and Kobayashi, K., "Application of Rectangular Hoop as Lateral Confinement for Concrete Beam Members," CAJ Proceedings of Cement & Concrete, No.43, pp.340-345, 1989.

13) Inoue, S., Takahashi, K., Igo, Y., Miyagawa, T. and Fujii, M., "Effects of Various Factors on the Accumulated Dissipated Energy of Concrete Beams under Reversed Cyclic Loading," Proc. of the 45th Annual Conference of the JSCE, Vol.5, pp.674-675, 1990. [in Japanese]

14) Fukushima, Y., Hattori, A., Inoue, S., Miyagawa, T. and Fujii, M., "Effects of Various Factors on the Dissipated Energy of Partially Prestressed Concrete Beams," Proc. of Annual Meeting of the JSCE Kansai Branch, pp.V-5-1-V-5-2, 1993. [in Japanese]

15) Inoue, S., Miyagawa, T. and Fujii, M., "Effects of Loading Histories on the Energy Dissipation of Partially Prestressed Concrete Beams," Proc. of the FIP Symposium on Modern Prestressing Techniques and Their Applications, 1993. [in printing]

16) Japan Society of Civil Engineers, "Standard Specification for Design and Construction of Concrete Structures," 1986 and 1991. [in Japanese]

17) Kawashima, K., Hasegawa, K., Koyama, T. and Yoshida, T., "Effects of Cyclic Loading Hysteresis on Dynamic Behavior of Reinforced Concrete Bridge Piers," Civil Engineering Journal, Vol.29, No.4, pp.33-38, 1987. [in Japanese]

18) Inoue, S., Hattori, T., Miyagawa, T. and Fujii, M., "Effect of Loading Histories on the Energy Dissipation of Partially Prestressed Concrete Beams and Their Damage Evaluation," Proc. of the JCI, Vol.15, No.2, pp.401-406, 1993. [in Japanese]

CHAPTER 6

ENERGY DISSIPATION OF REINFORCED CONCRETE BEAMS AND THEIR DAMAGE EVALUATION BASED ON DISSIPATED ENERGY

6.1 GENERAL REMARKS

The evaluation of seismic damage of concrete structures is very important in order to take early countermeasures, such as repair and strengthening, for the deteriorated structures after severe earthquakes. The degree of seismic damages in concrete structures is related closely to the maximum response deformation and hysteretic dissipated energy of their constituent members. In case of cyclic loading, as experienced during earthquakes, however, the latter seems to be more predominant. From this reason, it is essential to make clear the accumulating process of dissipated energy under reversed cyclic loads in order to make an accurate evaluation of seismic damages in concrete structures.

From this view point, energy dissipation properties of partially prestressed concrete beams were investigated in Chapter 5 and the accumulating process of dissipated energy under different loading histories was made clear in quantitative sense.

As for the reinforced concrete beams, however, their final failure mode under reversed cyclic loading tends to be different from that of partially prestressed concrete beams. Reinforced concrete beams tend to fail in shear after yielding of longitudinal steels due to remarkable reduction in concrete shear resistance caused by many load reversals and repetitions even if they are designed to fail in flexure under unidirectional monotonous loads. On the other hand, partially prestressed concrete ones fail in flexure as designed even under reversed cyclic loading due to the effectiveness of introduced prestress which contributes to the increase in shear resistance of concrete.

These facts suggest that influencing factors on the energy dissipation properties of reinforced concrete members are somewhat different from those of partially prestressed concrete ones. Therefore, the effects of different factors from those considered in case of partially prestressed concrete members should be made clear in order to evaluate seismic damage of reinforced concrete members

based on hysteretic dissipated energy.

In this chapter, investigations are done on the effects of longitudinal reinforcement ratio and shear reinforcement ratio on the energy dissipation properties of reinforced concrete beams under different loading histories. In addition, the idea of damage index indicated in Chapter 5 is also applied to the experimental results of reinforced concrete beam specimens and 1/3 scale bridge pier model specimens. From these results, applicability of the proposed damage index is discussed.

6.2 REVIEW OF PREVIOUS RESEARCH WORKS

6.2.1 Energy Dissipation of Reinforced Concrete Members

In order to use hysteretic dissipated energy as an indicator of seismic damage of concrete structures, the total dissipated energy must somehow be normalized so as to compare the results from different test specimens.

As indicated in Chapter 5, there have been few researches which dealt with the energy dissipation properties of reinforced concrete members in a quantitative sense.

Darwin et al. [1] normalized the energy dissipation capacity of a member with respect to the elastic energy stored in the member at yielding. This normalized value is expressed by "Energy Dissipation Index" defined as below.

$$D_i = \frac{E}{0.5P_y\Delta_y[1+(A'_s/A_s)^2]} \qquad (6-1)$$

Where,

D_i: Energy Dissipation Index.
P_y: yield load in the strong direction under reversed load.
Δ_y: yield deflection in the strong direction.
A_s: area of reinforcing steel in the strong direction.
A'_s: area of reinforcing steel in the weak direction.
E: total energy dissipated by a member during loading.

In case of $A_s=A'_s$, D_i represents the same meaning as $\Sigma E_{d\,ult.}$ adopted in

Chapter 5.

In general, longitudinal reinforcement ratio, transverse reinforcement ratio, compressive strength of concrete, shear span – effective depth ratio, arrangement of longitudinal and transverse reinforcement, axial force, loading histories, loading rate, and so on are considered as the factors having influences on energy dissipation of reinforced concrete members.

Darwin et al. [1] also indicated that D_i-value of reinforced concrete members were mainly influenced by three factors, which are maximum applied shear stress, concrete strength and transverse steel capacity. They proposed the following equation representing the relationship between D_i-value and these three factors from the analysis of the different experimental data [2-7].

$$D_i = 222\frac{(v_s f'_c)^{0.5}}{v_m^{1.5}} - 17 \qquad (6-2)$$

Where,

v_m: maximum shear stress ($=V_m/bd$).
v_s: nominal shear stress provided by shear reinforcement ($=A_w f_{wy}/bs$).
V_m: maximum shear force.
b: width of web.
d: effective depth.
A_w: area of stirrup.
f_{wy}: yield strength of stirrup.
s: spacing of stirrups.
f'_c: compressive strength of concrete.

They recommended a value of $D_i \geqq 35$ for reinforced concrete members in order to provide adequate performance under cyclic loading.

Uomoto et al. [8] indicated that the accumulative dissipated energy of reinforced concrete beams up to rupture of longitudinal steel showed almost the same value irrespective of applied deflection amplitude and deformation histories if the failure mode was the same among the specimens.

On the other hand, Kawashima et al. [9] reported the effects of applied loading history on the total dissipated energy of reinforced concrete bridge pier model specimens. They indicated that the total dissipated energy under gradually decreased deformation type loading became approximately 15% smaller than that

under gradually increased deformation type loading as usually done in laboratories.

These results suggest the possibility of damage evaluation based on hysteretic dissipated energy although the effects of various factors should be considered.

6.2.2 Assessment of Seismic Damage Using Damage Indexes

Some results have been reported as for damage assessment of reinforced concrete structures and members using damage indexes proposed in recent years.

Park et al. [10] related the calculated value of their damage index to the observed seismic damage during past earthquakes. They divided the degree of damage into five classes, that is, slight, minor, moderate, severe and collapse, and indicated that the repairable limit of structures is $D \leq 0.4$ (moderately damaged).

Stephens et al. [11] also related the value of their damage function and Park's damage index to the observed damage of small scale model structures. In this report, relationship between four types of descriptive damage, that is, safe, slightly damaged, damaged and critically damaged, and each calculated damage function and damage index was investigated. The results showed that both of Stephen's damage function and Park's damage index correlated well with descriptive damage although considerable scattering was observed at higher damage levels, especially at the level of critical damage.

These researches indicated that these damage indexes could be reasonable and potentially effective measures of the damage conditions of reinforced concrete structures. However, it was also indicated that the available data were considered to be insufficient to reliably determine the correlation between these damage indexes and damage state.

6.3 EXPERIMENTAL PROCEDURES [12]

6.3.1 Specimens and Test Variables

Specimens tested are reinforced concrete beams having a rectangular cross section of width x full depth = 10 x 20cm and a total length = 160cm as shown in Fig.6-1. Three levels of longitudinal reinforcement ratio (p), 1.43, 2.26 and 3.28%,

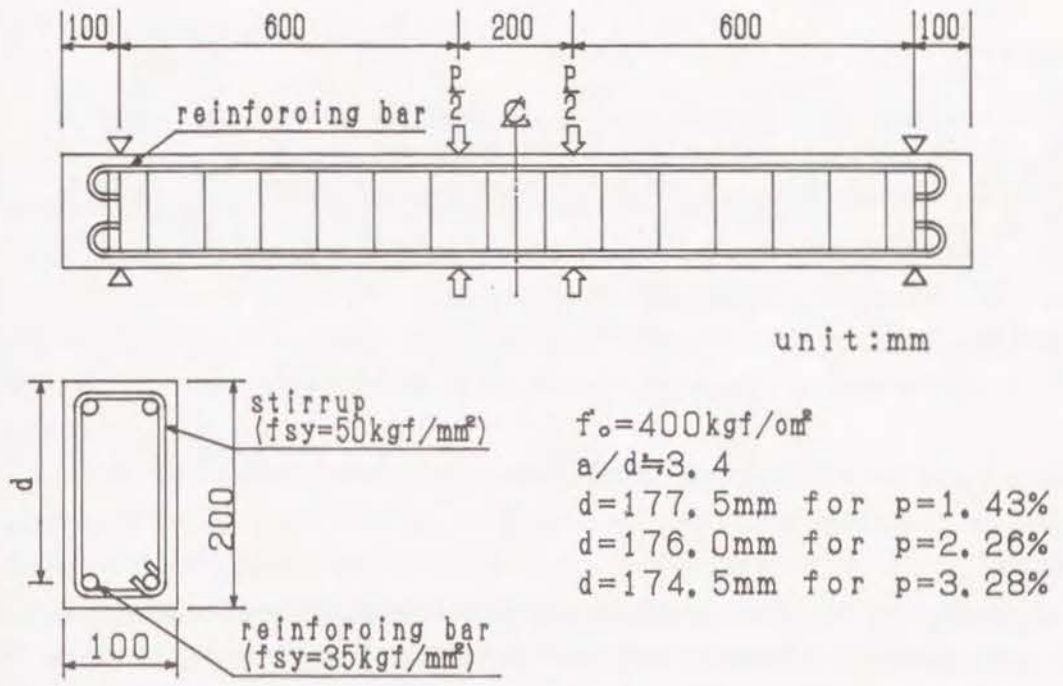

Fig.6-1 Dimensions of tested beams

and three levels of shear reinforcement ratio (p_w), 0.63, 0.95 and 1.26%, were selected. The reason to select shear reinforcement ratio as a test variable instead of volumetric ratio of lateral confinement is that the final failure mode of reinforced concrete members under reversed cyclic loading is affected by the shear resistance of concrete rather than the compressive ductility of concrete. The value of p_w=0.63% corresponds to the minimum required one prescribed in JSCE Standard Specification for Design and Construction of Concrete Structures [13]. Compressive strength of concrete (f'_c) was 400kgf/cm^2 for all of the specimens. The yield strength of longitudinal bars and stirrups was approximately 35kgf/mm^2 and 50kgf/mm^2, respectively.

6.3.2 Loading Histories

All of the beams were simply supported and loaded under symmetrical two-point load with a/d=3.4 (a: shear span length, d: effective depth). Two types of loading histories were adopted. The one (Series-A) was reversed cyclic loading with each one load reversal at gradually increased deflection amplitude of $\pm\delta_y$,

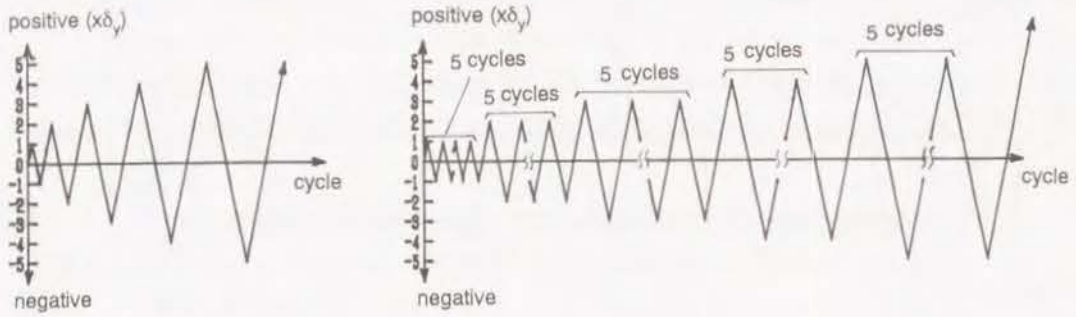

(a) Series–A (b) Series–B

Fig.6–2 Applied loading histories

$\pm 2\delta_y$, $\pm 3\delta_y$, --- (δ_y: yield deflection). The other (Series–B) had five load reversals at each gradually increased deflection amplitude. These loading histories are schematically shown in Fig.6–2.

6.4 RESULTS OF TESTS AND DISCUSSIONS [12]

6.4.1 Definition of the Ultimate State and Non–dimensional Dissipated Energy

It is necessary to define the ultimate state of members when the seismic damage of concrete structures should be evaluated. In this chapter, the same ultimate state as defined in Chapter 5 is adopted, that is, the point at which the reduction in load carrying capacity from the maximum load reached to 20% of the maximum load.

Non–dimensional dissipated energy at each deflection amplitude (E_d') as defined in Chapter 5 is also used in this chapter in order to eliminate the effect of difference in the maximum load carrying capacity among each specimen. Non–dimensional total dissipated energy until the ultimate state ($\Sigma E_{d\,ult.}'$) was calculated by summing each E_d'–value up to the ultimate state. In this case, the energy dissipated within the cycle at which the member reached its ultimate state is included in the $\Sigma E_{d\,ult.}'$–value.

6.4.2 Energy Dissipation in Series–A Beams

In Fig.6–3 are shown some examples of load – deflection hysteresis loops of Series–A beams. In addition, in Fig.6–4 are shown some examples of non–dimensional dissipated energy (E_d') at each deflection amplitude.

E_d'–value increases almost linearly with increasing deflection amplitude until the ultimate state, where the E_d'–value begins to decrease. The increasing ratio of the E_d'–value is influenced by the longitudinal reinforcement ratio, p, and it becomes smaller with increasing p–value, while the effect of the shear reinforcement ratio is not significant.

All of the beams tested failed finally in shear after yielding of longitudinal steels caused by significant reduction in shear resistance due to load reversals and repetition well into inelastic range. The deflection amplitude at which the E_d'–value begins to decrease becomes larger with increasing shear reinforcement ratio, p_w. In other words, shear reinforcement ratio determines the deflection amplitude at the ultimate state of reinforced concrete members subjected to load reversals well into the post–elastic range, as volumetric ratio of transverse hoops for lateral confinement does in case of partially prestressed concrete members. These facts imply that the predominant factor which determines the ultimate state of a member is different according to its ultimate failure mode.

6.4.3 Energy Dissipation in Series–B Beams

Fig.6–5 shows some examples of load – deflection hysteresis loops of Series–B beams. In Series–B, the energy dissipated in the first cycle at each deflection amplitude is affected by the previous load cycles. The ratio of $E_d'(B(1))/E_d'(A)$, where $E_d'(B(1))$ is non–dimensional energy dissipated at the first cycle at each deflection amplitude in Series–B beams and $E_d'(A)$ is non–dimensional energy dissipated in the corresponding deflection amplitude of Series–A beams, decreases approximately linearly with increasing deflection amplitude as seen in Fig.6–6, although scattering exists in the experimental data. This decreasing ratio is affected by the shear reinforcement ratio and becomes larger with decreasing p_w–value. In this case, the effect of longitudinal reinforcement ratio is not significant.

From these results, the following equation representing the relationship

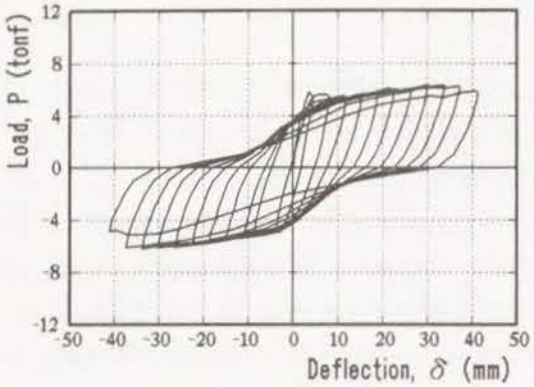

(a) p=1.43%, p_w=0.95%

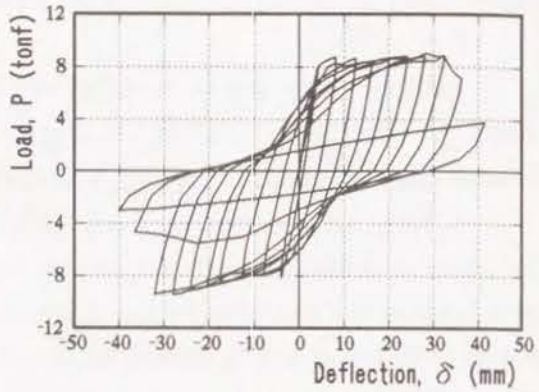

(b) p=2.26%, p_w=0.95%

Fig.6-3 Load – deflection hysteresis loops (Series-A)

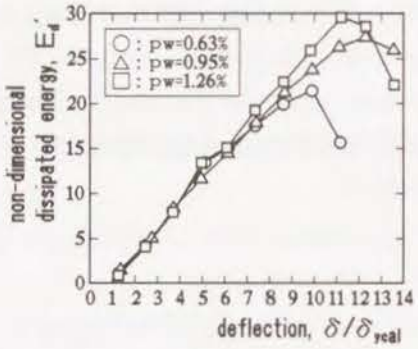

(a) p=1.43%

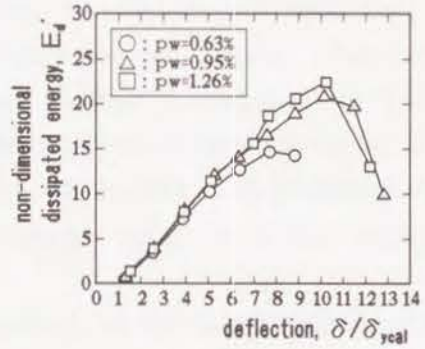

(b) p=2.26%

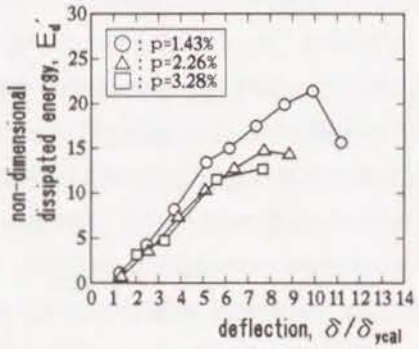

(c) p_w=0.63%

Fig.6-4 Changes of E_d'-value (Series-A)

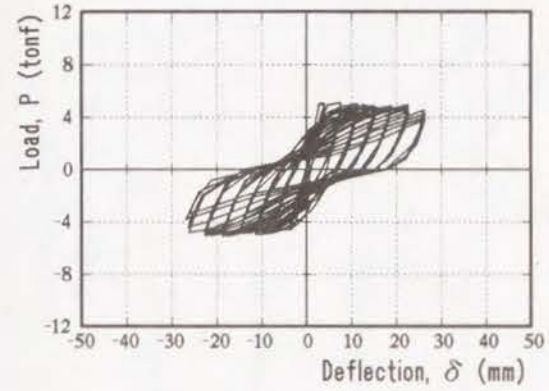

(a) p=1.43%, p_w=0.95%

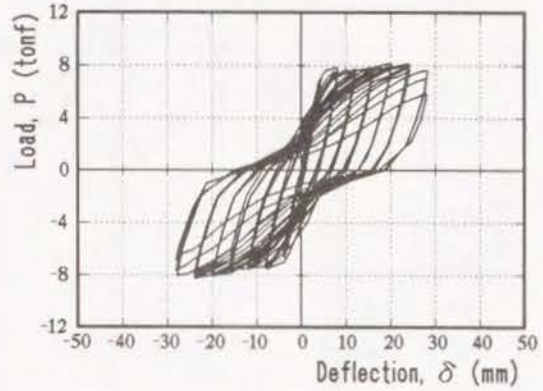

(b) p=2.26%, p_w=0.95%

Fig.6-5 Load – deflection hysteresis loops (Series-B)

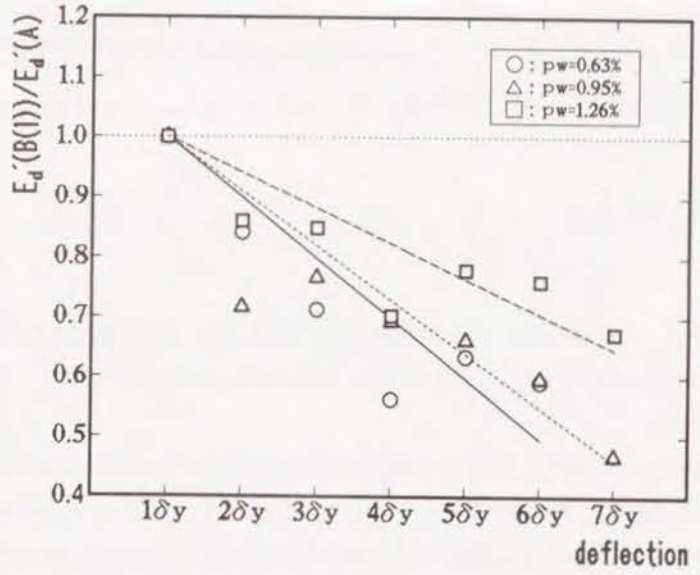

Fig.6-6 Relationship between E_d'(B(1))/E_d'(A) and applied deflection amplitude (p=1.43%)

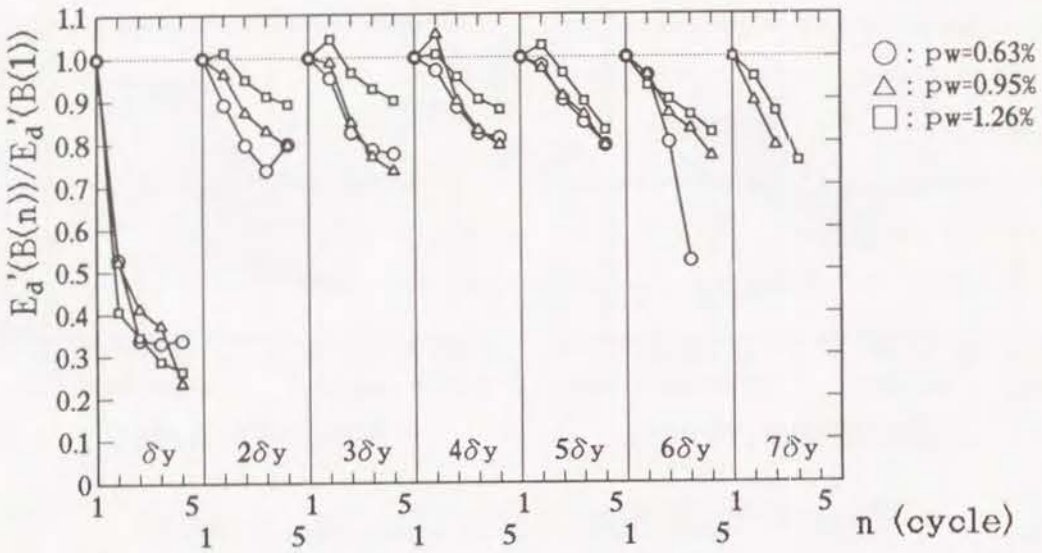

Fig.6–7 Relationship between $E_d'(B(n))/E_d'(B(1))$ and number of repeated cycles (p=1.43%)

between $E_d'(B(1))$ and $E_d'(A)$, which is a function of shear reinforcement ratio and applied deflection amplitude, was obtained.

$$\frac{E_d'(B(1))}{E_d'(A)} = 1-[\eta(\frac{\delta}{\delta_y})-1] \qquad (6-3)$$

Where δ is more than δ_y and η is a parameter affected by shear reinforcement ratio.

In this study, η=0.112, 0.082 and 0.056 was obtained for p_w=0.63, 0.95 and 1.26%, respectively.

On the other hand, the energy dissipated in each cycle at the same deflection amplitude of Series–B beams is affected by the number of repeated cycles (n), and the ratio of $E_d'(B(n))/E_d'(B(1))$, where $E_d'(B(n))$ is non–dimensional dissipated energy in the n–th cycle at each deflection amplitude, decreases with increasing n–value as shown in Fig.6–7. This decreasing ratio is influenced by the given deflection amplitude. At the deflection amplitude of $\delta=\delta_y$, the E_d'–value at the fifth cycle reduces to approximately 20% of that at the first cycle. At the deflection amplitude of more than $2\delta_y$, on the other hand, the E_d'–value at the fifth cycle reduces to at most 80% of that at the first cycle. In this case, the effects of

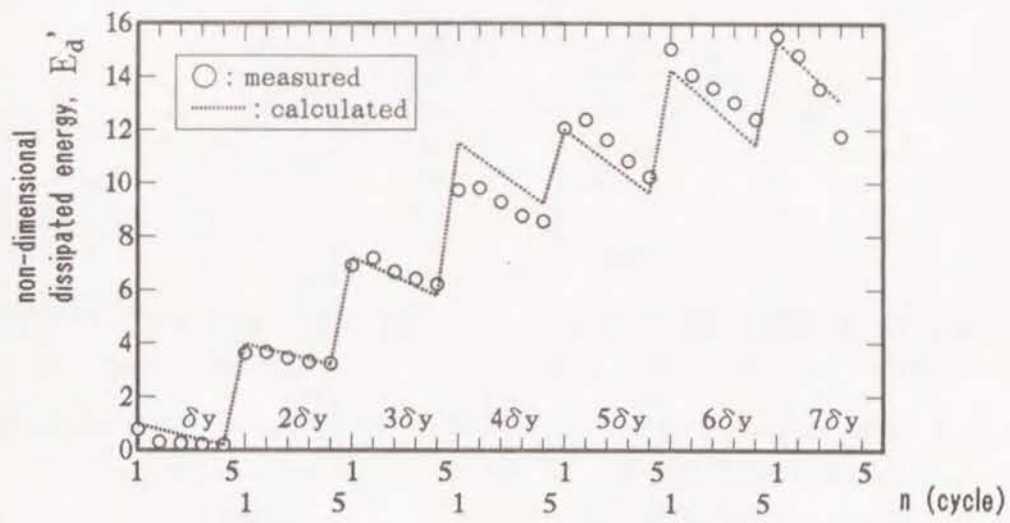

Fig.6–8 Comparison between the measured and calculated E_d'–values (Series–B, p=1.43%, p_w=1.26%)

longitudinal reinforcement ratio and shear reinforcement ratio are not significant.

From these results, the relationship between $E_d'(B(n))$ and $E_d'(B(1))$, which is given as a function of the number of the repeated cycles, were obtained as below.

$$\frac{E_d'(B(n))}{E_d'(B(1))} = 1-0.8\,\frac{n-1}{4} \qquad (\delta=\delta_y) \qquad (6-4)$$

$$= 1-0.2\,\frac{n-1}{4} \qquad (\delta\geq 2\delta_y) \qquad (6-5)$$

Where, n is the number of load repetitions not more than 5 at each deflection amplitude.

Fig.6–8 shows an example of the comparison between the measured and the calculated E_d'–values of a Series–B beam, where the latter is obtained from Eq.(6–3) to Eq.(6–5) using the E_d'–values of the corresponding Series–A beam. This figure indicates that the E_d'–values in Series–B beams can be well estimated by using the proposed equations if the energy dissipation properties under the fundamental loading process, in this case such as Series–A, is given.

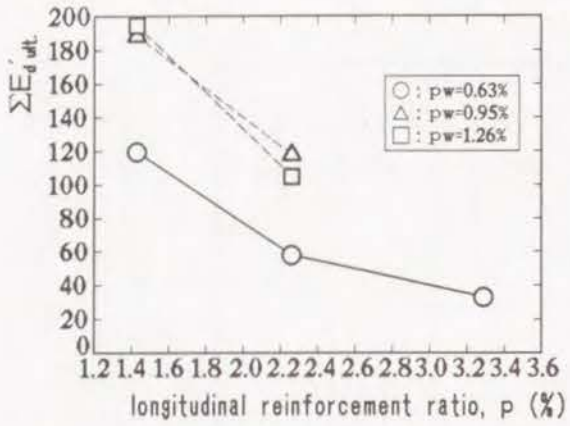

Fig.6–9 Effect of longitudinal reinforcement ratio on $\Sigma E_{d\,ult.}'$–value (Series–A)

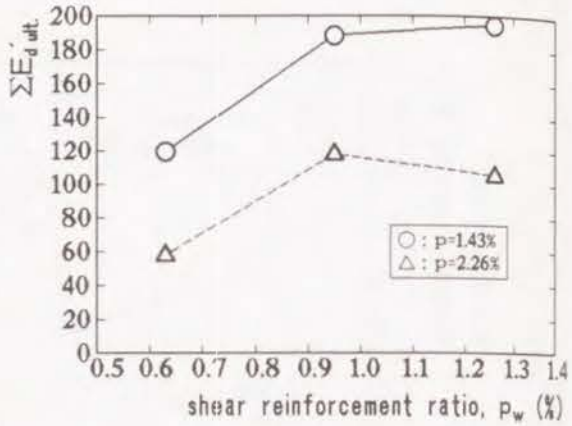

Fig.6–10 Effect of shear reinforcement ratio on $\Sigma E_{d\,ult.}'$–value (Series–A)

6.4.4 Total Dissipated Energy until the Ultimate State

Fig.6–9 and Fig.6–10 show the effects of the longitudinal reinforcement ratio and the shear reinforcement ratio on the non–dimensional total dissipated energy until the ultimate state ($\Sigma E_{d\,ult.}'$) of Series–A beams, respectively.

$\Sigma E_{d\,ult.}'$–value decreases with increasing p–value, while its decreasing ratio reduces with increasing p–value. On the other hand, $\Sigma E_{d\,ult.}'$–value increases with increasing p_w–value, although its increasing ratio decreases with p_w–value. These tendencies are also observed in Series–B beams. From these results, the equation representing the $\Sigma E_{d\,ult.}'$–values of the beams is proposed as Eq.(6–6) assuming that $\Sigma E_{d\,ult.}'$–values are in inverse proportion to longitudinal reinforcement ratio and expressed by a logarithmic function of shear reinforcement ratio.

$$\Sigma E_{d\,ult.}' = a*\ln(1+p_w)+b*\left(\frac{1}{p}\right)+c*\frac{\ln(1+p_w)}{p}+d \qquad (6\text{–}6)$$

Where, p and p_w are in percent, and a, b, c and d are experimental coefficients.

From the regression analysis of the experimental data, the values of the coefficients were obtained as a=44.54, b=123.27, c=266.89 and d=–69.89 for Series–A beams and a=449.50, b=205.93, c=–116.78 and d=–171.35 for Series–B beams. The $\Sigma E_{d\,ult.}'$–values calculated by Eq. (6–6) are compared with the

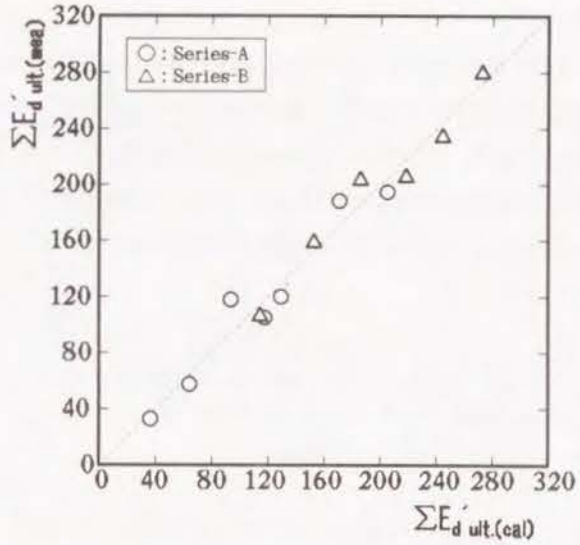

Fig.6–11 Comparison between the measured and calculated $\Sigma E_{d\,ult.}'$–values

measured ones in Fig.6–11. This figure indicates that the $\Sigma E_d'$–values of Series–A and Series–B beams can be well estimated by the proposed equation, although the number of used data is small.

6.5 DAMAGE EVALUATION OF REINFORCED CONCRETE MEMBERS [12]

6.5.1 Concept of Damage Index

As mentioned in Chapter 5, the degree of damage of a reinforced concrete member can be estimated by comparing the actual dissipated energy under a real earthquake with the total dissipated energy until the ultimate state. However, the $\Sigma E_{d\,ult.}'$–value of a member is essentially different according to the loading histories as seen in this study. In Chapter 5, therefore, hysteretic damage of a partially prestressed concrete member was evaluated by using respective $\Sigma E_{d\,ult.}'$–value corresponding to each loading history. However, that idea needs the estimation of several $\Sigma E_{d\,ult.}'$–values corresponding to different loading histories and is not rational in a sense. From these reasons, the following assumption is introduced in order to evaluate the damage of a member subjected to different loading histories as

adopted in Series-A and B.

When a member is subjected to more than two loading cycles at the same deflection amplitude, the real damage of the member after the second loading cycle is assumed to decrease with increasing loading cycles (n). If the damage of a member can be represented by the non-dimensional dissipated energy, the above assumption can be expressed by the following equations.

$$E_d''(n)=f(n)*E_d'(n) \tag{6-7}$$

$$f(n)=\frac{1}{n}*\frac{1+n(\kappa-1)}{\kappa} \tag{6-8}$$

Where, $E_d''(n)$ is the modified non-dimensional dissipated energy at the n-th loading cycle of the same deflection amplitude, f(n) is the damage reducing factor for the n-th cycle and κ is an experimental coefficient.

Here, the index evaluating the seismic damage is defined as

$$DI=\frac{\Sigma E_d''(n)}{\Sigma E_{d\,ult.}'(A)} \tag{6-9}$$

where, $\Sigma E_{d\,ult.}'(A)$ is the non-dimensional total dissipated energy until the ultimate state under a basic loading history, for example, gradually increased cyclic loading with one load repetition at each deflection amplitude adopted in Series-A.

Based on the above mentioned idea, the degree of damage of a member subjected to several load repetitions at the same deflection amplitude can be estimated by using Eq.(6-7)~Eq.(6-9) if the non-dimensional total dissipated energy until the ultimate state under a fundamental loading history, such as Series-A, is already known.

6.5.2 Application to Experimental Results

Damage index, DI, of Series-A and Series-B beams at each deflection amplitude was estimated by using Eq.(6-7)~(6-9). In this case, Eq.(6-6) was used for calculating the value of $\Sigma E_{d\,ult.}'(A)$ in Eq.(6-9).

As for the value of the coefficient κ, κ=1.1 for p=2.26% and κ=1.9 for

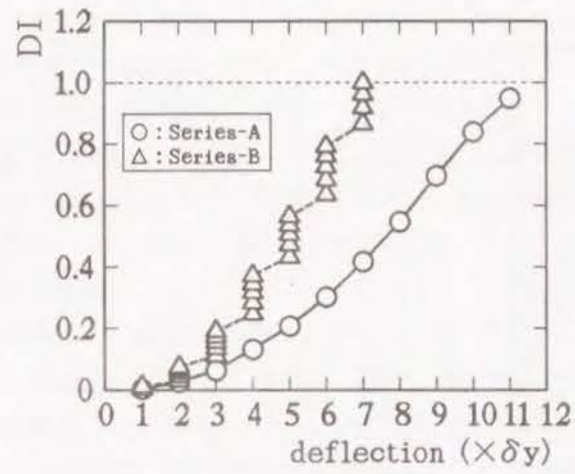

Fig.6-12 Example of the changes of DI (p=1.43%, p_w=1.26%)

p=1.43% was obtained in this study considering that the value of DI became 1.0 at the ultimate state of each specimen.

An example of the changes of DI in Series-A and Series-B beams is shown in Fig.6-12. It is indicated that the damage of the beams subjected to many load repetitions at the same deflection amplitude as Series-B in this study can be well estimated by the proposed method and that Series-B beams failed at smaller deflection amplitude than Series-A beams due to many load repetitions at each deflection amplitude.

6.5.3 Application to 1/3 Scale Bridge Pier Model Specimens

The proposed concept of damage index based on hysteretic dissipated energy was applied to the test results of 1/3 scale bridge pier model specimens conducted at Hanshin Expressway Public Corporation [14].

(1) Details of specimen and loading method

The size of the specimens (No.1 and No.2) is shown in Fig.6-13. They had a same rectangular cross section of width x full depth = 116.7 x 100 cm and a total height of 480 cm. The dimensions of this specimen were reduced precisely to 1/3 scale of those of standard bridge pier designed at Hanshin Expressway Public Corporation according to the law of similitude in order to eliminate the size effect.

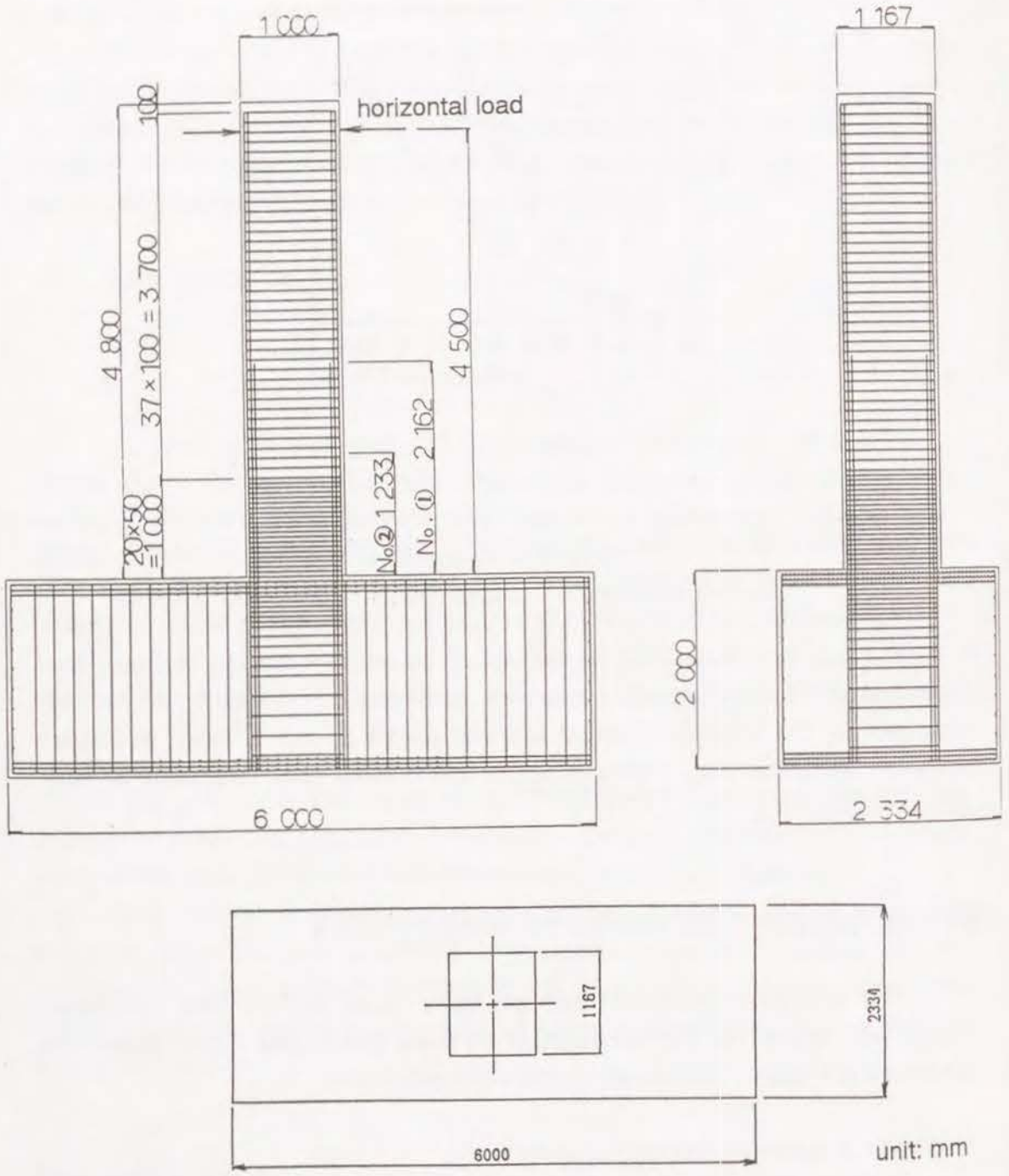

Fig.6-13 Dimensions of bridge pier model specimens [14]

Longitudinal reinforcement ratio of the specimen was 2.28% and reinforcing bars were arranged with three layers. No.1 specimen had a cut-off of longitudinal steel at the height of 216 cm, while No.2 at the height of 123 cm from the face of footing. On the other hand, shear reinforcement ratio was 0.326% irrespective of the specimens. Compressive strength of concrete was 283kgf/cm^2 and the yield strength of longitudinal steel and transverse steel was 38.3kgf/mm^2 and 32.4kgf/mm^2, respectively.

These specimens were subjected to reversed cyclic horizontal loads at the height of 450cm from the face of footing. The applied deflection amplitude was gradually increased as $\pm\delta_y$, $\pm2\delta_y$, $\pm3\delta_y$, --- and ten load repetitions was applied at each deflection amplitude. During the loading test, constant axial force of 160tonf (σ=13.7kgf/cm^2) corresponding to the dead load of superstructures was provided by four unbonded prestressing bars.

(2) Summary of test results

In Fig.6-14 are shown the load - deflection hysteresis loops of the specimens No.1 and No.2. In addition, in Fig.6-15 are shown their final failure modes. The specimen No.1 failed ultimately in flexure within the region near the face of the footing while the specimen No.2 failed in flexure within the cut-off zone of longitudinal steel. The summary of the visual change observed in the specimens during loading test is as follows.

(a) No.1 specimen

1) P=35.5tonf	Flexural cracking.
2) $\delta=\delta_y$	Flexural cracks at mid-height of the specimen turned to diagonal cracks.
3) $\delta=2\delta_y$	Diagonal cracks were observed in the bottom region near the footing face.
4) $\delta=4\delta_y$	Maximum load (121 tonf). Tendency of reduction in load carrying capacity due to load repetition. Spalling of cover concrete.
5) $\delta=5\delta_y$	Remarkable reduction in load carrying capacity. Significant spalling of cover concrete. Partial rupture of longitudinal steel.
6) $\delta=6\delta_y$	Further reduction in load carrying capacity.

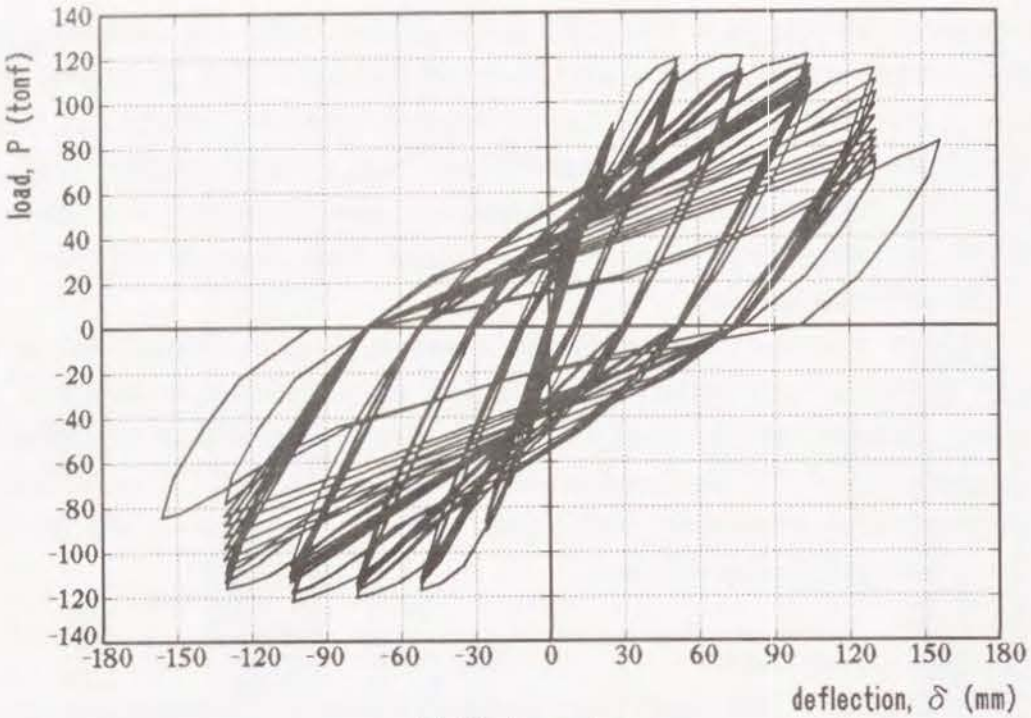

(a) No.1 specimen

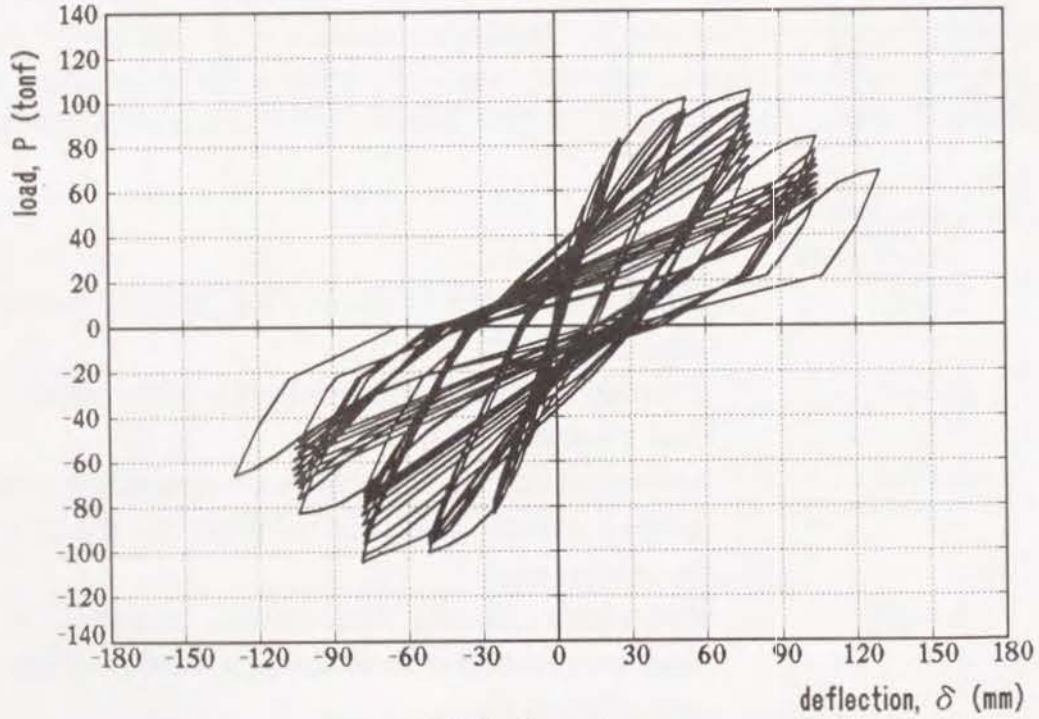

(b) No.2 specimen

Fig.6-14 Load – deflection hysteresis loops [14]

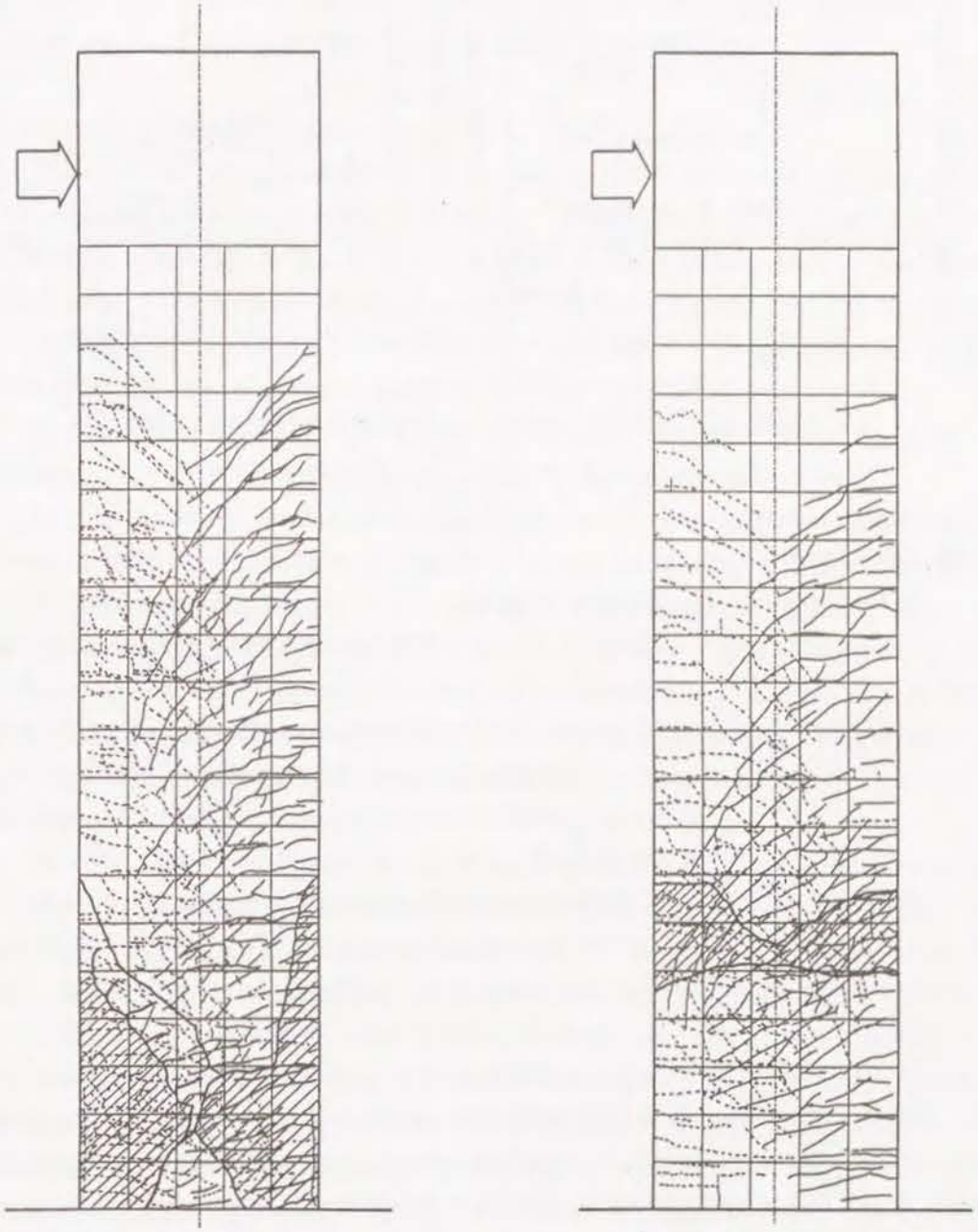

(a) No.1 specimen (b) No.2 specimen

Fig.6-15 Final failure mode [14]

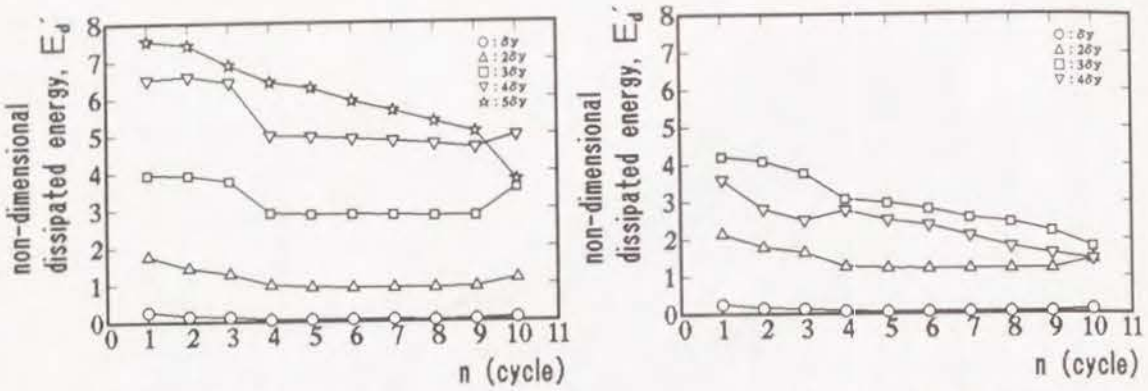

(a) No.1 specimen

(b) No.2 specimen

Fig.6-16 Changes of E_d'-value with repeated cycles

(b) No.2 specimen

1) P=13.3tonf — Flexural cracking.

2) $\delta=\delta_y$ — Flexural cracks at the cut-off zone turned to diagonal cracks.

3) $\delta=3\delta_y$ — Maximum load (105 tonf). Remarkable reduction in load carrying capacity due to load repetition. Spalling of cover concrete and buckling of longitudinal steel within the cut-off zone.

4) $\delta=4\delta_y$ — Further reduction in load carrying capacity. Partial rupture of longitudinal steel.

5) $\delta=5\delta_y$ — Furthermore reduction in load carrying capacity.

In Fig.6-16 are shown the changes of non-dimensional dissipated energy (E_d') with repeated cycles. At the deflection amplitudes less than $2\delta_y$, E_d'-value of these two specimens is almost the same and reduction in E_d'-value with repeated cycles is not remarkable. In No.2 specimen, however, E_d'-value becomes smaller with repeated cycles at $\delta=3\delta_y$ due to the pinching effect in P-δ hysteresis loops according to significant diagonal cracks at the cut-off zone, and E_d'-value at $\delta=4\delta_y$ becomes smaller than that at $\delta=3\delta_y$. This implies that No.2 specimen reached its ultimate state during the loading cycles of approximately $\delta=4\delta_y$. In No.1 specimen, on the other hand, E_d'-value increases with increasing the applied deflection amplitude until $\delta=5\delta_y$, although decreases remarkably during repeated cycles at

$\delta=5\delta_y$. This means that No.1 specimen reached its ultimate state during loading cycles at $\delta=5\delta_y$. These differences between No.1 and No.2 are supposed to be generated mainly from the difference of the location of final failure.

(3) Application of damage index

The concept of damage index proposed in this chapter was applied to the test results of the specimens No.1 and No.2. The ultimate state of each specimen was decided according to the definition adopted in this chapter, that is, the fourth cycle at $\delta=5\delta_y$ for the specimen No.1 and the first cycle at $\delta=4\delta_y$ for the specimen No.2. Damage index, DI, of these specimens at each loading cycle up to the ultimate state was calculated according to the following procedures.

In this case, $\Sigma E_{d\,ult.}'(A)$-value in Eq.(6-9) was calculated from Eq.(6-6) by substituting the actual p-value and p_w-value of each specimen.

As the value of coefficient κ in Eq.(6-8), $\kappa=1.1$ was adopted because the longitudinal reinforcement ratio of these specimens (p=2.28%) is almost equal to that (p=2.26%) corresponding to $\kappa=1.1$. Eq.(6-8) which gives the damage reducing factor, f(n), was obtained from the test results of the specimens subjected to five load repetitions at each deflection amplitude, while the specimen No.1 and No.2 were subjected to ten load repetitions at each deflection amplitude. Therefore, the values of f(n) after the sixth cycle were estimated by extrapolation up to n=10 in Eq.(6-8).

The changes of DI in each specimen are shown in Fig.6-17. The calculated value of DI corresponding to the ultimate state of each specimen is 1.83 for the specimen No.1 and 0.74 for the specimen No.2. These results imply that the ultimate state given by the proposed damage index is somewhat different from that obtained from test results. In case of the specimen No.1, DI-value reaches 1.0 during the loading cycles at $\delta=4\delta_y$, while remarkable reduction in load carrying capacity due to load repetition was not observed at that deflection amplitude. This implies that DI overestimates the actual damage of the specimen No.1. In case of the specimen No.2, on the other hand, the value of DI does not reach 1.0 even at $\delta=4\delta_y$ although significant reduction in load carrying capacity was observed during loading cycles at $\delta=3\delta_y$, that is, DI underestimated the actual damage of the specimen No.2.

These disagreements in the value of DI is supposed to originate mainly from the differences in final failure mode and some additional factors having influences on the energy dissipation properties. The specimen No.1 failed ultimately in flexure

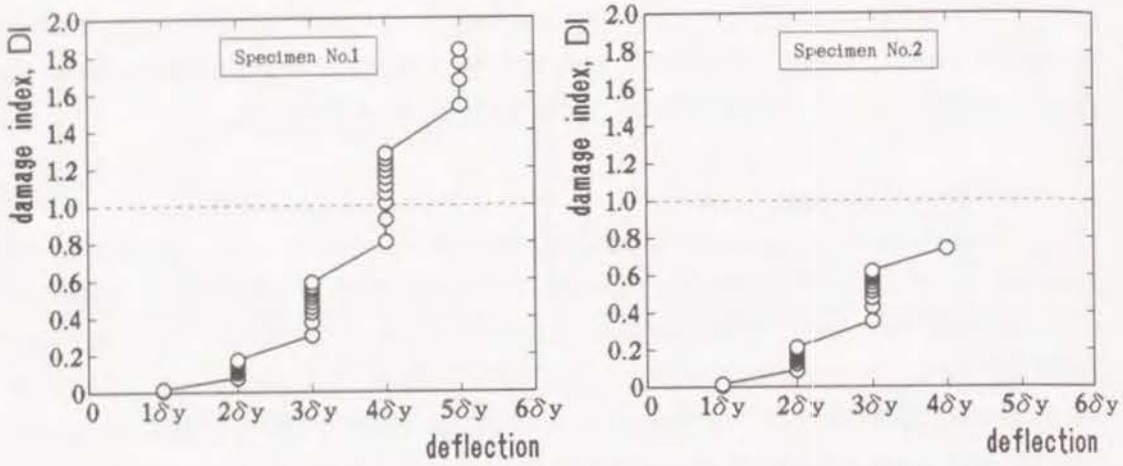

(a) No.1 specimen (b) No.2 specimen

Fig.6-17 Changes of DI

within the region near the footing face, while shear failure after yielding of longitudinal reinforcement is assumed when deriving the relationships between the non-dimensional total dissipated energy and the adopted test variables. In addition, introduced axial stress of approximately 14 kgf/cm^2 contributes to the increase in shear resistance of concrete under reversed cyclic loading. Therefore, the actual $\Sigma E_{d\,ult.}'(A)$-value of the specimen No.1 is supposed to be larger than that calculated by Eq.(6-6), resulting in overestimation of DI at the ultimate state. The specimen No.2, on the other hand, failed ultimately in flexure within the cut-off zone. In this case, the final failed region is concentrated at the cut-off zone as seen in Fig.6-15 and is much narrower than that of the specimen No.1. This concentration of failed region led to the pinching effect in load - deflection hysteresis loops at $\delta=3\delta_y$, resulting in the reduction in dissipated energy. As a result, the actual $\Sigma E_{d\,ult.}'(A)$-value of the specimen No.2 is supposed to be much less than that calculated by Eq.(6-6) and this led to the underestimation of DI in the specimen No.2.

As mentioned in Chapter 5, high degree of uncertainty exists in considering the effects of various factors on the non-dimensional total dissipated energy until the ultimate state and the accumulation process of damage due to load repetitions. In addition, the definition of the ultimate state adopted in Chapter 5 and 6 does not always reflect the real ultimate state of a member. Although damage evaluation based on hysteretic dissipated energy, which can consider the accumulative

damage due to cyclic loads, is supposed to be very effective, it is inevitable at the present state that some degree of disagreement should exist between the actual ultimate state of a member and the estimated one. Therefore, further investigations, for example, probabilistic approach on the uncertainty of the effects of various factors on the energy dissipation properties, is necessary.

6.6 CONCLUSIONS OF CHAPTER 6

In this chapter, energy dissipation properties of reinforced concrete beams are discussed by focusing mainly on the effects of longitudinal reinforcement ratio, shear reinforcement ratio and loading histories. In addition, a new damage index based on hysteretic dissipated energy is proposed and its applicability is examined by using the test results of 1/3 scale bridge pier model specimens. The main conclusions obtained in this chapter are as follows.

(1) Non-dimensional dissipated energy, which is normalized by the product of calculated yield load and yield deflection, of reinforced concrete beams becomes smaller with increase in longitudinal reinforcement ratio compared at the same deflection amplitude. Shear reinforcement ratio, on the other hand, determines the deflection amplitude at the ultimate state of tested beams subjected to reversed cyclic loading well into inelastic range.

(2) Non-dimensional dissipated energy are also influenced by the number of repetitions at the same deflection amplitude and the previous loading cycles at smaller deflection amplitude. The changes in non-dimensional dissipated energy according to the applied deflection amplitudes and the number of loading cycles of reinforced concrete beams under gradually increased reversed cyclic loads can be well estimated by the equations proposed in this study.

(3) Non-dimensional total dissipated energy until the ultimate state of reinforced concrete beams can be expressed by a function of longitudinal reinforcement ratio and shear reinforcement ratio although this relationship has been derived from limited data.

(4) A new damage index for reinforced concrete members based on hysteretic dissipated energy has been proposed, in which the damage reducing factor is introduced based on that actual damage corresponding to the energy dissipated at the same deflection decreases with increasing the number of load repetition.

(5) The applicability of the proposed damage index has been examined by using the test results of 1/3 scale bridge pier model specimens. The results showed the possibility of damage evaluation based on the proposed damage index. However, some degree of disagreement between the actual damage and the estimated one still exists at the present state due to the uncertainty of the effects of another factors besides those considered in this chapter. Therefore, further investigations should be necessary for more accurate evaluation of seismic damage of reinforced concrete members based on hysteretic dissipated energy.

REFERENCES OF CHAPTER 6

1) Darwin, D. and Nmai, C. K., "Energy Dissipation in RC Beams under Cyclic Load," Journal of Structural Engineering, ASCE, Vol.112, No.8, pp.1829–1846, 1989.
2) Nmai, C. K. and Darwin, D., "Cyclic Behavior of Lightly Reinforced Concrete Beams," Structural Engineering and Engineering Materials SM Report No.12, University of Kansas Center for Research, 1984.
3) Scribner, C. F. and Wight, J. K., "Strength Decay in Reinforced Concrete Beams under Load Reversals," Journal of the Structural Division, ASCE, Vol.106, No.ST4, pp.861–875, 1980.
4) Wight, J. K. and Sozen, M. A., "Strength Decay of RC Columns under Shear Reversals," Journal of the Structural Division, ASCE, Vol.101, No.ST5, pp.1053–1065, 1975.
5) Hwang, T. H. and Scribner, C. F., "R/C Member Cyclic Responses during Various Loadings," Journal of Structural Engineering, ASCE, Vol.110, No.3, pp.477–489, 1984.
6) Ma, S. M., Bertero, V. V. and Popov, E. P., "Experimental and Analytical Studies on the Hysteretic Behavior of Reinforced Rectangular and T–beams," Report No.EERC76–2, Earthquake Engineering Research Center, University of California, Berkeley, 1976.
7) Bertero, V. V., Popov, E. P. and Wang, T. Y., "Hysteretic Behavior of Reinforced Concrete Flexural Members with High Shear," Report No.EERC74–9, Earthquake Engineering Research Center, University of California, Berkeley, 1972.
8) Uomoto, T., Yajima, T. and Hongo, K., "Damage Evaluation of Reinforced Concrete Beams Subjected to Cyclic Bending Moment Using Dissipated Energy," Proc. of the Japan Society of Civil Engineers, No.460/V–18, pp.85–92, 1993. [in Japanese]
9) Kawashima, K., Hasekawa, K., Koyama, T. and Yoshida, T., "Effects of Cyclic Loading Hysteresis on Dynamic Behavior of Reinforced Concrete Bridge Piers," Civil Engineering Journal, Vol.29, No.4, pp.33–38, 1987. [in Japanese]
10) Park, Y. J., Ang, A. H.–S. and Wen, Y. K., "Seismic Damage Analysis of Reinforced Concrete Buildings," Journal of Structural Engineering, ASCE, Vol.111, No.4, pp.740–757, 1985.
11) Stephens, J. E. and Yao, J. T. P., "Damage Assessment Using Responce Measurements," Journal of Structural Engineering, ASCE, Vol.113, No.4, pp.787–801, 1987.
12) Inoue, S., Nakata, S., Miyagawa, T. and Fujii, M., "Energy Dissipation of Reinforced Concrete Beams under Reversed Cyclic Loading," Proc. of the Tenth World Conference on Earthquale Engineering, Vol.6, pp.3089–3093, 1992.
13) Japan Society of Civil Engineers, "Standard Specification for Design and Construction of Concrete Structures," 1991.
14) Research Committee on the Ductility of RC Bridge Piers, "Technical Report on Loading Tests of 1/3 Scale Bridge Pier Model Specimens," Hanshin Expressway Administration and Technology Center, 1993. [in Japanese]

CHAPTER 7

CONCLUSIONS

This research aimed at the clarification of the effects of various factors on the ductility and energy dissipation properties of reinforced, partially prestressed and prestressed concrete beam members, and in addition, the quantitative evaluation of seismic damage of these members based on hysteretic energy dissipation.

The main conclusions obtained in each chapter are summarized as follows together with some comments for future investigations.

In Chapter 2, a new stress – strain model for laterally confined concrete, which considers the strength degradation after the maximum stress, is proposed based on the results obtained from uniaxial loading tests on circular and square column specimens. In addition, the verification of the proposed model is done by comparing the moment – curvature relationships of concrete beam members calculated by using the proposed model with the measured ones.

Degree of compressive ductility improvement of confined concrete becomes significant with increase in volumetric ratio of transverse hoops and yield strength of transverse hoops while with decrease in compressive strength of concrete and spacing of transverse hoops (s/D ratio). The effects of these factors can be expressed quantitatively by confining coefficients defined for the maximum stress, the strain at the maximum stress and the stress degradation gradient after the maximum stress, respectively. The proposed stress – strain model for confined concrete, which considers the strength degradation after the maximum stress, can represent the measured ones under uniaxial loads well into large deformation and can be reasonably used for theoretical moment – curvature analysis of concrete members having ordinary under–reinforced section with longitudinal steel index of less than 0.3. However, further investigation should be done on the effects of strain gradient for a more precise estimation of moment – curvature relationship of flexural members.

In Chapter 3, investigations are done on the effective methods for determining the buckling initiation point of longitudinal bars in confined concrete in addition to the effects of various factors on the strain at buckling initiation of

longitudinal bars.

For the determination of buckling initiation point of longitudinal bars, the method which utilizes the separating point in load – longitudinal strain curves of the region including the buckled zone and the adjacent unbuckled zone, is considered to be effective as well as the method using the gradient of load – longitudinal strain curves. The strain at buckling initiation of longitudinal bars is mainly influenced by spacing of transverse hoops and diameter of bars. Closer spacing of hoops of $s/D' \leq 0.6$ (s: spacing of hoops, D': minimum leg of a hoop) is desirable in order to avoid premature buckling of longitudinal bars and attain a sufficient amount of inelastic deformability until the initiation of buckling. Further studies are desired as for the buckling of longitudinal bars under reversed cyclic loads and the load carrying capacity of longitudinal bars after buckling.

In Chapter 4, flexural inelastic deformation properties of partially prestressed concrete and unbonded prestressed concrete beams using confined concrete in compression zone of section under reversed cyclic loading are discussed.

The ductility of unbonded prestressed concrete beams as well as partially prestressed concrete ones can be effectively improved by arranging transverse hoops as lateral confinement at the spacing of, for example, one-fourth of the effective depth. Equivalent coefficient of damping of partially prestressed concrete beams tends to decrease with increasing mechanical degree of prestress. Equivalent coefficient of damping of unbonded prestressed concrete beams, on the other hand, is almost equal to that of corresponding bonded ones although the ultimate flexural strength of the former is 15%–20% smaller compared with the latter. Closer spacing of transverse hoops also improves elastic recovery of prestressed concrete beams even within the falling branch region. From the view point of ductility and energy dissipation under reversed cyclic loading, partially prestressed concrete with mechanical degree of prestress of less than 0.5 is found to have the most desirable inelastic deformation properties.

In Chapter 5, effects of various factors on the energy dissipation properties of partially prestressed concrete beams under reversed cyclic loading are discussed. Based on the results, a new damage index based on hysteretic dissipated energy is also proposed.

Energy dissipation properties of partially prestressed concrete beams are influenced mainly by mechanical degree of prestress, volumetric ratio of transverse

hoops and loading history. Non-dimensional dissipated energy, which is normalized by the product of calculated yield load and yield deflection, of partially prestressed concrete beams can be expressed by a linear function of applied deflection amplitude within deformation increasing process, while by a quadratic function of applied deflection amplitude within deformation decreasing process. The value of coefficients in these functions are mainly determined by mechanical degree of prestress, while the deflection amplitude at the ultimate state is dependent on volumetric ratio of transverse hoops. Non-dimensional total dissipated energy until the ultimate state can be also represented by a function of volumetric ratio of transverse hoops and mechanical degree of prestress. The proposed damage index, which is defined as the ratio of the non-dimensional total dissipated energy accumulated actually during loading cycles to the predicted non-dimensional total dissipated energy until the ultimate state, shows reasonable estimation of damage of tested partially prestressed concrete beams .

In Chapter 6, effects of longitudinal reinforcement ratio and shear reinforcement ratio on the energy dissipation properties of reinforced concrete beams are investigated. The concept of damage index proposed in Chapter 5 is also applied to the test results of reinforced concrete beams and 1/3 scale bridge pier model specimens in order to examine its possibility for seismic damage evaluation of concrete structures and members.

Non-dimensional dissipated energy, which is defined similarly to Chapter 5, at each deflection amplitude is affected mainly by longitudinal reinforcement ratio, while the deflection amplitude at the ultimate state is determined by shear reinforcement ratio. Non-dimensional total dissipated energy until the ultimate state can be expressed by a function of longitudinal reinforcement ratio and shear reinforcement ratio. The proposed damage index can represent the seismic damage of reinforced concrete members quantitatively. However, some degree of disagreement still exists between the actual damage and the estimated one due to the uncertainty of the effects of another factors which are not considered in this chapter.

From the whole results of this thesis, the effects of various factors on the ductility and energy dissipation properties of reinforced, partially prestressed and prestressed concrete beams can be predicted quantitatively with a certain accuracy. The effectiveness of the proposed damage index for seismic damage evaluation is

also indicated. However, a high degree of uncertainty still remains as for the ultimate deformability of a member under reversed cyclic loads with different loading histories as well as the effects of other factors which are not considered in this thesis. Therefore, further studies concerning about these points are earnestly desired in order to establish a rational evaluation method of seismic damage of concrete structures based on hysteretic energy dissipation.